2017

Tools and metrics to characterize extreme climate events and evaluate climatic datasets over the Upper Colorado River Basin for societal applications

Abayomi Abiodun Abatan
Iowa State University

Tools and metrics to characterize extreme climate events and evaluate climatic datasets over the Upper Colorado River Basin for societal applications

by

Abayomi Abiodun Abatan

A dissertation submitted to the graduate faculty

in partial fulfillment of the requirements for the degree of

DOCTOR OF PHILOSOPHY

Major: Meteorology

Program of Study Committee:
William J. Gutowski Jr., Major Professor
Kristie J. Franz
William A. Gallus Jr.
Raymond W. Arritt
Tsing-Chang Chen

The student author and the program of study committee are solely responsible for the content of this dissertation. The Graduate College will ensure this dissertation is globally accessible and will not permit alterations after a degree is conferred.

Iowa State University

Ames, Iowa

2017

TABLE OF CONTENTS

LIST OF FIGURES

LIST OF TABLES

ACKNOWLEDGEMENTS

This is my story. Gideon said to him, “But Lord, how can I deliver Israel? Just look! My clan is the weakest in Manasseh, and I am the youngest in my family.” The LORD said to him, “Ah, but I will be with you! (Judges 6 verse 11 – 16). It is not of him that willeth, nor of him that runneth, but of God that showeth mercy (Roman 9 verse 16). I thank God for strengthen me throughout the course of my study.

Further, I could not have done this without the support of my loving wife, Christy Abatan, and my wonderful children, Jacob and Joel Abatan. I appreciate your endurance and patience when for the most parts I was away to attend conferences and research events. Your moral and spiritual supports kept me going all the way.

More so, my utmost appreciation goes to Professor William J. Gutowski Jr., who in the past few years has been a great mentor. We first met in 2008 at a conference in Nigeria, and thereupon you believed in me and gave me the opportunity to join your research team for my doctoral degree. I am so grateful. It's been a great learning experience working with your collaborators; Barbara Brown, Caspar Ammann, Eric Gilleland, John Halley Gotway, Kaatz Laurna, Lawrence Buja, Randy Bullock, Tressa Fowler, through whom the NSF grants that supported my doctoral work came from.

I am also grateful to my POS committee Professors Kristie J. Franz, William A. Gallus Jr., Raymond W. Arritt and Tsing-Chang Chen. Your effort and support helped in honing my research skills and shaping my career.

The prayer and support from my family members; Abatan (paternal) and Ajose (maternal), and my in-laws (Pastor and Mrs. Bukola Komolafe) is high commendable. In

addition, my stay in Ames, Iowa, could not have been memorable and hospitable to me and my family without the support of Professor and Mrs. Tunde Adeleke, African Fellowship brethren, Grand Avenue Baptist Church Small Group members, and Christ Community Church prayer team. I am so grateful.

Finally, my sincere thanks to my office mates for the good times spent together. I appreciate Daryl Herzmann, Dave Flory, and all members of the Iowa State University Graduate Meteorology program. I acknowledge research collaboration with my dear friend Babatunde J. Abiodun (University of Cape Town, South Africa), who boosts my research skills. I am indeed very grateful to you all.

ABSTRACT

This study supports the Denver Water management goals by providing tools and metrics that are relevant for operational activities. The study focuses mainly on drought events, but with a slight mention of pluvial conditions over upper Colorado River basin (UCRB), the region that supplies water to Denver community. The study uses observed monthly minimum and maximum temperatures and monthly precipitation datasets (Climatic Research Unit; CRU and Precipitation-Elevation Regression on Independent Slopes Model; PRISM) and modeling outputs from 34 members of the Community Earth System Model Large Ensemble (CESM-LE) to monitor and characterize droughts over the region. With these datasets, we compute two multi-scalar moisture indices: standardized precipitation evapotranspiration index (SPEI) and standardized precipitation index (SPI) on a 36-month scale. We evaluate the capability of the CESM-LE to reproduce drought over the region using the more recently developed spatial verification tool, the Method for Object-based Diagnostic Evaluation (MODE) technique. In addition, the study examines the large-scale atmospheric circulation features associated with drought and pluvial conditions using reanalysis output. The results reveal the usefulness of these datasets, the drought indicators, and the spatial verification technique as important analytical tools to monitor and characterize extreme hydroclimatic conditions over UCRB.

CHAPTER 1. GENERAL INTRODUCTION

Extreme climatic events, in particular droughts and pluvials, have exhibited pronounced variability in many locations within the United States (US). The socioeconomic and ecologic impacts of these events are so enormous that they have gotten the attention of several researchers (e.g., Sheffield et al. 2004; Andreadis et al. 2005; Cayan et al. 2010; Wang et al. 2011). Drought is an unprecedented multiscalar phenomenon endowed with complex characteristics with significant impacts on several sectors of the economy. For instance, drought can affect all aspects of the agricultural sector: crop production, fisheries, and animal production. Also, drought can have great influence on every element of the hydrologic cycle (e.g., evaporation, runoff, percolation, precipitation, and transpiration). It is important to note that there are three basic types of drought: agricultural, meteorological, and hydrological drought. Each of these droughts has their own specific characteristics. As a result, several drought indices have been developed for drought monitor and analysis. Among such indices are the standardized precipitation index (SPI; McKee et al. 1993) and the standardized precipitation evapotranspiration index (SPEI; Vicente-Serrano et al. 2010).

In the past few decades and more recently, the southwest US including the upper Colorado River basin (UCRB) have experienced multi-year severe droughts that caused hardship through depletion of soil moisture and water storage levels in major lakes in the region. The impact of this extreme condition on water resources in this region has been a great concern to water resource managers. In order to improve the quality of services to the community, the Denver Water management's interest in gaining knowledge of variations in climate and large-scale atmospheric features in relation to drought conditions has increased.

However, the available datasets and tools in their standard formats are not directly useful for most planning and decision-making processes.

The focus of this study is to identify indices necessary to characterize drought episodes over UCRB, evaluate the usefulness of climate model outputs to Denver Water operation, and adapt a climate analysis weather validation tool that has been developed for numerical weather prediction.

In order to shed light on the aforementioned goals, several questions are addressed:

- How different, if any, is the drought pattern portrayed by SPI and SPEI at 36-month timescales?
- Is there any similarity in drought characteristics (e.g., onset, duration, cessation, intensity, and frequency) shown by SPI and SPEI?
- Are pluvials simply the mirror-image of droughts?
- What are the atmospheric large-scale features associated with the maintenance of drought?
- Does the CESM-LE simulate the drought objects depicted by the observed drought index? This question will be assessed by comparing the statistics of simulated drought objects with observed drought objects using the MODE technique.

Dissertation Organization

This dissertation contains a total of five (5) chapters. Chapter 1 contains a general introduction on drought conditions. Chapter 2 is a version of a published paper, while chapter 3 and chapter 4 are versions of the manuscripts that have been submitted for publication. The final chapter describes the general conclusions that can be drawn from the contents of this dissertation.

All of the analysis in chapter 2 was done by Abayomi Abatan. William J. Gutowski, Jr., Caspar M. Ammann, Laurna Kaatz, Barbara G. Brown, Lawrence Buja, Randy Bullock, Tressa Fowler, Eric Gilleland and John Halley Gotway contributed substantially to the paper through discussion and constructive comments. As in chapter 2, the analyses and interpretation of results in chapters 3 and 4 were carried out by Abayomi Abatan. The above-mentioned co-authors contributed also to the success of these chapters. The MODE diagnostic tool was developed by Barbara G. Brown, Randy Bullock, Tressa Fowler, and John Halley Gotway.

References

Andreadis, K. M., E. A. Clark, A. W. Wood, A. F. Hamlet, and D. P. Lettenmaier, 2005: Twentieth-century drought in the conterminous United States. *J. Hydrometeor.*, **6,** 985–1001, doi:10.1175/JHM450.1.

Cayan, D. R., T. Das, D. W. Pierce, T. P. Barnett, M. Tyree, and A. Gershunov, 2010: Future dryness in the southwest US and the hydrology of the early 21st century drought. *Proc. Natl. Acad. Sci.,* **107,** 21271–21276.

McKee, T. B., N. J. Doesken, and N. J. Kleist, 1993: The relationship of drought frequency and duration to time scales. Preprints, *Eighth Conf. on Applied Climatology*, Anaheim, CA, *Amer. Meteor. Soc*., 179–184.

Sheffield, J., G. Goteti, F. Wen, and E. Wood, 2004: A simulated soil moisture based drought analysis for the United States. *J. Geophys. Res.*, **109,** D24108, doi:10.1029/2004JD005182.

Vicente-Serrano, S. M., S. Beguería, and J. I. López-Moreno, 2010: A multiscalar drought index sensitive to global warming: The Standardized Precipitation Evapotranspiration Index. *J. Climate*, **23,** 1696–1718, doi:10.1175/2009JCLI2909.1.

Wang, D., M. Hejazi, X. Cai, and A. J. Valocchi, 2011: Climate change impact on meteorological, agricultural, and hydrological drought in central Illinois. *Water Resour. Res*.**,** W09527, doi:10.1029/2010WR009845.

CHAPTER 2. MULTI-YEAR DROUGHTS AND PLUVIALS OVER UPPER COLORADO RIVER BASIN AND ASSOCIATED CIRCULATIONS

A paper published in

The Journal of Hydrometeorology **2017,** 18, 799–818

Abayomi A. Abatan[1,*], William J. Gutowski, Jr.[1], Caspar M. Ammann[2], Laurna Kaatz[3], Barbara G. Brown[2], Lawrence Buja[2], Randy Bullock[2], Tressa Fowler[2], Eric Gilleland[2] and John Halley Gotway[2]

[1]Department of Geological and Atmospheric Sciences, Iowa State University, Ames, Iowa USA
[2]Research Applications Laboratory, National Center for Atmospheric Research, Boulder, Colorado USA
[3]Denver Water, Denver, Colorado USA
[*]Department of Meteorology and Climate Science, Federal University of Technology, Akure, Nigeria

Abstract

This study analyzes spatial and temporal characteristics of multi-year droughts and pluvials over the southwest United States with a focus on the upper Colorado River basin. The study uses two multi-scalar moisture indices: standardized evapotranspiration index

[1]Corresponding author address: Abayomi A. Abatan, 3134 Agronomy Hall, Department of Geological and Atmospheric Sciences, Iowa State University, Ames, Iowa 50011 USA.

E-mail address: abatanaa@iastate.edu yomiabatan69@gmail.com

(SPEI) and standardized precipitation index (SPI) on a 36-month scale. The indices are calculated from monthly average precipitation and maximum and minimum temperatures from the Precipitation-Elevation Regression on Independent Slopes Model dataset for the period 1950–2012. The study examines the relationship between individual climate variables as well as large-scale atmospheric circulation features found in reanalysis output during drought and pluvial periods. The results indicate that SPEI36 and SPI36 show similar temporal and spatial patterns, but that the inclusion of temperatures in SPEI36 leads to more extreme magnitudes in SPEI36 than in SPI36. Analysis of large-scale atmospheric fields indicates an interplay between different fields that yields extremes over the study region. Widespread drought (pluvial) events are associated with enhanced positive (negative) 500-hPa geopotential height anomaly linked to subsidence (ascent) and negative (positive) moisture convergence and precipitable water anomalies. Considering the broader context of the conditions responsible for the occurrence of prolonged hydrologic anomalies provides water resource managers and other decision makers with valuable understanding of these events. This perspective also offers evaluation opportunities for climate models.

Keywords: Drought; pluvial; SPEI and SPI indices; Denver Water; streamflow

1. Introduction

The southwestern United States, including the upper Colorado River basin (UCRB), is highly vulnerable to regional climatic extremes, such as droughts and pluvials, due to the region's geographic location and climatological characteristics (Laird et al. 1996; Hidalgo

2004). Multi-year droughts and pluvials have severe consequences for the agricultural sector and water resources management, such as for Denver Water, a major water utility in the region. Multi-year to multi-decadal extremes in precipitation occurred as droughts during the 1930s and 1950s (Woodhouse and Overpeck, 1998). The 1930s drought was characterized by numerous dust storms (Hughes, 1976), such that the choking billows of dust during these periods inspired the term "Dust Bowl" by Edward Stanley (Mencken, 1979). The drought that lasted from 1934-1937 occurred as a result of a climatic anomaly (Cook et al. 2014) exacerbated by unwise land use practices (Landsberg, 1982). The region had barely recovered from the devastating impacts of the 1930s drought when another persistent drought occurred in the 1950s. Drought episodes during the 1930s and 1950s marked the worst droughts experienced in the twentieth century over the region as well as for large areas in the United States (Andreadis et al. 2005). To this day, the 1953-1957 drought remains the reference drought for Denver Water to illustrate water management challenges.

More recently, severe multi-year regional droughts in the 2000s led to substantial impacts. A recent study over the UCRB by Woodhouse et al. (2016) observed that a warming trend has resulted in increased snowfall and earlier snow melt leading to increased runoff. At the same time, the evaporation also increased, causing a significant reduction in streamflow actually reaching the major reservoirs, especially during drought. The ongoing multi-year drought over the UCRB has been linked to warming (Nowak et al. 2012; Woodhouse et al. 2016) and has had substantial impact on the socioeconomic activities of the region as well as downstream. For example, the decline of water levels in Lake Powell and Lake Mead resulting from this drought combined with warming temperatures gives a situation where agriculture and hydropower production will likely suffer. A continued trend would yield the

potential for more costly extreme conditions, which calls for better understanding of the drought characteristics and associated dynamics in the UCRB. The work presented in this study is part of an effort by the research community and the Denver Water management to characterize long-term droughts and pluvials over the basin and to assess the quality of climate models in reproducing real world conditions. The work will inform scientific communities, water managers and policy makers, and through that information help making better decision on planning, distribution, and managing the best use of water resources.

There is no universal definition of drought, in large part because of different contexts and applications. However, in practice, drought is generally accepted as a natural hazard that originates from a precipitation deficit over an extended period of time (Wilhite and Buchanan, 2005) coupled with changes in other atmospheric variables including solar radiation, wind speed, evaporation, and temperature (Sheffield et al. 2012). Drought is a multi-scalar phenomenon (Vicente-Serrano et al. 2010a) with complex characteristics that can exert a great impact on the environmental and socio-economic condition of a nation (Palmer, 1965; Wilhite, 1993, 2000; Bryant, 2005).

The impacts of drought on water resources management and on the economy in the UCRB as well as the broader southwest have prompted numerous studies (e.g., McCabe et al. 2004; Seager et al. 2005, 2008; Christensen and Lettenmaier, 2007; McCabe and Wolock, 2007; Meko et al. 2007; Schubert et al. 2009; Dawadi and Ahmad, 2012; Nowak et al. 2012; Vano et al. 2014; Woodhouse et al. 2016). There is consensus that ongoing drought episodes in UCRB are related to both natural climate variability and, increasingly, to climate change associated with global warming. For example, Woodhouse et al. (2016) indicated that droughts over the basin have been amplified by warmer temperature relative to precipitation

deficits. Under the current warming conditions, Barnett and Pierce (2008) showed that there is a 50% chance that storage in Lake Powell will depleted by 2021. This projection is consistent with studies listed above that examined the impact of climate change on the basin. In addition, previous studies highlighted the link between UCRB hydroclimatic behavior during regional droughts and atmospheric/oceanic circulation patterns. These patterns are related to sea surface temperature (SST) anomalies over major ocean basins (e.g., tropical and North Pacific and North Atlantic) that are associated with major climatic modes. The effects of El Niño–Southern Oscillation (ENSO) and Pacific Decadal Oscillation (PDO) on UCRB's hydroclimatic variations was the focus of study by Hidalgo and Dracup (2003). They observed that during winter the basin was characterized by wetter than normal conditions during El Niño events (associated with tropical Pacific SST warming) and drier than normal conditions during La Niña events, consistent with previous studies. Hidalgo and Dracup (2003) further showed that hydroclimate shifts were even more significant when El Niño (La Niña) coincided with the positive (negative) phase of the PDO. Hoerling et al. (2009) also found that the southwestern United States' vulnerability to drought during 1946–1956 was a result of the region's sensitivity to SST anomalies in the tropical Pacific. In contrast, studies such as Kerr (2005) and Sutton and Hodson (2005) suggested that the Dust Bowl of the 1930s and the 1950s drought were associated with the warm phase of the Atlantic Multidecadal Oscillation. The results of these studies indicated the existence of several large-scale atmospheric patterns interacting to modulate droughts at different time scales.

Kingston et al. (2015) suggested that part of the uncertainty in the relationships between atmospheric circulation and drought comes from the method of drought identification. There

are different ways to characterize drought, such as agricultural, hydrological, and meteorological droughts. Agricultural drought is defined in terms of soil moisture deficit, hydrological drought in terms of anomalously low streamflow, while meteorological drought is defined in terms of precipitation deficit. Both soil moisture and precipitation deficits are prerequisites to hydrologic drought. These definitions are based on different objectives, and hence, several indices have been developed for representing different types and intensities of droughts or pluvials, and often with different time scales in mind. Among them are the Palmer drought severity index (PDSI; Palmer, 1965; Karl, 1983), the standardized precipitation index (SPI; McKee et al. 1993; Guttman, 1998), and the standardized precipitation evapotranspiration index (SPEI; Vicente-Serrano et al. 2010a). These indices are commonly used to provide useful information on drought detection and for monitoring evolving drought conditions to the public, water resources managers, and policy makers as part of an effective early warning system (Wilhite, 2002). They inform planning processes in water resources management for water allocations to minimize the impact of persistent drought (Yurekli and Anli, 2008).

Although these indices offer robust information on drought events, there are inherent limitations associated with them. For example, although PDSI is advantageous for characterizing soil conditions, it has limitations for use in climate studies (e.g., Karl, 1986; McKee et al. 1995; Guttman, 1998; Hu and Willson, 2000). Because of its inherently fixed time scale (between 9 and 12 months), the PDSI lacks the ability to distinguish different drought types given the multiscalar character that is important for assessing drought (McKee et al. 1993; Guttman, 1999; Vicente-Serrano et al. 2010a, 2010b). The SPI is a multiscalar index and can be applied across different geographical regions, at different time scales, but it

is based only on precipitation. It fails to account for the influence of changes in evaporation and transpiration on the climatic water balance. In addition, studies have indicated that SPI at shorter timescales can be misleading in regions with normally low seasonal precipitation totals (Hayes et al. 1999). Vicente-Serrano et al. (2010a) have proposed the SPEI as another important tool for drought evaluation. It is a modification of the SPI that incorporates potential evapotranspiration in its algorithm, thus allowing an evaluation of a complete climatic water balance. As a result, SPEI combines the advantages of being multiscalar (like the SPI) and being able to account for the role of temperature (like the PDSI) (Chen et al. 2013). Finally, studies such as Woodhouse et al. (2016) and work they cite show that trends in snowfall accumulation and earlier snow melt in the UCRB are influencing drought in the region. The indices above do not explicitly include effects of snow, which could influence characteristics of multi-year drought (Van Loon et al. 2014). However, Van Loon et al. (2014) also show that their results that included snow were consistent with earlier studies such as Vidal et al. (2010) that used other drought indicators that did not include snow.

This study uses 36-month SPEI and SPI to analyze drought and pluvial episodes over UCRB, the region that supplies water for Denver Water. Keeping in mind the example of the 1950s drought, Denver Water managers are especially interested in 36-month and longer droughts for planning water management, both for maintaining supply and for adequate operating revenue. Our analysis is part of an effort to understand the basis for past droughts and pluvials, and how they might change in the future, with an eye toward translating the knowledge to inform the water utility's needs. Aims of this study include: 1) diagnosing characteristics of multi-year droughts and pluvials (e.g., onset, duration, cessation, intensity, and frequency), 2) revealing the contrasts between drought and pluvial characteristics, and 3)

extracting atmospheric large-scale features associated with the initiation and maintenance of extended drought and pluvial periods.

2. Study location, data, and methods

a. The study area

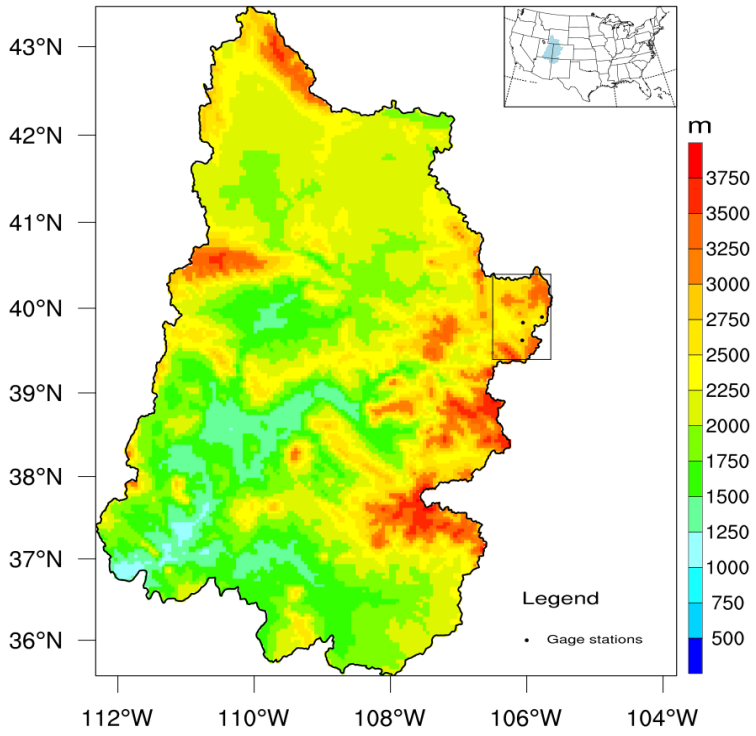

Figure 2.1 Topographic map of the UCRB with the locations of three streamflow gauge stations outlined in black box. The outline of the map of the contiguous United States showing the location of UCRB is shown in the inset.

The UCRB is located between 35 °N and 44 °N latitude, 105 °W and 113 °W longitude, and drains an area of about 284,380 km^2 across five states: Wyoming, Colorado, New Mexico, northern Arizona and Utah (Figure 2.1). The basin has diverse topographic features

with the Rocky Mountains on the eastern half and Wasatch Mountains on the western half. The relief ranges from 3,636 m (highest peak of the Wasatch; Mount Nebo) to 4,400 m (highest peak of the Rocky Mountains; Mount Elbert) above sea level. The topographic setting leads to complex regional microclimates across the basin, with a general transition of more maritime climates in the west to more pronounced continental conditions in the interior (Hirschboeck, 1991; Pitlick, 1994).

The climate of the UCRB is semiarid, with highly varied climate regimes that occur in the cold (October-March) and warm seasons (April-September). During the study period, the annual average temperature ranged from 5.1 to 7.9 °C, and the mean annual precipitation ranged from 510 to 1,060 mm. A large portion of the UCRB's accessible water comes from snowmelt during spring and heavy rainfall during summer (Christensen et al., 2004; Christensen and Lettenmaier, 2007). The precipitation events come mainly from frontal storms from the Pacific Ocean and convective storms whose moisture comes from the Gulf of Mexico or the Gulf of California (Barry, 1992).

The overall Colorado basin, whose water is often referred to as the life blood of the southwestern United States, supplies water for domestic use by approximately 26 million people, including residents of several major cities, such as Denver, and for various forms of recreation, irrigation and hydropower production (Hidalgo, 2004).

b. Data

The analysis in this study uses monthly maximum and minimum temperatures, potential evapotranspiration, precipitation, streamflow, and reanalysis datasets.

The monthly precipitation and maximum and minimum temperatures over UCRB are from the archives of the Precipitation-Elevation Regression on Independent Slopes Model (PRISM; Daly et al. 1994, 2008) datasets[2]. PRISM use a statistical interpolation method involving point measurements and digital elevation data. Further information on the dataset is available at the Oregon State University Climate Service website. The gridded datasets are available on a 4 km × 4 km grid from 1895–2012. Specifically, this study uses data for the 1948–2012 period to overlap with atmospheric reanalyses. The usefulness of this dataset in climate and many other applications is evident by its wide use (e.g., McCabe and Wolock, 2007; Nowak et al. 2012; Woodhouse et al. 2016).

We use monthly streamflow data aggregated over three gauging stations as representative streamflow data for the UCRB. The stations are Blue River below Dillon, Fraser River near Winter Park, and Williams Fork near Leal (see Fig. 2.1). The streamflow data were sourced from a combination of the State of Colorado's Division of Water Resources website[3], the United States Geological Survey National Water Information System website[4], and the Raw Water Operations database of Denver Water records. The data are available from October 1915 to December 2014. For consistency with the length of the period of the other datasets used in this study, we use the streamflow data starting from January 1948 and ending in December 2012.

The large-scale atmospheric conditions associated with droughts and pluvials during the study period are examined by analyzing reanalysis fields from two reanalysis datasets; the

[2] http://www.prism.oregonstate.edu

[3] http://www.dwr.state.co.us/SurfaceWater/Default.aspx

[4] http://waterdata.usgs.gov/nwis

National Centers for Environmental Prediction – National Center for Atmospheric Research (NCEP–NCAR) reanalysis dataset (Kalnay et al. 1996) and the European Centre for Medium-Range Weather Forecasts (ECMWF) Interim (ERA-I) reanalysis dataset (Dee et al. 2011). The NCEP-NCAR reanalysis uses a comprehensive analysis/forecast system with 3-D variational analysis to perform data assimilation from 1948 to the present. The reanalysis output is available every six hours on a 2.5° × 2.5° grid and at 17 pressure levels from 1000 to 10 hPa. Although NCEP–NCAR resolution is coarser than ERA-I's, we chose this dataset because it has a relatively long temporal record. Also, the dataset has been widely used in several studies and found to produce reasonable results. We use it to examine composites during droughts and pluvials in the UCRB of precipitable water, geopotential height, omega vertical velocity, and u and v components of wind anomalies. The ERA-I dataset is available at both coarser and finer resolutions at 37 pressure levels from 1000 to 1 hPa, for the period 1979–2012. The gridded data products available online include, among others, 6-hourly and monthly upper-air fields covering the troposphere and stratosphere. We use the monthly time scale at 0.125° × 0.125° resolution. In particular, we use ERA-I data to analyze and examine the vertical integral of zonal and meridional moisture flux and the flux divergence.

c. Methods of analysis

The SPI developed by McKee et al. (1993) to estimate and monitor drought has received widespread application, and it is commonly recommended by the research community and the World Meteorological Organization (WMO, 2006) as a key tool to quantify drought at different locations and time scales. It is calculated by fitting a parametric statistical distribution to precipitation data that have been accumulated over a period of time, from

which non-exceedance probabilities are transformed to the standard normal distribution (Stagge et al. 2014). Detailed descriptions can be found in McKee et al. (1993) and Guttman (1998). The second drought index used in this study, SPEI, was developed by Vicente-Serrano et al. (2010a) to characterize droughts at different time scales. The SPEI is obtained by fitting a log-logistic Pearson III distribution to the climatic water balance. Details are provided in Vicente-Serrano et al. (2010a), Beguería et al. (2014), and Yu et al. (2014). Unlike the SPI, the SPEI incorporates temperature effects and thus PET in its algorithm, which allows for an evaluation of a more complete climatic water balance, defined here as precipitation (input) minus PET (loss).

There are several methods for estimating PET (Vörösmarty et al. 1998). However, there are three commonly used approximations: Thornthwaite (Th; Thornthwaite, 1948), Hargreaves (Hg; Hargreaves and Samani, 1985), and Penman-Monteith (PM; Monteith, 1965). While Th requires only mean temperature and latitude of the location, the PM formulation requires temperature, solar radiation, relative humidity, and wind speed. However, the third equation, Hg, requires only maximum and minimum temperatures. Although PM is recommended for the estimation of PET, and it has been widely used, its extensive data requirement for variables that are not routinely measure by many meteorological stations (Beguería et al. 2014) has limited its application. Th, on the other hand, has been found by previous studies to overestimate PET with increasing temperature (Beguería et al. 2014, van de Schrier et al. 2011). Also, Th does not give reliable results in semiarid regions, as it underestimates PET (Jensen et al. 1990). This study uses Hg to compute PET in the climatic water balance. We use Hg because PRISM does not have all variables required to estimate PET by PM, but it does have those needed by Hg. In addition,

PET estimated from the Hg and PM equations at monthly and annual timescales are very similar (Beguería et al. 2014, Droogers and Allen, 2002).

Because the three methods use different input variables to compute PET, there may be differences in the SPEI results obtained from these methods. We present the evolution of the 36-month SPEI obtained from the three methods in the Appendix. The SPEI series from the three methods are identical, although there are slight differences in magnitude. The drought events during the 1950s, 1960, and the more recent drought episodes during the 2000s are well captured by the three PET methods, except for Th method that underestimated the 1950s drought episodes.

Recently, Beguería et al. (2014) updated the SPEI algorithm to allow the user to select between different approaches to calculate the potential evapotranspiration (PET), with some consequences for climate studies. This study uses the revised SPEI algorithm to compute SPEI and SPI at 36-month time scale (hereafter SPEI36 and SPI36) based on PRISM monthly precipitation and maximum and minimum temperatures at each grid point over the UCRB using the SPEI function developed and made available through an R-package by Beguería and Vicente-Serrano (2013). The classification of the intensity of dryness (negative values) and wetness (positive values) used in this study for the drought and pluvial episodes is given in Table 1, consistent with literature (Hayes et al. 1999; Lloyd-Hughes and Saunders, 2002). We focus on 36-month periods ending in December, identified by the year of their ending month. We develop the time series at each grid point using an overlapping 36-month running mean window. For example, data designated as “December 1950” comes from the mean of January 1948 – December 1950; similarly December 1951 data comes from the mean of January 1949 – December 1951, etc. For the temperatures and precipitation

series, these are running averages; for the drought indices, these are moving windows of more complex cumulative quantities as derived in the index calculations.

Table 2.1 Classification scale for drought/pluvial indicator values.

Category	Index range
Extreme dry	index ≤ -2.0
Severe dry	$-2.0 <$ index ≤ -1.5
Moderate dry	$-1.5 <$ index ≤ -1.0
Normal	$-1.0 <$ index < 1.0
Moderate wet	$1.0 \leq$ index < 1.5
Severe wet	$1.5 \leq$ index < 2.0
Extreme wet	$2.0 \leq$ index

Recall that SPEI and SPI are standardized anomalies, as implied by their names. For ease of comparison of the hydroclimate variables with these indicators, we also determine the anomaly of all the data used in this study. The anomalies were computed by subtracting the long-term mean from the monthly value at each grid point. Standard deviations at each grid points were also calculated. We use 1981–2010 as the baseline period for consistency with the baseline used in the SPEI algorithm. Then, we obtain the normalized anomalies of the variables by dividing the anomalies by the standard deviations. This method has been used in several research studies involving extremes and synoptic-scale events (e.g., Grumm and Hart, 2001; Hart and Grumm, 2001; Junker et al. 2008). The trends in the hydroclimatic variables are calculated and the statistical significance of the trends at the 5% significance level are assessed using the modified Mann-Kendall test statistics (Hamed and Rao, 1998).

Finally, we examine the large-scale atmospheric features associated with the extreme events by focusing on so-called widespread extreme events. We define conditions as a widespread extreme event when 50% or more of the grid points in the target region exhibit

drought (pluvial) intensity of –1.0 and below (+1.0 and above). We tested the number of events retained for composites by varying the spatial coverage threshold for drought/pluvial from 50 to 60%. We found that despite considerable reduction in the number of events, the spatial patterns of the composites varied only slightly, which implies that the choice of a 50% threshold is reasonable for this study. We develop composite maps of atmospheric variables corresponding to the average conditions of all the widespread drought or pluvial events for each of the two indices. Prior to compositing, we detrend the time series of the large-scale fields by removing the linear fit to the time series at each grid point. This is done in order to remove potential effects of trends that might yield false indication of significant behavior. We present analyses only for composites developed using the widespread events derived from SPEI because the two indices, SPEI and SPI, have nearly identical extreme event years. In addition to the composites, we also present analyses for two selected periods when the study region experienced widespread drought and pluvial conditions. This enables us to compare and contrast the large-scales atmospheric features influencing droughts and pluvials events over UCRB.

Results and discussion

a. Mean climatology

In order to understand the nature of extreme conditions over UCRB, we first examine the climatology of the region by analyzing the 36-month moving average of the surface variables used in this study to compute the drought indices. In particular, we analyze and examine the spatial distributions and time series of maximum temperature (TX36), minimum temperature

(TN36), potential evapotranspiration (PET36) and precipitation (P36) during the period of study using the PRISM 4km data.

The spatial pattern of mean TX36 is shown in Fig. 2.2a, with a distinct spatial variability. The eastern sector and parts of the northern axis, the mountainous regions with height at 2750 m and above, are characterized by lower temperatures, while higher values with slight-to-moderate temperature gradients dominate the northern and the southern parts of the basin. The areal mean maximum temperature over the basin is about 14.7 ℃, with a mean standard deviation of about 3.9 ℃. The temperature range is 20.7 ℃, with maximum value of 23.0 ℃ and minimum value of 2.3 ℃. Unlike the maximum temperature, a clear north-south temperature gradient is shown by the spatial distributions of minimum temperature (Fig. 2.2b). Temperatures over the eastern sector of the basin are generally cooler. The core of the minimum temperature over the basin is located at the southwestern regions extending in narrow strip over the central part. Areal mean temperature is –0.6 ℃, with a standard error of 3.7 ℃. The temperature range is 19.2 ℃, with maximum value of 9.0 ℃ and minimum value of –10.2 ℃.

Figure 2.2c shows the spatial pattern of mean PET36 over the UCRB during the period of study. This pattern shows a close resemblance to that of mean TX36 (Fig. 2.2a), with higher evapotranspiration characterizing the lower parts of the basin while the high-elevation regions are characterized by lower evapotranspiration. As expected, the observed pattern of the long-term average PET36 (Fig. 2.2c) is very similar to that of mean T36, as the potential evapotranspiration in this study is calculated using temperature. Areal mean potential evapotranspiration over UCR is 90.4 mm, with a standard deviation 15.1 mm and a median value of about 89.3 mm. The climatological minimum and maximum values of PET are 45.3

and 120.7 mm, respectively. The similarities between the spatial distributions of maximum temperature and potential evapotranspiration over the basin suggest their important roles in extreme conditions over the basin.

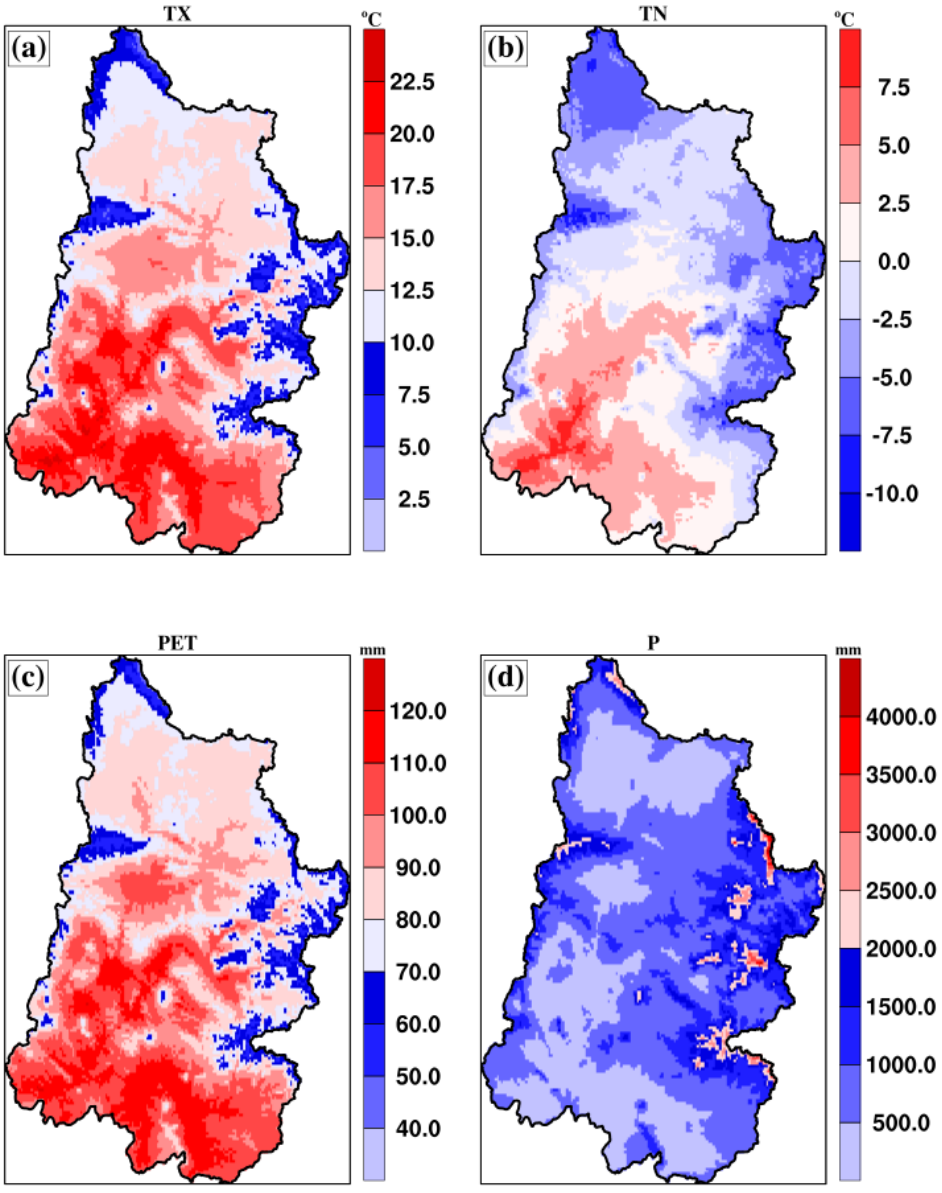

Figure 2.2 The spatial pattern of mean climatology of (a) TX36, (b) TN36, (c), PET36, and (d) *P*36 in December during the period 1950–2012.

Figure 2.2d shows the mean P36 over UCRB. Unlike the other three hydroclimatic fields, large parts (well over 90% of the area) of the basin have precipitation below the average value (815.4 mm). However, several portions of the high-elevation regions, have precipitation above the spatially averaged mean value (815.4 mm). Pockets of maximum values of about 4457.7 mm can be seen over the mountainous regions. The precipitation over the low lying areas can be as low as 293.6 mm with a standard deviation of about 495.4 mm. The relatively lower values of precipitation over large fractions of the basin suggest, in general, that the basin has drier conditions at lower elevations.

b. Spatial and temporal distributions of hydroclimate variables and drought indices

1) Temporal characteristics of climate variables and drought indices

In consideration of the climate variability over the UCRB, we examine the temporal evolution of the normalized anomalies of maximum temperature, potential evapotranspiration, precipitation, and the drought indices at 36-month timescale, averaged over the study domain (Fig. 2.3) and a sub-region (Fig. 2.4). The sub-region contains the locations of the streamflow observations used here (outlined black box in Fig. 1). The streamflow observations are concentrated in the extreme northeastern portion of the UCRB, the region that supplies water for Denver. Thus, we also examine the time series of the surface hydroclimates and drought indices along with the streamflow (SF36) data spatially averaged over this sub-region. The result of the streamflow analysis over this region will be used as a proxy for the characteristics of streamflow for the entire basin region.

Figure 2.3 shows the temporal evolution of normalized TX36, PET36, P36, SPEI36 and SPI36 anomalies spatially averaged over our study domain. The normalized TX36 anomalies

show clusters of hot and cool periods (Fig. 2.3a). Hot years are found during 1954–1964 (with a break in 1957), 1977–78, 1981–82, 1988–1990, 1996–97, and 2000–2008, while there have been cool years during 1950–53, 1965–1976, 1979–80, 1983–87, 1991–95, and 2009–11. Of the clusters, the most obvious are the positive anomalies spanning 1954–64 and 2000–08, and negative anomalies spanning 1965–1976, 1983–87, and 1991–95. TX36 shows a statistically significant cooling trend (–0.40 per decade, p = 0.0084) from 1950–80 and a non-significant warming trend (0.41 per decade, p = 0.1660) from 1981–2012, which is consistent with Gleason et al. (2008). In general, the linear trend in normalized TX36 anomalies during the period 1950–2012 shows non-significant warming at a rate of 0.05 per decade (p = 0.6311).

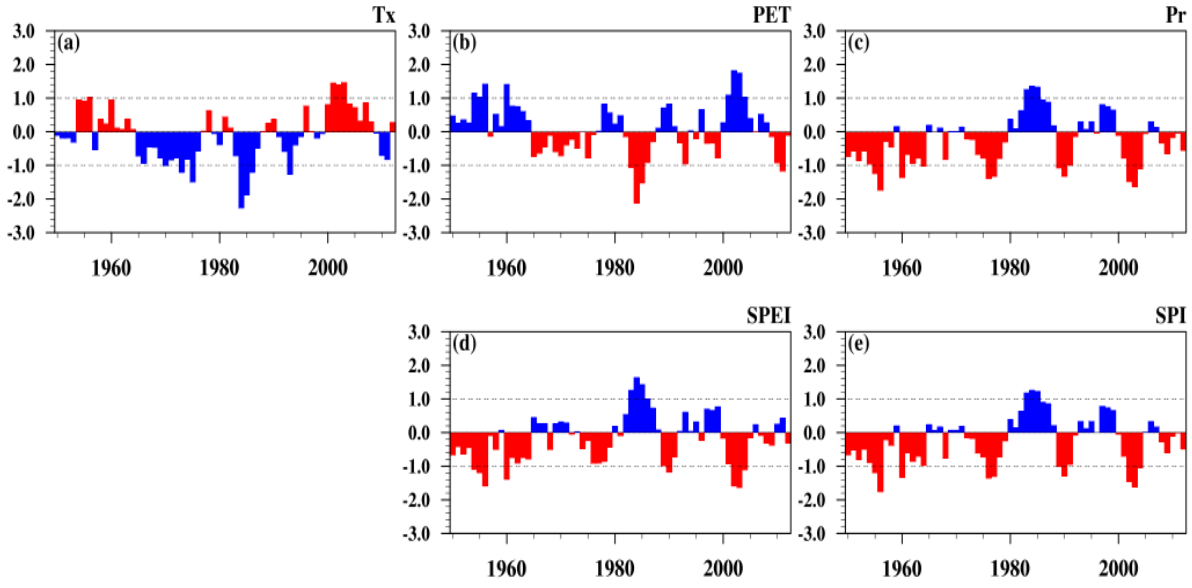

Figure 2.3 Time series of (a) TX36, (b) PET36, (c) *P*36, (d) SPEI36, and (e) SPI36 over UCRB. Drought is identified as –1.0 std dev from the 1981–2010 baseline period.

Figure 2.3b shows the temporal evolution of PET36. This pattern is similar to that of TX36 (Fig. 2.3a), although with slight differences in timing and duration. For example, in contrast to T36, PET36 shows a cluster of positive anomalies during 1950–53. The longer duration of positive PET36 anomaly during the periods 1950–64 and 2000–08 indicate the higher evaporative demand by the atmosphere over UCRB during those periods. The temporal pattern of PET36 shows a decreasing trend (–0.33 per decade, p = 0.1577) in the field during the first half of the period and an increasing trend (0.24 per decade, p = 0.4606) during the later period. Overall, normalized PET36 anomaly is characterized by a non-significant decreasing trend (–0.07 per decade, p = 0.4667). The time series of normalized P36 anomalies is shown in Fig. 2.3c. In general, clusters of dry years span the periods 1950–64, 1972–79, 1989–1992, 2000–05, and 2008–12, while the other periods are characterized by positive anomalies, with the longest duration in 1980–88, respectively. The trend in P36 shows a non-significant increase (0.08 per decade, p = 0.3409) during 1950–80 and a statistically significant decrease (–0.45 per decade, p = 0.0362) during 1981–2012.

As shown in the time series of SPEI36 (Fig. 2.3d) the dry episodes (negative anomalies) span 1950–58, 1960–64, 1974–79, 1989–1991, 2000–09, and 2007–09, while wet episodes (positive anomalies) occur during 1965–71 with breaks in 1968, 1982–1988, 1992–95 and 1997–99, respectively. Figure 2.3e shows that the time series of SPI36 (Fig. 2.3e) exhibit a temporal pattern consistent with P36. The similarity is due to the sole contribution of precipitation in the SPI calculation. Although the temporal patterns of SPEI36 and SPI36 are similar, indicating the influence of precipitation in both indices, the opposite-phase relationship of SPEI36, in particular, with TX36 and PET36 suggest that warming coupled

with higher evaporative demand may also be playing significant role in variations of extreme SPEI36 events over UCRB.

Examination of trend analysis during the two periods considered above indicate that trends in these drought indicators show increases during the first half of the period from 1950–80, with changes of 0.09 and 0.17 per decade for SPI36 and SPEI36, respectively. The upward trend is a result of the reduction in drought intensity towards the end of the period. However, during 1981–2012, trends in SPI36 and SPEI36 are –0.41 (significant; $p = 0.0320$) and –0.35 per decade, respectively. The downward trend in the drought indicators may be due to the weakening in intensity of the wet conditions and subsequent intensification in intensity during the dry conditions, especially during the 2000s. The drying during the recent decades is consistent with the results by other researchers, who studied PDSI (e.g., Cook et al. 2004; Dai et al. 2004). The results suggest, in agreement with other studies, that the increase in P36 over UCRB between the first half and second half of the period is the main cause for the upward (moistening) trends observed in the drought indicators. Also, the warming trend during the second half of the period and simultaneous significant decrease in precipitation is responsible for the later drying trends.

The time series of normalized anomaly of SF36, hydroclimatic variables, and the drought indices for the sub-region is shown in Fig. 2.4. It can be seen that there is a close resemblance between the hydroclimatic variables and drought indices in Fig. 2.4 with those in Fig. 2.3 for the UCRB. The few differences that occur are related to the onset and cessation of events. Also, the magnitudes appear higher in Fig. 2.4 than in Fig. 2.3. The disparities may be due to the difference in spatial coverage, coupled with elevation effect.

The streamflow data shown in Fig. 2.4d indicates that the periods of anomalous positive and negative SF36 are in good agreement with the wet and dry years presented by both SPEI36 (Fig. 2.4e) and SPI36 (Fig. 2.4f). More specifically, the correlation of SF36 and SPEI36 is 0.78, whereas the correlation of SF36 and SPI36 is 0.79; both indices appear to be indicators of streamflow into Denver Water's reservoirs. The trends in SF36 during both the first half and second half of the period show weaker non-significant decreases (–0.13 {p = 0.6833} and –0.07 {p = 0.8793} per decade), respectively. Overall, the pattern displayed by the normalized SF36 anomalies indicates an increasing trend with magnitude of about 0.07 per decade.

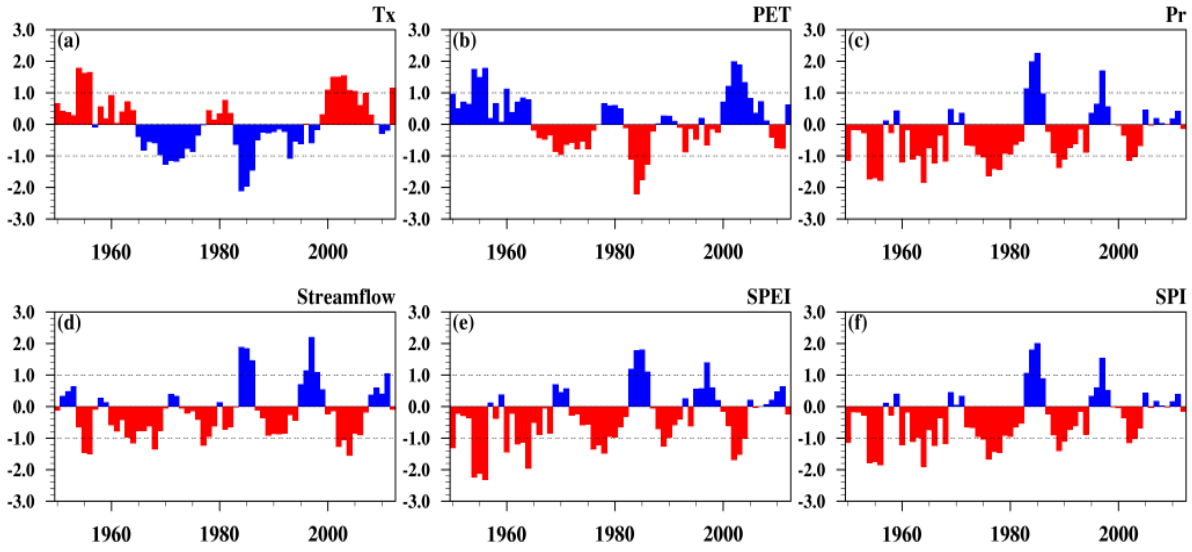

Figure 2.4 Time series of (a) TX36, (b) PET36, (c) *P*36, (d) SF36, (e) SPEI36, and (f) SPI36 averaged over the subbasin (black outlined box in Fig. 2.1). Drought is identified as –1.0 std dev from the 1981–2010 baseline period.

Figure 2.5 shows the percentage area of the UCRB in moderate and severe-to-extreme droughts (left panels) and pluvials (right panels). The panels each consist of the temporal evolution of the SPEI (solid) and SPI (dash) at 36-month. In general, although the two indices have similar patterns, there are slight differences in percent area and period. For example, SPEI result indicates that 58% of the UCRB experienced moderate drought in 2004, while in 2002 about 54% of the region had moderate drought according to the SPI (Fig. 2.5a). For severe-to-extreme drought (Fig. 2.5b), there are about 83% (76%) and about 62% (37%) of the region in this classification of drought in 2003 (2002) as indicated by SPEI36 and SPI36, respectively. Furthermore, the period with the highest percentage area in moderate-to-extreme drought over UCRB is 1956 with about 66% as indicated by SPI36. Droughts during these periods have a significant impact on water resources over the western region of the United States.

As in the temporal patterns depicted in Figures 2.5a and 2.5b for the moderate and severe droughts over UCRB, there is a similarity in the time series of each category of pluvial events according to SPEI36 and SPI36 (Figs. 2.5c and 2.5d). We see that 1983, 1984, and 1985 had the largest percentage of area in moderate and severe-to-extreme wet conditions, respectively. In 1983 and 1984, about 61% and 80% of UCRB was affected by moderate wet conditions as indicated by SPEI36 and SPI36, while SPEI36 (SPI36) indicated that about 46% (33%) of the area experienced severe-to-extreme wet conditions in 1984 (1985).

Overall, the percentage of area in drought in the 2000s stands out as a prominent feature of the temporal pattern over the region, with a peak in 2003. The other prominent features of the time series of percentage area in drought over UCRB are the mid-1950s, 1960s, 1970s, and 1988 to 1990. The 1980s and late 1990s are characterized by pluvial conditions. These

results are in agreement with other studies over the western United States (e.g., Andreadis et al. 2005).

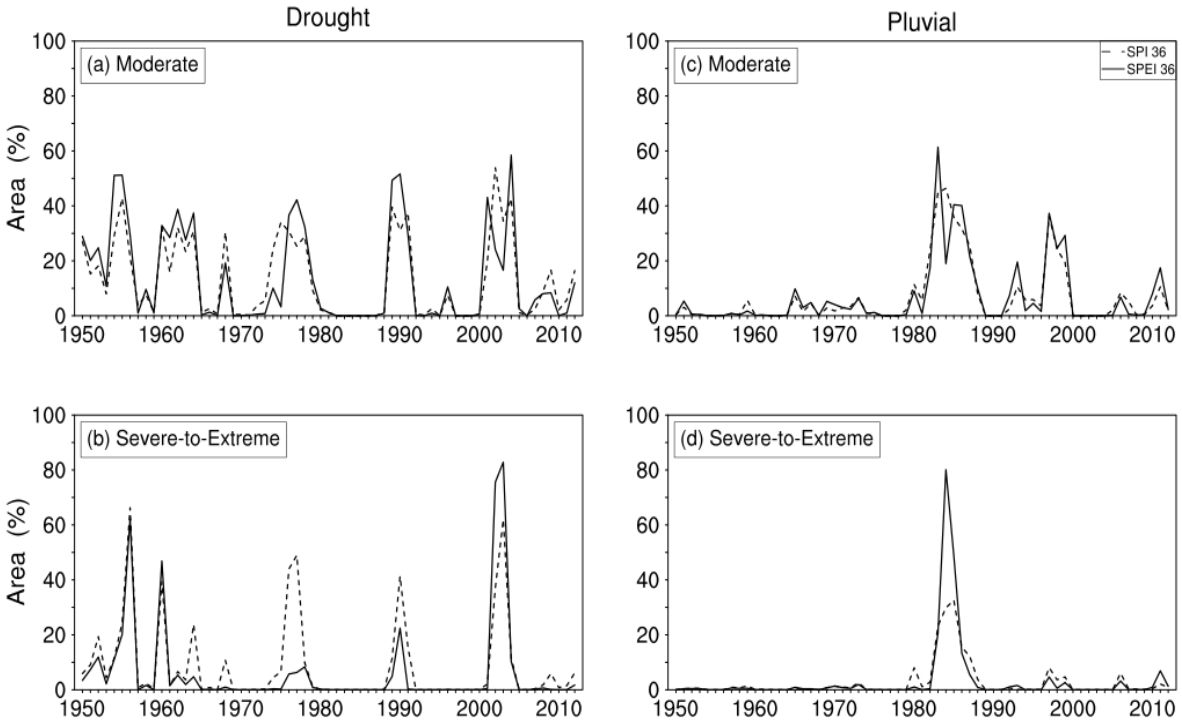

Figure 2.5 Areas (%) of the UCRB in (a) moderate and (b) severe-to-extreme drought and (c) moderate and (d) severe-to-extreme pluvial conditions at the 36-month time scale ending in December from 1950 to 2012. The solid line is for SPEI, while the dashed line is for SPI. See text for the classification of the indices values.

2) Spatial patterns of SPEI36 and SPI36

In Colorado, the recent drought conditions, which started in late 1999 and initially peaked in the summer of 2002, had a great impact on the Colorado River basin. The basin

experienced the worst 11-year drought in the last century (Bureau of Reclamation 2012) and the reservoir storage declined. Snowpack was much below average, and in 2002 it was extremely low throughout the state. The natural annual flow volume at Lees Ferry stood at 6.03 million acre-feet (MAF) below average annual flow of approximately 14.8 MAF (https://www.doi.gov/water/owdi.cr.drought/en/). To better understand the climate variability over this region for planning purposes requires the application of appropriate tools. In an effort to show the similarities and/or differences in the patterns depicted by the two indices, we examine the spatial patterns of the indices in that extreme drought year of 2002 and compare conditions with the years 1956 and 1984 when the drought indicators exhibit the largest percentage of area in either drought or pluvial conditions over UCRB.

We show the spatial patterns of SPEI36 and SPI36 during the periods ending 1956, 1984, and 2002 in Figure 2.6. Although the spatial patterns of the two indices bear a clear resemblance to each other, there are slight differences in magnitude. This suggests that different large-scale atmospheric features may be responsible for extreme events over the UCRB. In 1956, the magnitude of drought in SPI36 (Fig. 2.6d) is slightly higher than in SPEI36 (Fig. 2.6a). The drought intensity appears to be higher over the southern parts of the region and over the sub-region. Previous studies have shown that the 1950s drought over the United States was related to a deficit in precipitation rather than a warming temperature (Dai et al. 2004). Unlike the spatial patterns in 1956, the regions in severe droughts in 2002 are spatially larger in SPEI36 (Fig. 2.6c) than in SPI36 (Fig. 2.6f) (see also Figure 2.5), indicating that drought intensity in SPEI36 is larger than in SPI36. The 2002 drought was accompanied by warming during the second half of the study period (Fig. 2.3). This is

consistent with Dai et al. (2004), which indicated that increases in percentage areas after the mid-1980s were primarily caused by surface warming.

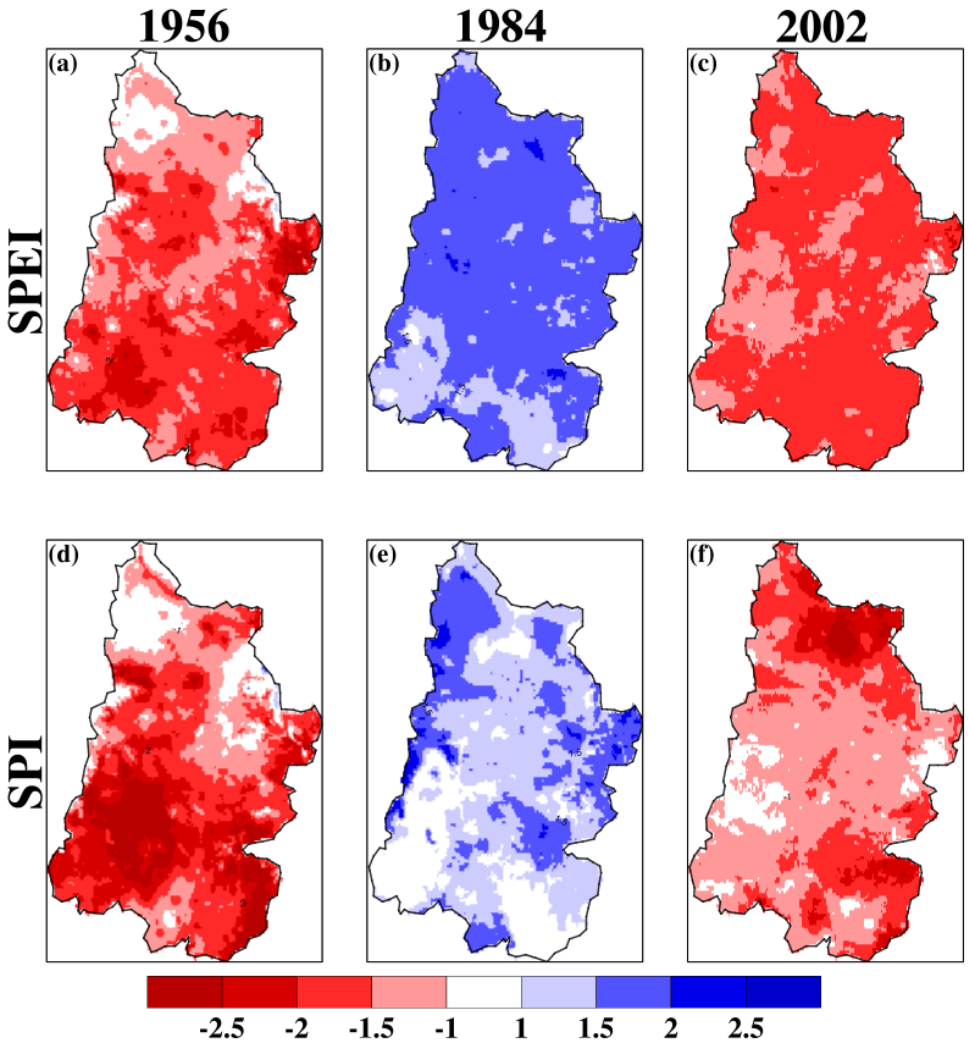

Figure 2.6 Spatial patterns of the (top) SPEI and (bottom) SPI at the 36-month time scale ending in December for (a),(d) 1956; (b),(e) 1984; and (c),(f) 2002.

The spatial structure of the pluvial event in 1984 is shown in Figures 2.6b and 2.6e. This study finds that while SPEI classifies large areas as having severe pluvial conditions, SPI

displays more areas in normal-to-moderate pluvial conditions. Fig. 2.4 shows that anomalies in temperature and potential evapotranspiration were below normal indicating that evaporative demand over the river basin was lower. Concurrently, there was a positive precipitation anomaly that then could yield higher streamflow (Fig. 2.4d). Finally, the SPI in Fig. 2.6 shows more spatial heterogeneity than the SPEI. This difference may be a consequence of the inherently larger spatial scale of temperature anomalies that are part of an SPEI computation.

The temporal and spatial analysis of drought and pluvial conditions indicated, for example, that droughts during the 1950s were a response to precipitation deficits, while droughts during the 2000s show an increasing influence of temperature in addition to rainfall deficits, although the patterns portrayed by SPEI36 and SPI36 are spatially similar. This result, however, underscores the potential advantage of SPEI as an appropriate tool for drought monitoring, especially under climate change because it takes the effect from rising temperatures into account.

c. Atmospheric large-scale features associated with drought and pluvial events

Previous studies indicated that extreme events over the southwest United States are likely related to changes in atmospheric circulation. A few examples were highlighted in the section 1. In this section, we analyze the spatial arrangement of composites of large-scale atmospheric features, including the precipitable water, zonal and meridional moisture transport, geopotential height, and omega vertical velocity, to examine their physical structure during widespread droughts and pluvials as indicated by SPEI36 over UCRB, using the NCEP-NCAR reanalysis dataset. The robustness of these large-scale fields was examined

using the finer spatial scale ERA-I dataset, in particular, for the divergence of vertically integrated moisture flux. In order to put the large-scale patterns influencing extreme events over UCRB into perspective, we repeat the above analyses for two periods; 1984 and 2002. The selection of these two years is motivated by the time series of the drought indices shown in Figs. 3 and 5. The results presented in this section refer to composite fields that have been detrended to remove the influence of linear trends. For ease of readability and interpretation, the outline of the study region is shown in green.

Figures 2.7–2.9 show the anomaly maps of precipitable water content *W* in the atmospheric column superposed on wind at 925-hPa (Fig. 2.7), 500-hPa geopotential height Z500 and wind at 500-hPa (Fig. 2.8), and a vertical cross sections outlining the vertical velocity field ω with meridional wind (Fig. 2.9). Figures 2.7a and 2.7b, 2.8a and 2.8b, and 2.9a and 2.9b are the composites of widespread droughts and pluvials, while the spatial patterns of the 2002 drought and 1984 pluvial are shown in Figs. 2.7c and 2.7d, 2.8c and 2.8d, and 2.9c and 2.9d.

The result shows that drought events (Fig. 2.7a) are associated with anomalous negative W in the atmospheric column over the Pacific Ocean with an extension over the basin. The low level circulation shows a band of weaker anticyclonic circulation between 30 °N and 40 °N. The reduced strength of the westerlies thus act to promote dryness over the region. The reduced W content in the atmospheric column over UCRB is associated with enhanced Z500 (Fig. 2.8a). Overall, the CONUS region is dominated by a ridge with positive Z500 anomalies. The maximum height anomaly is located over the western United States, encompassing the UCRB. Thus, the dry conditions coupled with warmer than normal climate over the region are directly associated with this positive height anomaly, consistent with

previous studies (Schubert et al. 2004). The anomalies of enhanced easterly wind vectors over the region are linked with negative W anomaly, and this suggests the presence of mid-tropospheric subsidence air over the region, which acts to promote the dryness. This feature is supported by the latitude-height analysis of ω displayed in Figure 2.9a. The figure showed the pattern of ω and wind spatially averaged over the longitudinal extent of UCRB (Fig. 2.1). It is seen that, while the northern part of the basin is characterized by shallow ascent below the 500-hPa level, the entire basin is dominated by anomalous positive omega vertical velocity (descent) with the core axis extending over a wider atmospheric levels.

The widespread pluvial events (Figures 2.7b, 2.8b, and 2.9b) over the UCRB exhibit large-scale atmospheric circulation patterns that are different from, but not mirror images of, the anomalous behavior of the widespread drought events. Figure 2.7b displays the spatial distribution of W anomaly during widespread pluvial events. This figure features a northeast-southwest oriented positive W anomaly that extend eastwards from the eastern tropical Pacific Ocean over the basin, with two maxima; one over the Oceanic area and the other over the inland area. This core, over the Pacific Ocean acts as the source of moisture transport from the Gulf of California to inland regions, while the inland core acts as the sink. The strong southwesterly wind anomaly with circulations over the basin indicate the transport of moisture over the basin. In contrary to Figure 2.8a, the Z500 during widespread pluvial events (Fig. 2.8b) shows a height anomaly pattern that is oriented northwest to southeast. The core of the anomalous height is seen over the basin. The positive W and negative Z500 anomalies are associated with deeper and enhanced cyclonic anomaly at 500-hPa level. The enhanced low-level and mid-tropospheric winds indicate the presence of stronger ascent

through the depth of the atmosphere over the region. In fact, Fig. 2.9b lends support to these analyses, where enhanced ascending motion is the dominant feature over the basin.

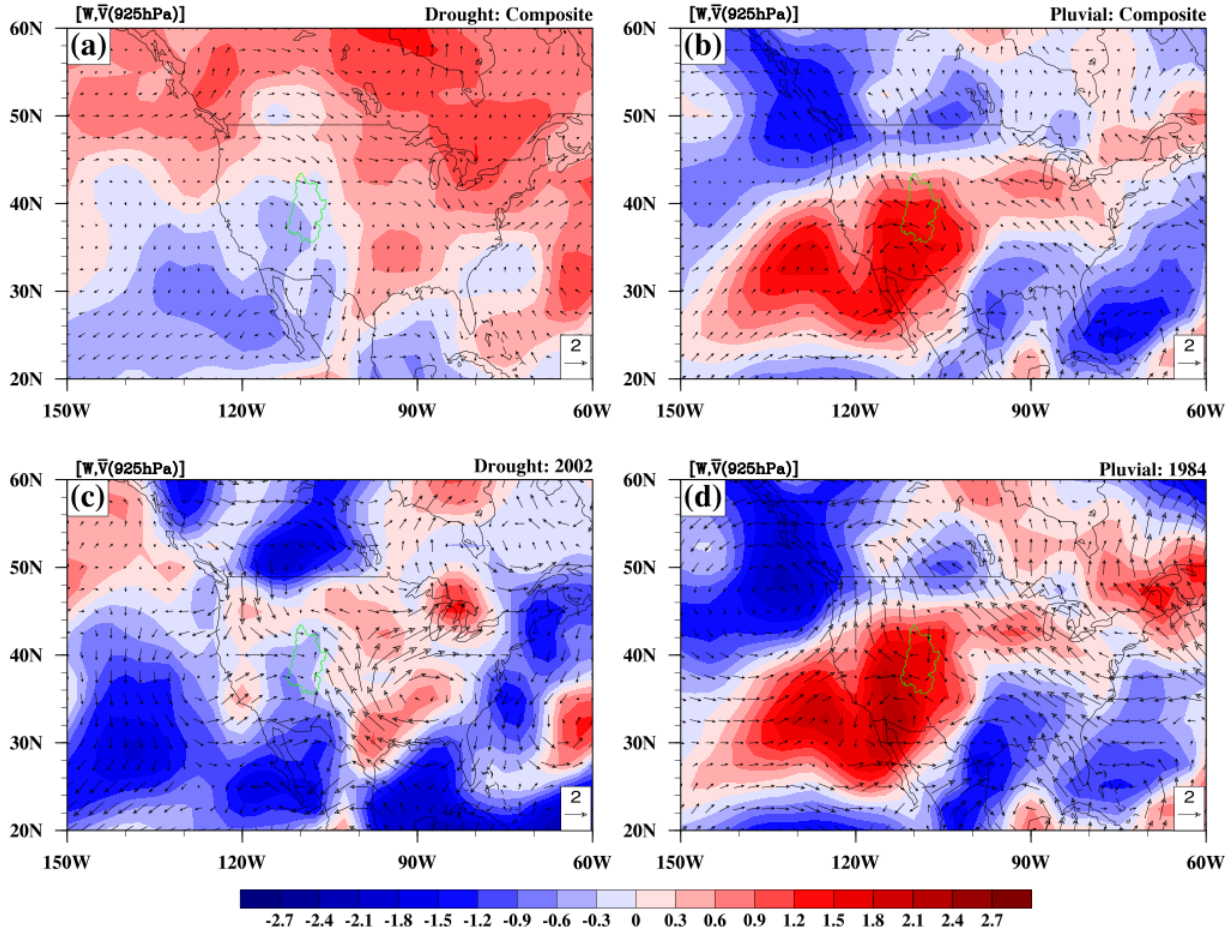

Figure 2.7 Composite mean standardized anomaly of *W* superimposed with 925-hPa wind vector during widespread (a) drought and (b) pluvial events and mean standardized anomaly of *W* superimposed with 925-hPa wind vector for (c) 2002 drought and (d) 1984 pluvial from SPEI at the 36-month time scale over UCRB. The shading interval is 0.3σ, where σ is std dev.

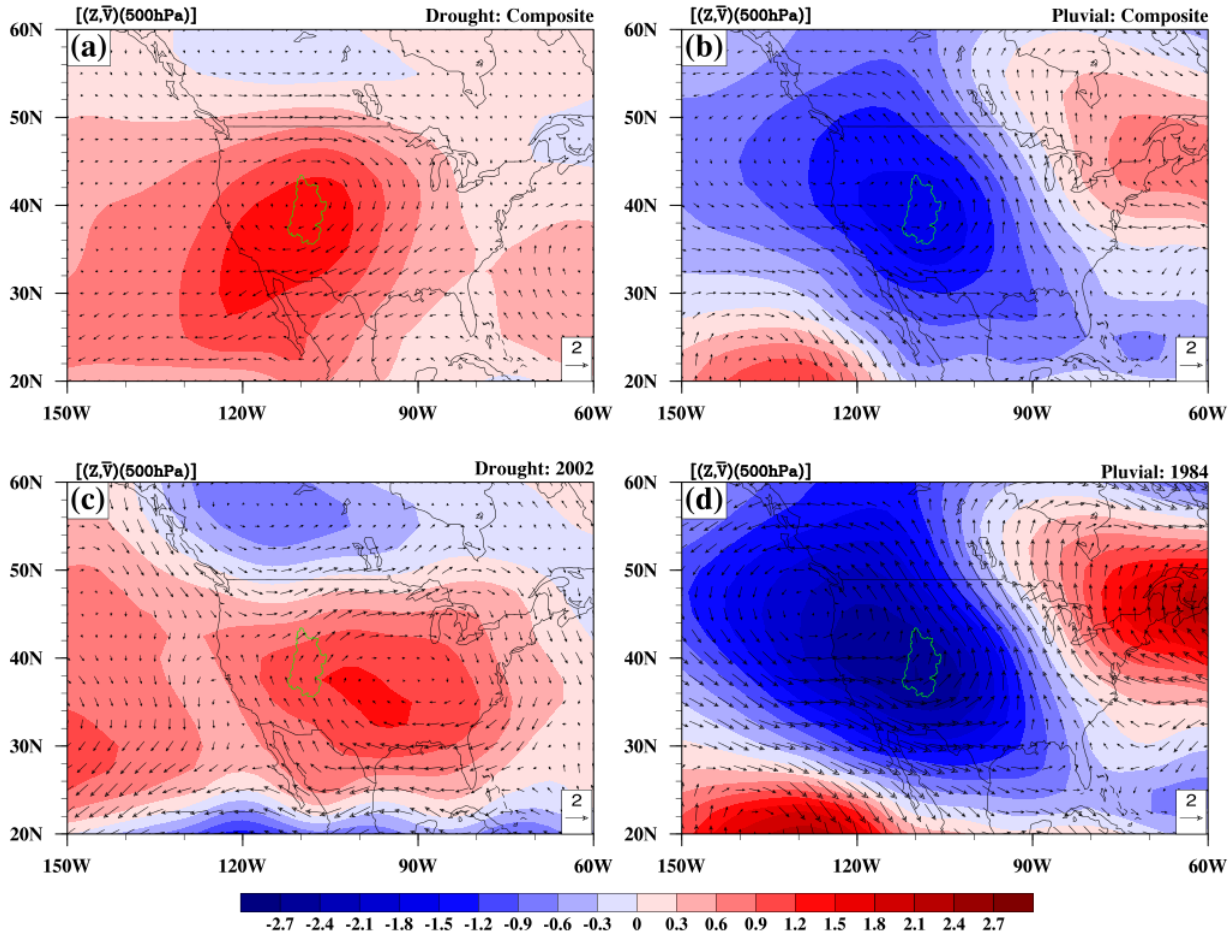

Figure 2.8 Composite mean standardized anomaly of Z500 superimposed with 500-hPa wind vector during widespread (a) drought and (b) pluvial events and mean standardized anomaly of Z500 superimposed with 500-hPa wind vector for (c) 2002 drought and (d) 1984 pluvial from SPEI at the 36-month time scale over UCRB. The shading interval is 0.3σ.

The composites of normalized large-scale atmospheric anomaly fields during widespread drought and pluvial events derived from SPEI36 over UCRB show patterns that are spatially dissimilar. These result indicate, to a first approximation, that drought and pluvial events are

not simply mirror images of each other and that they are modulated by different large-scale features. This is further confirmed by the spatial distributions during two specific periods with opposing events (Figures 2.7c,d; 2.8c,d; 2.9c,d) over the region. Differences occur in spatial distributions of W and wind vectors between Fig. 2.7c (a component of Fig. 2.7a) and Fig. 2.7a. Analysis of individual drought events (figures not shown) that made up Fig. 2.7a indicates that drought episodes over UCRB are associated with large-scale features of different magnitudes and patterns in W and 925-hPa wind vectors. By and large, there tends to be an easterly wind component during drought (e.g., Fig. 2.10). Further study on pattern classification of features linked with drought episodes over the region will contribute to knowledge on drought events over the region.

The results presented above indicate differences in moisture availability during widespread drought and pluvial events over UCRB. So, in order to further differentiate between drought and pluvial characteristics, and also to put into perspective the large-scale anomaly associated with extremes over the UCRB, we analyze the moisture transport and its convergence over the region. Since the divergence of the vertically integrated moisture flux is readily available from ERA-I dataset, we multiply this field by minus 1 to obtain moisture convergence. The NCEP-NCAR reanalysis is too coarse to resolve well this field for the UCRB. Figure 2.10 shows the anomalies of vertically integrated moisture convergence and the moisture flux vector during extreme events over UCRB. Consistent with the anomalous positive Z500 (Fig. 2.8a) and omega vertical velocity (Fig. 2.9a), the enhanced easterly moisture flux during drought conditions is linked with anomalous negative moisture convergence (Fig. 2.10a), with maximum anomalies over the eastern half of the basin. There

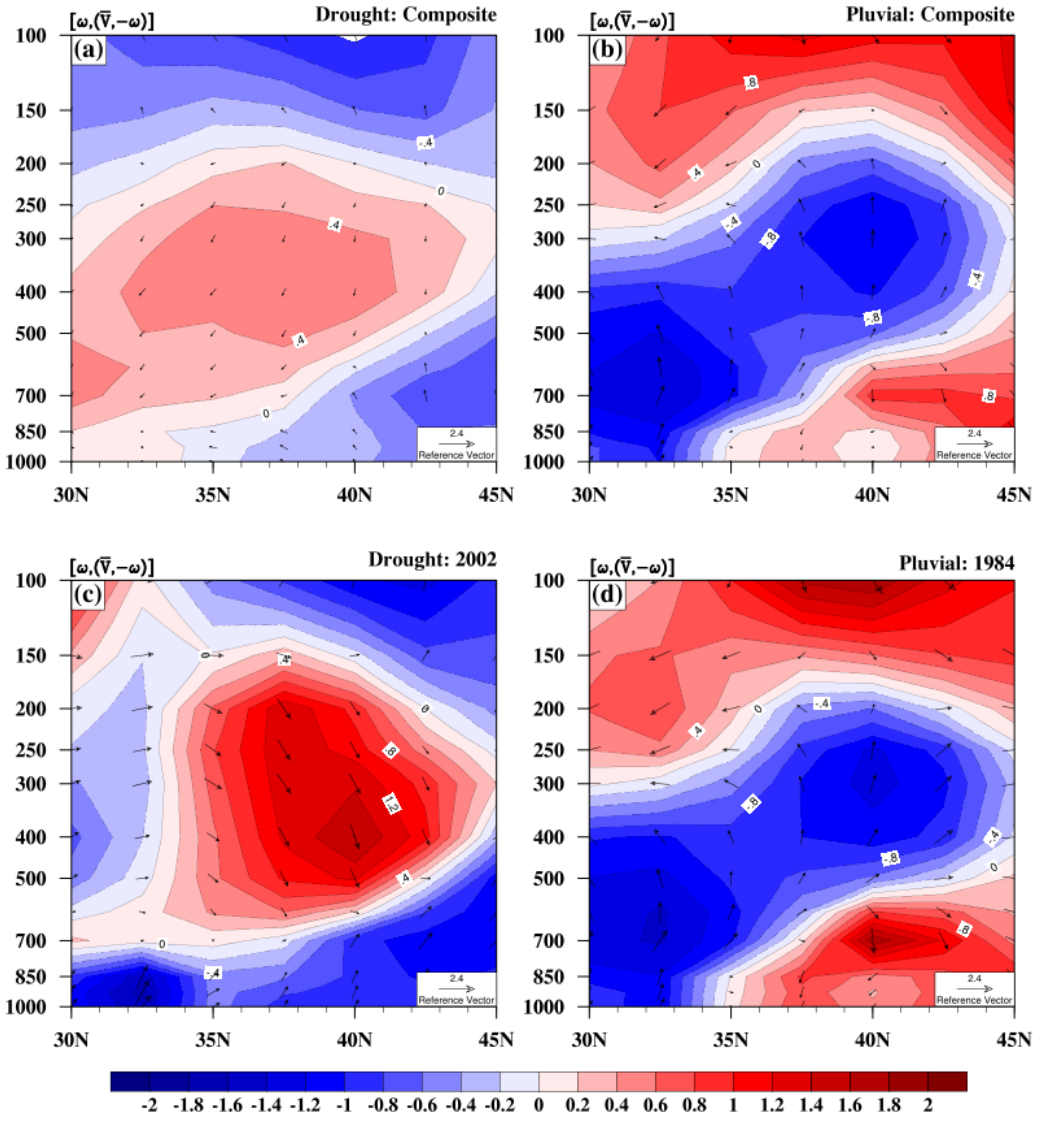

Figure 2.9 Vertical structure of composite mean standardized anomaly of ω and wind vector (v, -ω) averaged between the longitudinal length of UCRB during widespread (a) drought and (b) pluvial events and mean standardized anomaly of ω and wind vector (v, -ω) for (c) 2002 drought and (d) 1984 pluvial from SPEI at the 36-month time scale over UCRB. The shading interval is 0.2σ.

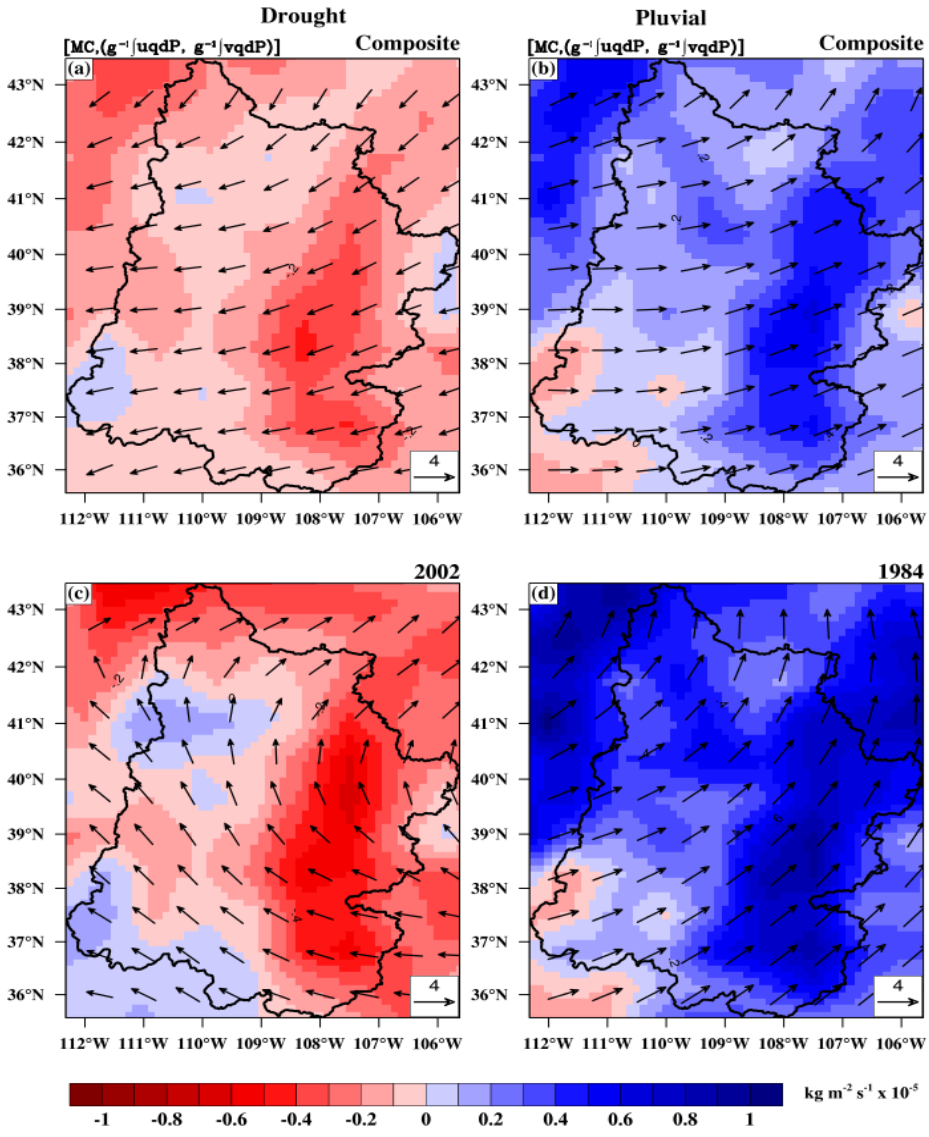

Figure 2.10 Composite mean anomaly of moisture convergence (MC) superimposed with vertically integrated moisture flux anomaly (arrows) during widespread (a) drought and (b) pluvial events and mean anomaly of MC superimposed with vertically integrated moisture flux for (c) 2002 drought and (d) 1984 pluvial from SPEI at the 36-month time scale over UCRB. The climate variables are from ERA-Interim dataset.

appears to be an interplay between these large-scale fields, as the enhanced sinking motions in anomalous positive Z500 results in enhanced moisture divergence. In addition, the enhanced easterlies here seem to suppress the moisture-bearing westerlies over the Ocean and thus act to promote a drought-conducive environment over the river basin. In contrast, for pluvial events, Fig. 2.10b displays different patterns compared to the drought events. For the pluvial events, the enhanced westerly moisture flux is associated with increased moisture convergence, consistent with the enhanced rising motion (Fig. 2.9b) associated with anomalous negative Z500 (Fig. 2.8b) over the basin area. The persistent rising motion coupled with abundant precipitable water in the atmospheric column and enhanced westerlies promoting orographic precipitation favors the conversion of atmospheric moisture into clouds and precipitation (Liu et al. 2004). Thus, the interplay between these fields in the atmospheric column over UCRB acts to promote the moisture convergence during widespread pluvial events. Overall, this pattern indicates an enhancement above the long-term mean of moisture transport from the Gulf of California and from the Gulf of Mexico. Similar large-scale environmental features displayed during 2002 drought and 1984 pluvial in comparison with the composite patterns during all drought and pluvial events, respectively suggest that extreme events over UCRB are associated with anomalous negative moisture convergence (droughts) and anomalous positive moisture convergence (pluvials) concomitant with other interrelated anomalies of large-scale atmospheric fields.

All the figures presented in previous sections indicate the links between hydroclimatic variables and drought indicators. Also, the results show the relationships between extremes and large-scale atmospheric features over UCRB. The patterns indicate that there is a

difference in the physical mechanisms responsible for widespread droughts and pluvials over UCRB during the period of study.

4. Conclusions

This study focused on diagnosing characteristics of multi-year droughts and pluvials over the upper Colorado River basin (UCRB), using two drought indicators. We examined and compared the temporal and spatial patterns of droughts and pluvials depicted by SPEI and SPI at the 36-month timescale. We chose this longer time scale because Denver Water managers are interested in persistent, multi-year droughts for planning water management. Shorter anomalies can be managed with the existing reservoirs and other infrastructure. The data used for this study included monthly mean maximum temperature, minimum temperature, and precipitation from the PRISM datasets for the period 1948–2012. The streamflow data came from the archive of the United States Geological Survey National Water Information System. The two drought/pluvial indices (SPEI36 and SPI36), were calculated using monthly mean maximum temperature and precipitation from the PRISM datasets. The study also examined large-scale physical processes associated with widespread droughts and pluvials over UCRB using NCEP–NCAR reanalysis for 1948–2012 and ERA-I reanalysis for 1979–2012.

The results of our analyses can be summarized as follows:

- There has been a marked warming with increased potential evapotranspiration and decreased precipitation leading to widespread droughts.

- Clusters of warm anomalies in T36 coupled with positive anomalies of PET36 and negative anomalies of P36 coincide with periods of severe to extreme droughts, while periods of severe to extreme pluvials are associated with cool anomalies in T36 in conjunction with negative anomalies of PET36 and positive anomalies of P36. Clusters of warm and cool anomalies in T36 coupled with positive (negative) and negative (positive) anomalies of PET36 (P36) coincide with periods of severe to extreme droughts and pluvials.
- SPEI36 and SPI36 exhibit similar temporal evolution, but the SPEI36 variations are greater than SPI36 variations. Also the magnitude of the trend in SPEI36 is greater than that of SPI36 during the two sub-periods of 1950–1980 and 1981–2012.
- The SPEI36 shows a higher percentage of area in drought or pluvial conditions in comparison with SPI36. According to the SPEI36, the largest area affected by moderate, severe, and extreme droughts occurred in 2004, 2003 and 1956. The year 1999 marked the period with the highest percent area of UCRB in moderate wet conditions, while severe and extreme wet conditions occurred especially in 1984.
- Reduced precipitable water anomaly coupled with easterly wind anomalies are associated with widespread droughts, while enhanced positive anomaly of precipitable water and associated strong westerly wind anomalies are linked with widespread pluvials over UCRB.
- The anomalous high geopotential height field during widespread drought is linked with reduced precipitable water content in the atmospheric column over UCRB, while the deepened geopotential height anomaly over the region during widespread pluvial conditions is linked with increased precipitable water. The Pacific Ocean, the Gulf of

California, and the Gulf of Mexico are important sources of moisture transport into the region. However, the enhanced high geopotential height anomaly is responsible for blocking moisture transport from reaching the interior of the U.S. through subsidence associated with the circulation; this results in dry conditions over the region.

- Consistent with reduced precipitable water and positive height anomaly, an area of descending motion over the latitudinal extent of the basin is observed during drought conditions. In contrast, pluvial conditions over the basin occur as a result of the interplay between positive precipitable water content, low height anomalies, and sustained rising motions.
- Because of the links between the previously discussed large-scale fields, the moisture convergence is anomalously low during drought episodes and anomalously high during pluvial episodes.

In conclusion, the findings of this study have shown that widespread droughts (pluvials) as represented by SPI36 and SPEI36 occur in association with anomalous warm and dry (cool and wet) conditions over UCRB. The analysis further shows that droughts and pluvials are not simply mirror images of each other in their characteristics, so that one is not simply the opposite phase of the other. This is particularly true of the large-scale circulation patterns associated with droughts and pluvials. Furthermore, the results of this study underline the impacts of warming on regional water balance and climates. Corroborating other studies that have shown that the frequency and severity of drought increases with rising temperature (Dai 2011; Lorenzo-Lacruz et al. 2010; Vicente-Serrano et al. 2010a), results here demonstrate

that drought indicators that incorporate the influence of temperature would be more appropriate for monitoring drought and pluvial conditions in this region. In this regard, this study indicates that SPEI as an alternative to SPI better captures and quantifies drought conditions. Thus, SPEI appears to be well suited for Denver Water to estimate streamflow, and thus is a better climate indicator for water management than precipitation-based indicators alone.

Acknowledgements

The work has been supported by the National Science Foundation through the Earth System Modeling (EaSM) Grant AGS-1243030. This work contributes tools and information to serve the needs of Denver Water resource management to identify the most applicable climate data that influence decision-making and understanding of key physical processes. We thank them for their consultation on this study. The calculations and analyses in this study have been done using the National Center for Atmospheric Research (NCAR) Command Language (NCL Version 6.3.0). We acknowledge high-performance computing support from Yellowstone (ark:/85065/d7wd3xhc) provided by NCAR's Computational and Information System Laboratory. NCAR is supported by the National Science Foundation, and managed by the University Corporation for Atmospheric Research. We also acknowledge the support of the Federal University of Technology, Akure, Nigeria, for granting study leave to the first author to pursue his Ph.D. The reviewers are also acknowledged for their comments, which helped improve the quality of the paper.

Appendix: Comparison of SPEI using different PET methods

The SPEI time series in Fig. A1 use the PET methods described in the main body of the paper, applied to the datasets discussed there, except that the SPEI data obtained from PM approach using the Climatic Research Unit dataset is from the SPEIbase v.2.4 archive (Beguería et al. 2014). The correlations between the SPEI series from the three methods are high ($r > 0.85$) and statistically significant ($p < 0.0001$) at the 5% significance level (values shown in Appendix A1: d, e, and f). Using the test statistics for difference of two means (Devore, 1995, sec. 9.1), the result indicate that there are no significant differences between the means of the SPEI series from the three methods. In fact, for most part, the difference is below 0.5. The t-test for the difference of two means for PM versus Hg is substantially higher ($t = 1.14$) than that of PM versus Th ($t = –0.24$) and Hg versus Th ($t = –1.46$). These results indicate that using PET obtained from Hg method instead of PM method will not affect the SPEI results.

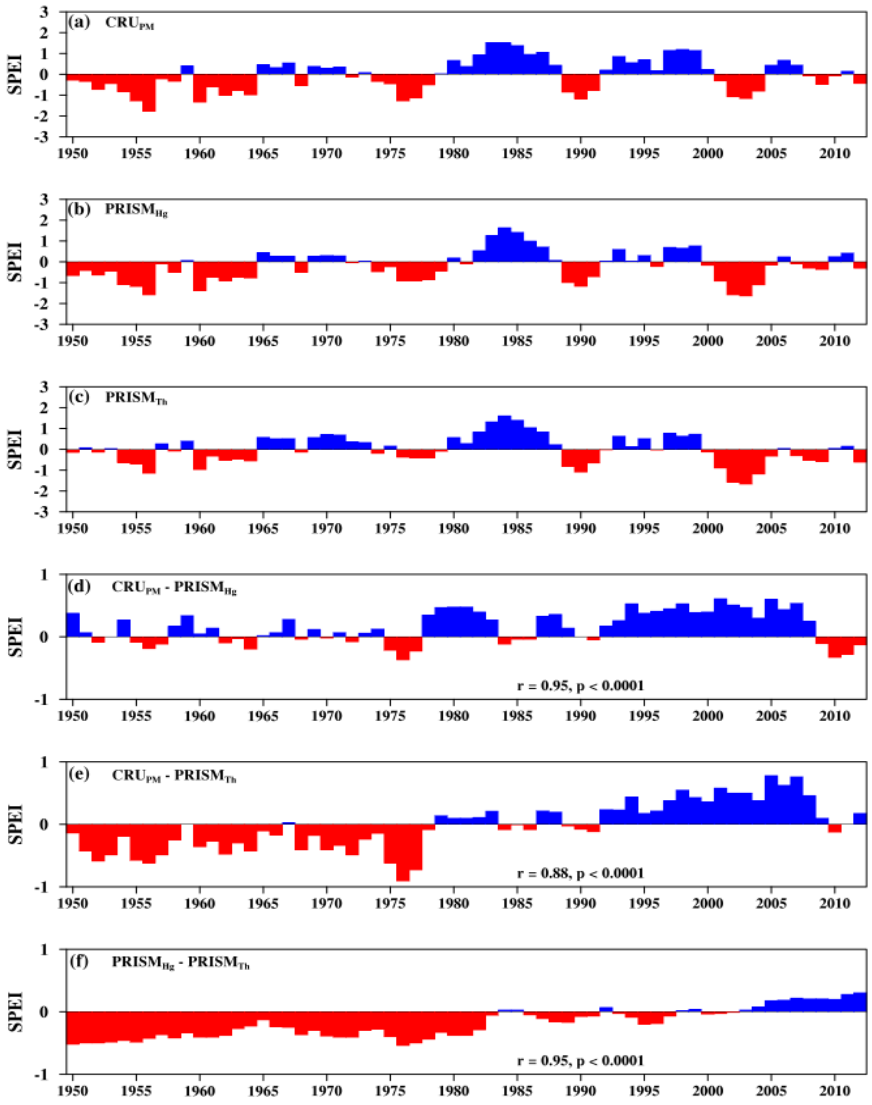

Figure 2.A1 Time series of the 36-month SPEI over UCRB obtained using (a) PM (SPEIbase v.2.4 data available online at http://digital.csic.es/handle/10261-/128892), (b) Hg, and (c) Th PET methods. The differences between the SPEI evolution from the three methods are shown in the lower three panels: (d) CRU_{PM} – $PRISM_{Hg}$, (e) CRU_{PM} – $PRISM_{Th}$, and (f) $PRISM_{Hg}$ – $PRISM_{Th}$. The correlation coefficients and the statistical significance value between one method vs the other is indicated in the lower three plots.

References

Andreadis, K. M., E. A. Clark, A. W. Wood, A. F. Hamlet, and D. P. Lettenmaier, 2005: Twentieth-century drought in the conterminous United States. *J. Hydrometeor.*, **6,** 985–1001, doi:10.1175/JHM450.1.

Barnett, T. P., and D. W. Pierce, 2008: When will Lake Mead go dry? *Water Resour. Res.*, **44,** W03201, doi:10.1029/2007WR006704.

Barry, R. G., 1992: *Mountain weather and climate*. Routledge, 402 pp.

Beguería, S., and S. M. Vicente-Serrano, 2013: Calculation of the standardised precipitation-evapotranspiration index (SPEI). R Project, 16 pp. [Available online at http://cran.r-project.org/web/packages /SPEI/SPEI.pdf.]

——, ——, F. Fergus, and B. Latorre, 2014: Standardized precipitation evapotranspiration index (SPEI) revisited: parameter fitting, evapotranspiration models, tools, datasets and drought monitoring. *Int. J. Climatol*. **34,** 3001–3023, doi:10.1002/joc.3887.

Bryant, E., 2005: *Natural Hazards*. 2nd edd.Cambridge University Press, 312 pp.

Bureau of Reclamation, 2012: Colorado River basin water supply and demand study: Executive summary. USBR Rep., 28 pp. [Available online at https://www.usbr.gov/lc/region/programs/crbstudy/finalreport/.]

Chen, T., G. R. van der Werf, R. A. M. de Jeu, G. Wang, and A. J. Dolman, 2013: A global analysis of the impact of drought on net primary productivity. *Hydrol. Earth Syst. Sci.*, **17,** 3885–3894, doi:10.5194/hess-17-3885-2013.

Christensen, N. S., and D. P. Lettenmaier, 2007: A multimodel ensemble approach to assessment of climate change impacts on the hydrology and water resources of the

Colorado River Basin. *Hydrol. Earth System Sci.*, **11,** 1417–1435, doi:10.5194/hess-11-1417-2007.

——, A. W. Woods, N. Voisin, D. P. Lettenmaier, and R. N. Palmer, 2004: The effects of climate change on the hydrology and water resources of the Colorado River Basin. *Climatic Change*, **62,** 337–363, doi:10.1023/B:CLIM.0000013684.13621.1f.

Cook, B. I., J. E. Smerdon, R. Seager, and S. Coats, 2014: Global warming and 21st century drying. *Climate Dyn.*, **43**, 2607–2627, doi:10.1007/s00382-014-2075-y.

Cook, E. R., C. A. Woodhouse, C. M. Eakin, D. M. Meko, and D. W. Stahle, 2004: Long-term aridity changes in the western United States. *Science*, **306**, 1015–1018, doi:10.1126/science.1102586.

Dai, A., 2011: Drought under global warming: A review. *Wiley Interdiscip. Rev.*: *Climate Change*, **2,** 45–65, doi:10.1002/wcc.81.

——, K. E. Trenberth, and T. Qian, 2004: A Global Dataset of Palmer Drought Severity Index for 1870–2002: Relationship with soil moisture and effects of surface warming. *J. Hydrometeor.*, **5,** 1117–1130, doi:10.1175/JHM-386.1.

Daly, C., R. P. Neilson, and D. L. Phillips, 1994: A statistical–topographic model for mapping climatological precipitation over mountainous terrain. *J. Appl. Meteor.*, **33,** 140–158, doi:10.1175/1520-0450(1994)033<0140:ASTMFM>2.0.CO;2.

——, M. Halbleib, J. I. Smith, W. P. Gibson, M. K. Doggett, G. H. Taylor, J. Curtis, and P. P. Pasteris, 2008: Physiographically sensitive mapping of temperature and precipitation across the conterminous United States. *Int. J. Climatol*., **28,** 2031–2064, doi:10.1002/joc.1688.

Dawadi, S., and S. Ahmad, 2012: Changing climatic conditions in the Colorado River basin: Implications for water resources management. *J. Hydrol.*, **430–431**, 127–141, doi:10.1016/j.jhydrol.2012.02.010.

Dee, D., and Coauthors, 2011: The ERA-Interim reanalysis: Configuration and performance of the data assimilation system. *Quart. J. Roy. Meteor. Soc*., **137,** 553–597, doi: 10.1002/qj.828.

Devore, J. L., 1995: *Probability and Statistics for Engineering and the Sciences*. 4th ed. Wadsworth Publishing Company, 741 pp.

Droogers, P., and R. G. Allen, 2002: Estimating reference evapotranspiration under inaccurate data conditions. *Irrig. Drain. Syst.* **16**: 33–45, doi:10.1023/A:1015508322413.

Gleason, K. L., J. H. Lawrimore, D. H. Levinson, and T. R. Karl, 2008: A revised U.S. climate extremes index. *J. Climate,* **21,** 2124–2137, doi:10.1175/2007JCLI1883.1.

Grumm, R. H., and R. Hart, 2001: Standardized anomalies applied to significant cold season weather events: Preliminary findings. *Wea., Forecasting,* **16,** 736–754, doi:10.1175/1520-0434(2001)016<0736:SAATSC>2.0.CO;2.

Guttman, N. B., 1998: Comparing the Palmer drought index and the standardized precipitation index. *J. Amer. Water Resources Assoc*., **34,** 113–121, doi:10.1111/j.1752-1688.1998.tb05964.x.

——, 1999: Accepting the standardized precipitation index: A calculation algorithm. *J. Amer. Water Resources Assoc*., **35,** 311–322, doi:10.1111/j.1752-1688.1999.tb03592.x.

Hamed, K. H., and A. R. Rao, 1998: A modified Mann-Kendall trend test for autocorrelated data. *J. Hydrol.* **204,** 182–196, doi:10.1016/S0022-1694(97)00125-X.

Hargreaves, G. L., and Z. A. Samani, 1985: Reference crop evapotranspiration from temperature. *Appl. Eng. Agric.*, **1**, 96–99, doi:10.13031/2013.26773.

Hart, R., and R. H. Grumm, 2001: Using normalized climatological anomalies to rank synoptic-scale events objectively. *Mon. Wea. Rev.*, **129,** 2426–2442, doi:10.1175/1520-0493(2001)129<2426:UNCATR>2.0.CO;2.

Hayes, M. J., M. D. Svoboda, D. A. Wilhite, and O. V. Vanyarkho, 1999: Monitoring the 1996 drought using the Standardized Precipitation Index. *Bull. Amer. Meteor. Soc*., **80,** 429–438, doi:10.1175/1520-0477(1999)080<0429:MTDUTS>2.0.CO;2.

Hidalgo, G. H., 2004: Climate precursors of multidecadal drought variability in the western United States. *Water Resour. Res.*, **40,** W12504, doi:10.1029/2004WR003350.

——, and J. A. Dracup, 2003: ENSO and PDO effects on hydroclimatic variations of the upper Colorado River basin. *J. Hydrometeor*., **4,** 5–23, doi:10.1175/1525-7541(2003)004<0005:EAPEOH>2.0.CO;2.

Hirschboeck, K., 1991: Climate and floods. National water summary 1988–89: Hydrologic events and floods and droughts, USGS Water Supply Paper 2375, 67–88. [Available online at https://pubs.er.usgs.gov/publication/wsp2375.]

Hoerling, M., X.-W. Quan, and J. Eischeid, 2009: Distinct causes for two principal U.S. droughts of the 20th century. *Geophys. Res. Lett*., **36,** L19708, doi:10.1029/2009GL039860.

Hu, Q., and G. D. Willson, 2000: Effects of temperature anomalies on the Palmer drought severity index in the central United States. *Int. J. Climatol*., **20,** 1899–1911, doi:10.1002/1097-0088(200012)20:15<1899::AID-JOC588>3.0.CO;2-M.

Hughes, P., 1976: Drought: The Land Killer: *American Weather Stories*, Environmental Data Service, 77–87.

Jensen, M. E., R. D. Burman, and R. G. Allen, Eds., 1990: *Evapotranspiration and Irrigation Water Requirements. ASCE* Manuals and Reports on Engineering Practices No. 70, ASCE, 360 pp.

Junker, N. W., R. H. Grumm, R. Hart, L. F. Bosart, K. M. Bell, and F. J. Pereira 2008: Use of normalized anomaly fields to anticipate extreme rainfall in the mountains of North California. *Wea. Forecasting*, **23,** 336–356, doi:10.1175/2007WAF2007013.1.

Kalnay, E., and Coauthors, 1996: The NCEP/NCAR 40-Year Reanalysis Project. *Bull. Amer. Meteor. Soc*., **77,** 437–471, doi:10.1175/1520-0477(1996)077<0437:TNYRP>2.0.CO;2.

Karl, T. R., 1983: Some spatial characteristics of drought duration in the United States. *J. Climate Appl. Meteor*., **22,** 1356–1366, doi:10.1175/1520-0450(1983)022<1356:SSCODD>2.0.CO;2.

——, 1986: The sensitivity of the Palmer drought severity index and the Palmer's Z-Index to their calibration coefficients including potential evapotranspiration. *J. Climate Appl. Meteor*., **25,** 77–86, doi:10.1175/1520-0450(1986)025<0077:TSOTPD>2.0.CO;2.

Kerr, R. A., 2005: Climate Change: Atlantic Climate Pacemaker for Millennia past, Decades Hence? *Science*, **309,** 41–43, doi:10.1126/science.309.5731.41.

Kingston, D. G., J. H. Stagge, L. M. Tallaksen, and D. M. Hannah, 2015: European-scale drought: Understanding connections between atmospheric circulation and

meteorological drought indices. *J. Climate*, **28**, 505–516, doi:10.1175/JCLI-D-14-00001.1.

Laird, K. R., S. C. Fritz, K. A. Maasch, and B. F. Cumming, 1996: Greater drought intensity and frequency before AD 1200 in the Northern Great Plains, USA. *Nature,* **384,** 552–554, doi:10.1038/384552a0.

Landsberg, H. E., 1982: Climatic aspects of droughts. *Bull. Amer. Meteor. Soc*., **63**, 593–596, doi:10.1175/1520-0477(1982)063<0593:CAOD>2.0.CO;2.

Liu, J., R. E. Stewart, and K. K. Szeto, 2004: Moisture transport and other hydrometeorological features associated with the severe 2000/01 drought over the western and central Canadian Prairies. *J. Climate*, **17**, 305–319, doi:10.1175/1520-0442(2004)017<0305:MTAOHF>2.0.CO;2.

Lloyd-Hughes B., and M. A. Saunders, 2002: A drought climatology for Europe. *Int. J. Climatol.,* **22,** 1571–1592, doi:10.1002/joc.846.

Lorenzo-Lacruz, J., S. M. Vicente-Serrano, J. I. López-Moreno, S. Beguería, J. M. García-Ruiz, and J. M. Cuadrat, 2010: The impact of droughts and water management on various hydrological systems in the headwaters of the Tagus River (central Spain). *J. Hydrol*, **386,** 13–26, doi:10.1016 j.jhydrol.2010.01.001.

McCabe, G. J., and D. M. Wolock, 2007: Warming may create substantial water supply shortages in the Colorado River basin. *Geophys. Res*. Lett., **34,** L22708, doi: 10.1029/2007GL031764.

——, M. A. Palecki, and J. L. Betancourt, 2004: Pacific and Atlantic Ocean influences on multidecadal drought frequency in the United States. *Proc. Natl. Acad. Sci. USA*, **101**, 4136–4141, doi:10.1073/pnas.0306738101.

McKee, T. B., N. J. Doesken, and N. J. Kleist, 1993: The relationship of drought frequency and duration to time scales. Preprints, *Eighth Conf. on Applied Climatology*, Anaheim, CA, *Amer. Meteor. Soc*., 179–184.

——, ——, and ——, 1995: Drought monitoring with multiple time scales. Preprints, *Ninth Conf. on Applied Climatology*, Dallas, TX, Amer. Meteor. Soc., 233–236.

Meko, D. M., C. A. Woodhouse, C. A. Baisan, T. Knight, J. J. Lukas, M. K. Hughes, and M. W. Salzer, 2007: Medieval drought in the upper Colorado River Basin. *Geophys. Res*. Lett., **34,** L10705, doi:10.1029/2007GL029988.

Mencken, H. L., 1979: *The American Language.* One-Volume Abridged ed., Knopf, 206 pp.

Monteith, J. L., 1965: Evaporation and environment. *Sympos. Soc. Exp. Biol*. **19,** 205–234.

Nowak, K., M. Hoerling, B. Rajagopalan, and E. Zagona 2012: Colorado River basin hydroclimatic variability. *J. Climate*, **25**, 4389–4403, doi:10.1175/JCLI-D-11-00406.1.

Palmer, W. C., 1965: Meteorological drought. U.S. Weather Bureau Research Paper 45, 58 pp. [Available online at http://www.ncdc.noaa.gov/temp-and-precip/drought/docs/palmer.pdf.]

Pitlick, J., 1994: Relation between peak flows, precipitation, and physiography for five mountainous regions in the western USA. *J. Hydrol.*, **158,** 219–240, doi:10.1016/0022-1694(94)90055-8.

Schubert, S. D., M. J. Suarez, P. J Pegion, R. D. Koster, and J. T. Bacmeister, 2004: Causes of long-term drought in the U.S. Great Plains. *J. Climate*, **17,** 485–503, doi:10.1175/1520-0442(2004)017<0485:COLDIT>2.0.CO;2.

——, and Coauthors, 2009: A U.S. CLIVAR project to assess and compare the responses of global climate models to drought-related SST forcing patterns: Overview and results. *J. Climate*, **22,** 5251–5272, doi:10.1175/2009JCLI3060.1.

Seager, R., Y. Kushnir, C. Herweijer, N. Naik, and J. Velez, 2005: Modeling the tropical forcing of persistent droughts and pluvials over western North America: 1856–2000. *J Climate*, **18,** 4065 – 4091, doi:10.1175/JCLI3522.1.

——, ——, M. Ting, M. Cane, N. Naik, and J. Miller, 2008: Would advance knowledge of 1930s SSTs have allowed prediction of the Dust Bowl drought? *J. Climate*, **21,** 3261–3281, doi:10.1175/2007JCLI2134.1.

Sheffield, J., E. F. Wood, and M. Roderick, 2012: Little change in global drought over the past 60 years. *Nature*, **491**, 435–438, doi:10.1038/nature11575.

Stagge, J. H., L. M. Tallaksen, C-Y. Xu, and H. A. J. Van Lanen, 2014: Standardized precipitation-evapotranspiration index (SPEI): Sensitivity to potential evapotranspiration model and parameters. *IAHS Publ.*, **363,** 367–373.

Sutton, R. T., and D. L. R. Hodson, 2005: Atlantic Ocean forcing of North American and European summer climate. *Science*, **309,** 115–118, doi:10.1126/science.1109496.

Thornthwaite, C. W., 1948: An approach toward a rational classification of climate. *Geogr. Rev.*, **38**, 55–94 doi:10.2307/210739.

van der Schrier, G., P. D. Jones, and K. R. Briffa, 2011: The sensitivity of the PDSI to the Thornthwaite and Penman-Monteith parameterizations for potential evapotranspiration. *J. Geophys. Res.,* **116**: D03106, doi:10.1029/2010JD015001.

Van Loon, A. F., E. Tijdeman, N. Wanders, H. A. J. Van Lanen, A. J. Teuling, and R. Uijlenhoet, 2014: How climate seasonality modifies drought duration and deficit. *J. Geophys. Res. Atmos.,* **119,** 4640–4656, doi:10.1002/2013JD020383.

Vano, J. A., B. Udall, D. R. Cayan, J. T. Overpeck, L. D. Brekke, T. Das, H. C. Hartmann, H. G. Hidalgo, M. Hoerling, G. J. McCabe, K. Morino, R. S. Webb, K. Werner, and D. P. Lettenmaier, 2014: Understanding uncertainties in future Colorado River streamflow. *Bull. Amer. Meteor. Soc*., **95**, 59–78, doi:10.1175/BAMS-D-12-00228.1.

Vicente-Serrano, S. M., S. Beguería, and J. I. López-Moreno, 2010a: A multiscalar drought index sensitive to global warming: The Standardized Precipitation Evapotranspiration Index. *J. Climate*, **23,** 1696–1718, doi:10.1175/2009JCLI2909.1.

——, ——, ——, M. Angulo, and A. EL Kenawy, 2010b: A new global 0.5º gridded dataset (1901–2006) of a multiscalar drought index: Comparison with current drought index datasets based on the Palmer Drought Severity Index. *Amer. Meteor. Soc.,* **11,** 1033–1043, doi:10.1175/2010JHM1224.1.

Vidal, J.-P., E. Martin, L. Franchistéguy, F. Habets, J.-M. Soubeyroux, M. Blanchard, and M. Baillon, 2010: Multilevel and multiscale drought reanalysis over France with the Safran-Isba-Modcou hydrometeorological suite. *Hydro. Earth Syst. Sci.,* **14,** 459–478, doi:10.5194/hess-14-459-2010.

Vörösmarty, C. J., C. A. Federer, and A. L. Schloss, 1998: Potential evaporation functions compared on US watersheds: Possible implications for global-scale water balance and terrestrial ecosystem modeling. *J. Hydrol.*, **207**, 147–169, doi:10.1016/S0022-1694(98)00109-7.

Wilhite, D. A., 1993: *Drought Assessment, Management, and Planning*: *Theory and Case Studies*. Natural Resource Management and Policy Series, Vol. 2, Kluwer, 293 pp.

——, 2000: Drought as a natural hazard: Concepts and definitions. *Drought: A Global Assessment,* Vol. 1, D. A. Wilhite, Ed., Routledge, 3–18.

——, 2002: Combating drought through preparedness. *Nat. Resour. Forum*, **26**, 275–285, doi:10.1111/1477-8947.00030.

——, and M. Buchanan, 2005: Drought as hazard: Understanding the natural and social context. *Drought and Water Crisis: Science, Technology, and Management Issues*, D. A. Wilhite, Ed., CRC Press, 3–29.

WMO, 2006: Drought monitoring and early warning: Concepts, progress and future challenges. WMO 1006, 24 pp. [Available online at http://www.wamis.org/agm/pubs/brochures/WMO1006e.pdf.]

Woodhouse, C. A., and J. T. Overpeck, 1998: 2000 years of drought variability in the central United States. *Bull. Amer. Meteor. Soc*., **79,** 2693–2714, doi:10.1175/1520-0477(1998)079<2693:YODVIT>2.0.CO;2.

——, G. T. Pederson, K. Morino, S. A. McAfee, and G. J. McCabe, 2016: Increasing influence of air temperature on upper Colorado River streamflow. *Geophys. Res*. Lett., **43,** 2174–2181, doi: 10.1002/2015GL067613.

Yu, M., Q. Li, M. J. Hayes, M. D. Svoboda, and R. R. Heim, 2014: Are droughts becoming more frequent or severe in China based on the Standardized Precipitation Evapotranspiration Index: 1951–2010? *Int. J. Climatol.*, **34,** 545–558, doi:10.1002/joc.3701.

Yurekli, K., and A. S. Anli, 2008: Analyzing drought based on annual total rainfalls over Tokat province. *Int. J. Nat. Eng. Sci*., **2** (2)**,** 21–26.

CHAPTER 3. STATISTICS OF MULTI-YEAR DROUGHTS FROM THE METHOD FOR OBJECT-BASED DIAGNOSTIC EVALUATION (MODE)

A paper submitted to

The International Journal of Climatology

Abayomi A. Abatan[5,1,*], William J. Gutowski, Jr.[1], Caspar M. Ammann[2], Laurna Kaatz[3], Barbara G. Brown[2], Lawrence Buja[2], Randy Bullock[2], Tressa Fowler[2], Eric Gilleland[2] and John Halley Gotway[2]

[1]Department of Geological and Atmospheric Sciences, Iowa State University, Ames, Iowa USA
[2]Research Applications Laboratory, National Center for Atmospheric Research, Boulder, Colorado USA
[3]Denver Water, Denver, Colorado USA
[*]Department of Meteorology and Climate Science, Federal University of Technology, Akure, Nigeria

Abstract

This study uses the Method for Object-based Diagnostic Evaluation (MODE) technique to examine and compare the statistics of drought attributes over the upper Colorado River basin (UCRB). The drought objects are based on the standardized precipitation index (SPI) and the standardized precipitation evapotranspiration index (SPEI) on a 36-month timescale

[5]Corresponding author address: Abayomi A. Abatan, 3134 Agronomy Hall, Department of Geological and Atmospheric Sciences, Iowa State University, Ames, Iowa 50011 USA.

E-mail address: abatanaa@iastate.edu yomiabatan69@gmail.com

(SPI36 and SPEI36, respectively). The drought indicators are calculated using monthly precipitation as well as minimum and maximum temperatures from the Precipitation-Elevation Regression on Independent Slopes Model datasets from 1948 to 2012. MODE uses paired object attributes such as centroid distance, orientation angle, area ratio, and intersection area and a combination of parameter thresholds to determine the number of objects identified and retained in the merging and matching process in the two fields. Using MODE run with convolution radius of 0 (no smoothing) and an area threshold of 4 grid points, this study computes and analyzes object statistics including centroid locations, areas and intensity percentiles. Results of the analysis show that SPI36 produces more drought objects than SPEI36, although the spatial patterns are roughly similar leading up to almost similar statistics of object attributes, such as locations of the object centroids. The largest difference between SPEI36 and SPI36 occurs for the area of the drought objects. This contrast is obvious during the early 2000s when the region experienced multi-year drought resulting from increased warming of the atmosphere. This study demonstrates the use of MODE as a tool to evaluate and monitor drought event over the UCRB.

Keywords: MODE, SPEI, SPI, Drought objects, Pluvial objects, UCRB, Denver Water

1. Introduction

Droughts and pluvials are at the heart of many research studies because of their profound impact on water supplies (e.g., McCabe et al. 2004; Seager et al. 2008; Schubert et al. 2009; Cook et al. 2014a, 2014b). Recently, the potential changes in frequency, duration, magnitude

and impacts of such events over the coming decades have gained attention (Meehl et al. 2000; Cook et al. 2015). Droughts and pluvials are opposing events that historically have had significant economic impact on various sectors including agriculture and water resources management. This makes them events of interest to a major water utility in our region of study, Denver Water. For example, the U.S. Department of the Interior Bureau of Reclamation reported that "*Since 2000, the Colorado River Basin has been experiencing a historic, extended drought that has impacted regional water supply and other resources, such as hydropower, recreation, and ecologic services*". Reservoir storage in Lake Mead and Lake Powell has declined since the beginning of this persistent drought. Recently, Burgman and Jang (2015) estimated that drought-related agricultural loss in 2012 was worth tens of billions of U.S. dollars. Matthai (1969) reported that the 1965 flood on many streams in the South Platte River basin, resulting from three days of intense rains, caused damage worth US$508.2 million, with 75% of the losses recorded in the Denver metropolitan area. The 1976 catastrophic flash flood along the Big Thompson River left 139 dead, with an estimated property damage of US$35 million (Jarrett, 1990) while the historic Boulder flood of 9 – 15 September 2013 resulted in disaster emergencies being declared in 14 counties. These events can play an important role in depleting and polluting water systems and can lead to water shortages for both human consumption and agricultural purposes. Because of the potential impacts on ecosystems, humans, and animals, there is a great need for further understanding of the spatial characteristics of these extreme events.

Drought is complex in nature and it can be defined in different ways: agricultural, hydrological, meteorological, and socioeconomic (American Meteorological Society 1997; Dracup et al. 1980; Trenberth et al. 2007). The complexity of this extreme has resulted in its

monitoring and characterization using different indices. This study builds on our previous work (Abatan et al. 2017) that used the standardized precipitation index (SPI; McKee et al. 1993; Guttman, 1998) and standardized precipitation evapotranspiration index (SPEI; Vicente-Serrano et al. 2010) to examine extended droughts and their associated physical processes for a multi-decadal period (36-month) in the upper Colorado River basin (UCRB). We use the SPI and SPEI because of their simplicity, widespread application, and endorsement by the World Meteorological Organization (WMO, 2006) and the research community as an important tool to monitor drought at different time scales and locations.

Previous drought assessments have typically relied on traditional verification metrics based on contingency tables and/or various forms of subjective visual evaluations. Often, these techniques can be misleading (Ahijevych et al. 2009), and they may not provide much information that is of interest to users (Davis et al. 2006a). The inherent limitations associated with traditional approaches have led to the development of novel, new spatial verification techniques, including various object-based methods (Ahijevych et al. 2009; Brown et al. 2011; Gilleland et al. 2009). Object-based techniques have obvious direct application to the study of drought and pluvial areas; these methods include the Contiguous Rain Area approach (CRA; Ebert and McBride, 2000; Ebert and Gallus 2009), the Method for Object-based Diagnostic Evaluation (MODE; Davis et al. 2006a, 2006b, 2009), and the Structure-Amplitude Location approach (SAL; Wernli et al. 2008), amongst others. The SAL approach provides information about three specific characteristics of objects but has limited ability to directly compare sets of objects (Gilleland et al. 2009). The CRA approach estimates the magnitude of forecast error associated with forecast displacements, as well as biases in overall intensity, and thus provides guidance regarding the amount of error that is

not explained by these factors (denoted pattern error in the CRA formulation). One limitation of the CRA is that objects are matched only when they are contiguous (Gallus 2010). In contrast, the MODE approach does not require matched objects to be contiguous and is able to measure and compare a wide variety of object attributes (e.g., area, location, size, shape). This method makes it possible to evaluate characteristics of matched and unmatched objects in observed and model fields that would not be considered by the CRA (Davis et al. 2006a). Moreover, MODE is highly configurable and can be set up to meet the specific interests of individual users for specific applications (Bullock et al. 2016).

MODE was specifically developed for verification of gridded forecasts (e.g., from numerical weather prediction systems) compared to gridded observations. The method has largely been used to verify the forecasts of rainfall fields (e.g., Davis et al. 2006a, 2006b; Ahijevych et al. 2009; Davis et al. 2009; Gallus, 2010), which are difficult to evaluate due to the "double-penalty" issue in which displaced forecast fields are penalized as both false alarms and misses. Also, MODE has been applied to other meteorological variables, such as vector wind fields (Fowler and Bullock 2010). Mittermaier and Bullock (2013) used MODE and the time-domain version of MODE (which adds time as a third dimension) to explore the spatial and temporal characteristics of total cloud cover over the United Kingdom. However, until now, the application of object-based methods to climatological applications, such as drought evaluation have remained largely unexplored.

Here, we apply MODE to a climatological study of drought. We perform this exploration by comparing attributes of drought objects defined using the SPEI and SPI. We apply MODE to examine the spatial structure of spatially extensive droughts treated as objects. For this study, the drought objects are produced by SPEI and SPI at a 36-month timescale over

UCRB. We focus on object attributes such as the location of object centroids, object areas, and intensity percentiles.

2 Study area, data and methods

2.1. The study area

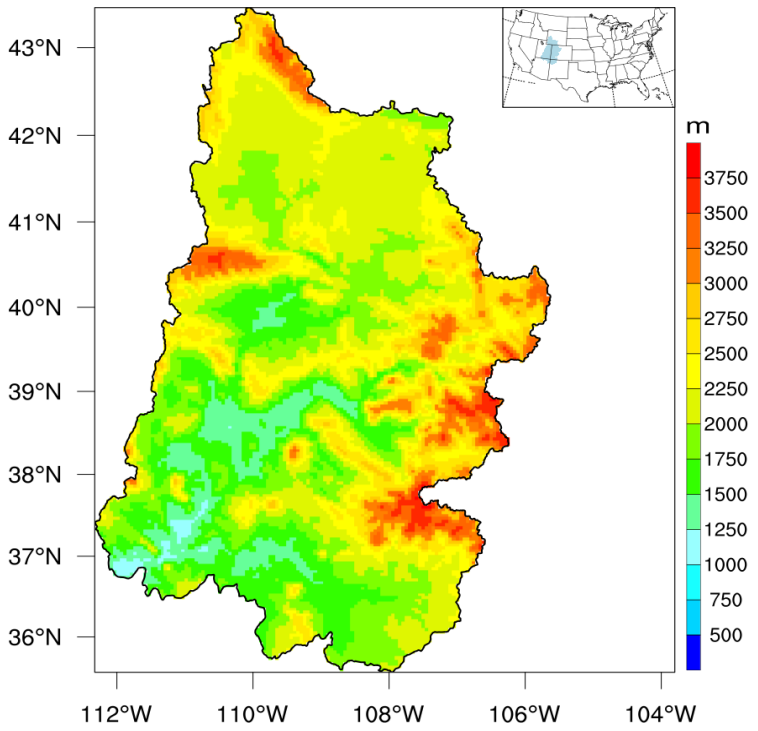

Figure 3.1 Topographic map of the upper Colorado River basin (UCRB). The outline of the map of the contiguous United States showing the location of UCRB is shown in the inset.

As the name implies, UCRB is the upper division of the Colorado River in the American Southwest. The basin occupies an expanse of about 284,380 km^2. The flow from the UCRB, which is highly regulated by several compacts, serves the water requirements of the five

basin states: northern Arizona, Colorado, New Mexico, Utah, and Wyoming (Figure 3.1). Diverse topographic features with the Wasatch Mountains in the west and the Rocky Mountains in the east characterize the basin. The relief ranges from 3,636 m (highest peak of the Wasatch; Mount Nebo) to 4,400 m (highest peak of the Rocky Mountains; Mount Elbert) above sea level. The complex topographic features result in the region experiencing difference climatic conditions. While the west is characterized by the maritime climatic conditions, the interior is characterized by continental climatic conditions. The region is semiarid in nature and the climate regimes over the basin that occur in the cold (October-March) and warm seasons (April-September) is highly variable. The annual average temperature ranged from 5.1 to 7.9 °C, and the mean annual precipitation ranged from 510 to 1,060 mm. A large portion of the UCRB's accessible water comes from snowmelt during spring and heavy rainfall during summer (Christensen et al., 2004; Christensen and Lettenmaier, 2007). The precipitation events come mainly from frontal storms from the Pacific Ocean and convective storms whose moisture comes from the Gulf of Mexico or the Gulf of California (Barry, 1992).

2.2 Data

We use the monthly mean maximum and minimum temperatures and precipitation datasets from the Precipitation-Elevation Regression on Independent Slopes Model (PRISM; Daly et al. 1994, 2008) to derive the drought indices. We use PRISM as opposed to, say, station data because it provides observation-based data on a regular grid and it attempts to account for elevation effects that could be important in a mountainous region like the UCRB. The gridded datasets are available on a 4 km × 4 km spatial resolution from 1895–2012.

However, we analyze data for the period 1948–2012 for consistency with our earlier study (Abatan et al., 2017). The analysis focus on 36-month periods ending in December. For example, using a 36-month running window, the data for December 1950 is aggregated from the mean from January 1948 to December 1950. Similarly, data for December 1951 come from the mean from January 1949 to December 1951, etc. The focus on the 36-month timescale was chosen to properly address the climate information needs of the Denver Water resources managers; in particular, the information necessary for planning water management, both for maintaining supply and adequate operating revenue.

2.3 Indices

Since there is no single method of assessing and describing drought severity that is suitable for all circumstances and users (Lloyd-Hughes, 2014), this study relies on the analyses of 36-month timescale SPEI and SPI to examine drought episodes over UCRB. The use of this timescale arises because Denver Water managers are especially interested in 36-month droughts for regional water resources planning and management.

The SPI is a multiscalar index developed for use in Colorado by McKee to monitor drought and wet spells. The SPI algorithm, based solely on precipitation, permits expression of drought and wet spells in terms of precipitation deficits, percent of normal and probability distribution. The SPI is advantageous as it is simple to calculate and can be used effectively in all seasons of the year because of its avoidance of a dependence on soil moisture. This makes the index important for characterizing drought (wet spells) conditions for different applications. The multiscalar and standardization properties of SPI offers robust application of the index across different geographical regions at different timescales. At shorter

timescales (e.g., 3 and 6 months) SPI can be used to indicate agricultural and meteorological drought, while at longer timescale it is useful for hydrological drought.

But there are also shortcomings to SPI. Since SPI is based on precipitation data alone, it fails to account for the influence of evaporation and transpiration on the climatic water balance. Hayes et al. (1999) indicated that application of SPI at shorter timescales (1, 2, or 3 months) in regions with normally low seasonal precipitation totals can be misleading because SPI gives a similar result to the percent of normal representation of precipitation. Despite these limitations, SPI has gained widespread acceptance and use because of its versatile and simple nature. Detailed expositions of the SPI methodology and applications can be found in studies such as McKee et al. (1993), Guttman, (1998), Lloyd-Hughes and Saunders (2002).

Vicente-Serrano et al. (2010) proposed the SPEI as an extension to the SPI as a more sensitive tool for drought evaluation for a changing climate. It is a modification of the SPI that incorporates potential evapotranspiration in its algorithm using the Hargreaves formula (Hargreaves and Samani, 1985), thus allowing for a more refined evaluation of the surface water balance. As a result, SPEI combines the advantages of being multiscalar (like the SPI) and accounting for the contribution of temperature to water balance (Chen et al. 2013). The SPEI is obtained by fitting a log-logistic Pearson III distribution to the climatic water balance. Details appear in Vicente-Serrano et al. (2010), Beguería et al. (2014), and Yu et al. (2014).

We calculate the 36-month SPEI and SPI (hereafter SPEI36 and SPI36) based on the PRISM monthly rainfall and temperature (minimum and maximum) values at each grid point over the UCRB using the SPEI library (Beguaría and Vicente-Serrano, 2013) developed for the R software suite (R Development Core Team, 2012). As stated earlier, we define the

drought indices at 36-month starting from January and ending in December of the third year for annual increments over the period 1950–2012 and we focus further analysis only on the periods ending in December.

2.4 MODE

MODE is an object-based technique that represents a class of spatial verification methods. The MODE technique was developed independently for weather forecast verification purposes by Davies et al. (2006a, 2006b), but follows the same overall paradigm as earlier work in the field of image analysis proposed by Chen and Wang (2002). The objective is to identify localized and episodic features of interest in 2-dimensional scalar fields and compare features in the two fields (generally a forecast and an observed field) to identify which features best correspond to each other (Davies et al. 2009). The MODE process involves object identification based on specified thresholds, object attributes measurement, objects merging, objects matching, and comparison of object attributes between the two fields. MODE is inherently flexible. It allows users to determine how merging and matching of objects in two fields are implemented. In addition, as in this study, MODE can be adapted to better meet the specific verification needs of the user (Davies et al. 2006a). This implies that the user can specify parameters of interest (such as centroid location, shape {orientation angle and aspect ratio}, intensity, area) and compute their statistics (such as standard deviation, median of intensity percentiles, maximum of median interest (MMI)) for individual objects in either field, and for the identified (matched) pairs of objects between the two fields. Therefore, MODE offers users a flexible way to learn about specified characteristics in individual datasets, but also immediately about commonalities

(hits) and differences (misses) between, traditionally, a forecast and observations. Of course, we can use MODE to characterize any one or more fields, none has to be an observation, and both can be different observational datasets without involving forecast or other model output. In essence, MODE may be used to compare any two fields (field1 and field2). In this study, field1 is SPEI36, while field2 is SPI36. As MODE normally operates on two input datasets, we use SPEI36 and SPI36, respectively as input fields.

MODE uses two basic steps to identify objects in meteorological fields. First, the raw data is convolved. This is basically a smoothing process using a convolution radius to remove unnecessary local scale variability. Secondly, the convolved data field is masked by applying a threshold (T) on the intensity of the fields, returning a binary matrix of zeroes, where the threshold was not surpassed, and non-zeroes (ones), where the selection criteria (threshold) were fulfilled. This can be done for multiple criteria, and where all of them pass their corresponding thresholds, these locations are then further analyzed, while any other information in cells that don't fulfill the thresholds are eliminated.

To identify coherent objects, and to compare objects between the fields, a step called "merging and matching" is performed (for details see Davies et al. 2006a, 2006b, and Bullock et al. 2016). MODE uses a fuzzy logic algorithm (Yager et al. 1987) to merge the retained information of the masked convolution fields into contiguous areas (objects). This is done individually in both forecast and observed fields. Using an iterative process, the "matching" step then attempts to identify corresponding objects between forecast and observed fields. The fuzzy logic algorithm considers many attributes of the objects to calculate a metric known as the total interest function that ultimately determines which objects are to be merged and matched. The attributes of each object pair used as input in the

fuzzy logic engine to calculate the total interest are centroid distance separation, orientation angle difference, intersection area, and area ratio. Given two objects, the area ratio is calculated by dividing the area of the smaller object by the area of the larger object, while the intersection area is the fraction of the overlap area divided by the average of the areas of the two objects. Other attributes of interest include union area and symmetric difference. The union area is the total area that is in either one or both of the two objects, and the symmetric difference is the area inside at least one object, but not both. Further details on the object pair attributes and the computation of the total interest appear in Davies et al. (2009) and Johnson and Wang (2012). For guiding the precise identification of a match between objects in the two fields, the total interest function is assigned a threshold value. MODE typically uses a total interest threshold value of 0.7. Pairs of objects in the two fields that exceeds this threshold value are considered a match. For all matches, the values in the masked convolution field are then replaced with the original values in order to retain the real intensities (note, the convolution led to an artificial smoothing to reduce noise, but for locations identified as part of objects, the true intensities are needed). All statistics are then calculated for each pair of matched objects as well as for each single objects in the separate fields.

MODE is run once all the necessary input and parameter thresholds are set. The summary statistics generated are written separately for each 36-month into the MODE output database, where they are available for inspection, analysis, and synthesis. The output files contain information for all of the attributes for individual drought objects (simple single and merged cluster single) and matched drought objects (simple pairs and cluster pairs). Among the information in the output file for individual objects is the percentile of intensities (e.g., 10th,

50th, and 90th) inside the object, the centroid locations of the object, and the area of the object. However, for matched objects, MODE output such statistics as critical success index, total interest, and intersection area. Other statistics such as bias can be calculated for the matched objects. For the climatology analysis in section 3.3, we extract the median value of the attributes of interest for each drought index separately and for each year to form a time series (an example is shown in Table 3.3 for 1960). Then we compare the temporal evolution of the median of the attributes of drought objects from SPEI36 and SPI36 using a box-whisker plot. Prior to the analysis in this study, we perform a normality test on the time series of the attributes to assess if the data series are normally distributed (see Appendix 3A1–3A2). For the time series that are normally distributed, we use the Welch Student's *t* test to assess the significant of the difference of two means for SPEI36 and SPI36 series, while we use Kolmogorov-Smirnov test statistics for the non-normally distributed series. Because the area of drought objects vary spatially, we take the logarithm of the area time series for clarity of analysis.

2.5 Parameter threshold

Objects are identified in the two fields and statistics of attributes of the objects are calculated and compared. Next, we take average of the statistics of object attributes in order to obtain the climatological characteristics of SPEI36 and SPI36 drought and pluvial objects. Thus, comparisons are at the climatological level.

As previously stated, MODE determines the number of objects retained in the merging and matching process by a combination of the convolution radius, area threshold, and the intensity threshold. This implies that variations in these parameters can impact the number of

objects identified. It is worth noting that Davies et al. (2006a) suggested a minimum convolution radius of four grid lengths. We performed a sensitivity analysis to examine the influence of different parameter choices on the number of objects. For the drought analysis (intensity threshold <= –1.0), four cases were examined to compare the number of resulting objects. We use: 1) convolution radius equal 0 (no smoothing) and an area threshold of 4 (hereafter; R0A4D), meaning that only contiguous regions of at least 4 connected grid-cells would make up objects; 2) convolution radius equal 4 and area threshold of 4 (R4A4D); 3) convolution radius equal 0 and area threshold of 6 (R0A6D); and 4) convolution radius equal 4 and area threshold of 6 (R4A6D). We repeated the same case samples for pluvial (intensity threshold of +1.0), leading to 1) R0A4P; 2) R4A4P; 3) R0A6P and 4) R4A6P. For the analysis presented in the next section, we focus on some of the attributes relevant for the study domain, such as centroids location, area and intensity percentiles. Lastly, we compute and compare the statistics of these attributes for the SPEI36 and SPI36.

3. Results and discussion

3.1 Sensitivity to threshold selection

In order to explore the sensitivity of the results to the retained number of objects and to selected parameter threshold, we applied MODE analysis to PRISM-derived SPI and SPEI using different combinations of area threshold and convolution radius. Figure 3.2 shows the temporal evolution of the number of drought objects identified for different combinations of parameter choices. For clarity of text, Table 3.1 gives an overview of the number of objects for each index and for each parameter threshold. It can be seen that the number of objects is

very sensitive to the combination of parameter choices. In particular, it appears that the number of objects depends more strongly on the value of convolution radius, and less on the area threshold. Although R0A4 and R0A6 show similar patterns (Figs. 3.2a, b), the number of objects produced by both SPEI36 and SPI36 for the R0A4 combination is higher than in R0A6 (Table 3.1).

Table 3.1 Number of objects identified by drought indices relative to parameter threshold.

	Drought parameter			
Drought index	**R0A4**	**R0A6**	**R4A4**	**R4A6**
SPEI	617	534	260	249
SPI	680	573	244	241

A similar temporal pattern (Figs. 3.2c, d) and approximately an equal number of objects (Table 3.1) is found for the comparison between R4A4 and R4A6 for drought events. However, there is a large disparity in the number of objects between R0A4 and R4A4, and also between R0A6 and R4A6. The R0A4 objects is more than two-third of R4A4 objects, while R0A6 drought objects is slightly more than twice R4A4 objects. The contribution of convolution radius to the number of objects is noteworthy; while the area threshold has little influence, the convolution radius is dominant in determining the number of retained objects. Comparison of the number of retained objects due to a combination involving R0 and R4 indicates that the higher number of objects in this study benefits from the case with no convolution radius (R0). Because we use indices based on monthly average data that are aggregated over a further 36-month timescale, it is reasonable to suggest that the resulting fields are already very smooth, and further smoothing of the indices using a convolution

radius of four grid lengths as suggested by Davies et al. (2006a) is not necessary for this study, and in fact, convolution might further water down the signal.

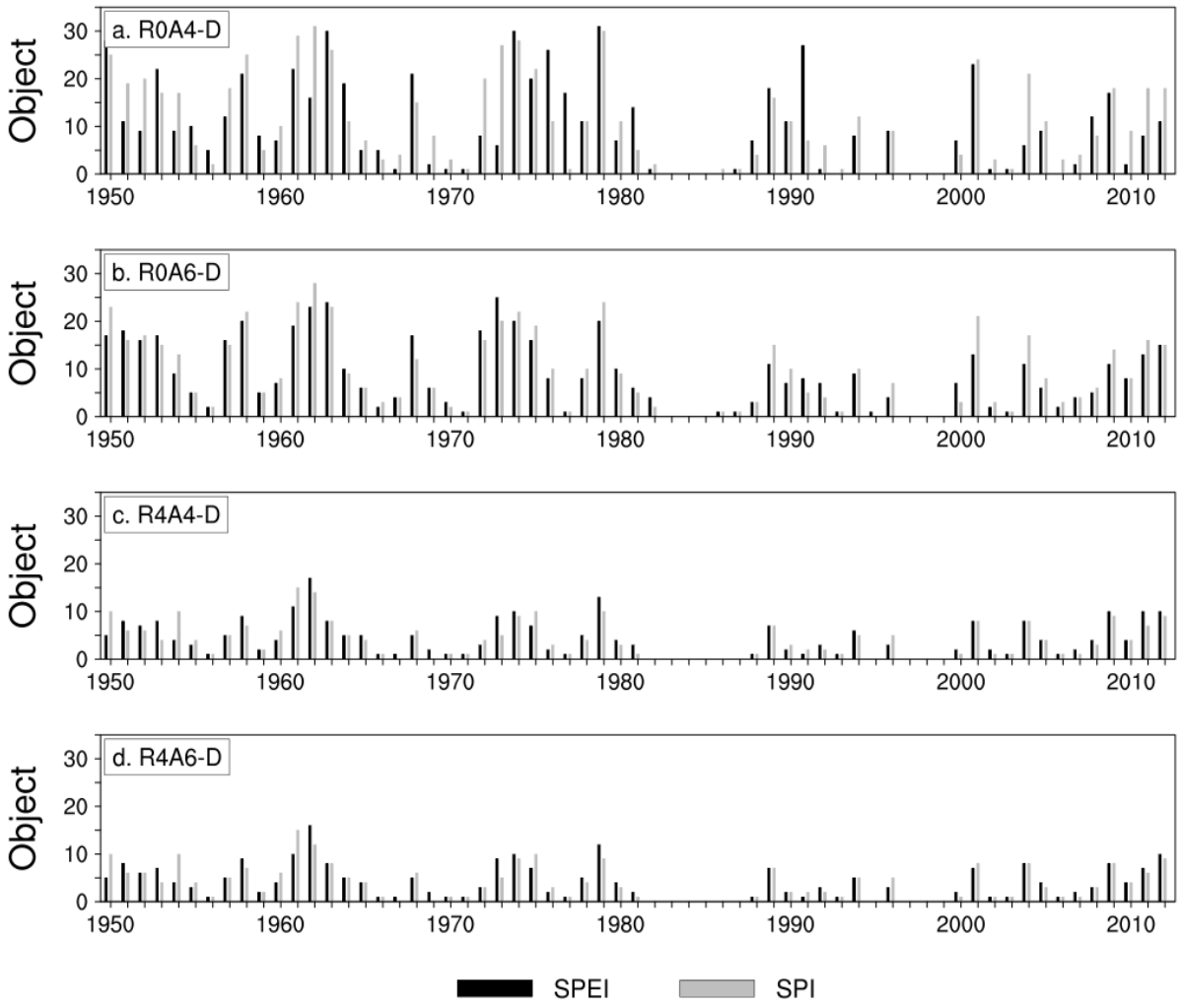

Figure 3.2 Time series of the number of drought objects for different combinations of parameter choices in MODE.

The figures give evidence on the selection of reasonable values of area threshold for defining objects. So, given the above results, we conclude that a combination of convolution radius of zero (R0) and area threshold of four grid lengths (A4) is ideal for producing

sufficient number of objects to allow statistical analyses, while avoiding objects with only one or two grid points, which might represent a structure too small to resolve. Having a good number of objects will also permit an adequate statistical analysis of the object attributes. Hence, for the remaining analysis in this study, we compare the statistics of SPEI36 and SPI36 drought objects attributes using MODE run with R0A4 parameter selection.

3.2 Sample output of MODE objects and attributes

Figure 3.3 shows the results of the application of MODE to SPEI36 and SPI36 datasets for 1960. The spatial distribution of drought in SPEI36 and SPI36 is shown in Figs. 3.3a and 3.3b, while the clusters of single drought objects identified for SPEI36 and SPI36 is shown in Figs. 3.3c and 3.3d. The colored numbers in the figures indicate cluster pairs of objects that were matched between the two fields. While Table 3.2 presents the total interest values of the single drought objects between the two indices, Table 3.3 gives the information and statistics of cluster single of drought objects identified by the two drought indices (Fig. 3.3). From Table 3.2, there are 7 simple single drought objects in SPEI36 and 10 simple single drought objects in SPI36 fields.

The aggregated total interest values (Table 3.2) indicate a good match between the simple single drought objects depicted by the two drought indices (not shown). The total interest values for the matched objects are considerably higher than the 0.7 thresholds; the values range from 0.7046 to 1.00. In particular, there is a perfect match in SPEI36–SPI36 simple drought object pairs (1, 1), (2, 2), and (6, 7), with a total interest of 1.00. The statistics of some of the attributes of these objects reflect this good match (Table 3.3). Using the 0.7 total interest threshold, we observe a match between SPEI36 object 4 and SPI36 objects 4 and 5.

Table 3.2 The total interest matrix for each SPEI36–SPI36 simple drought object pair for December 1960.

		SPEI36						
	Object	**1**	**2**	**3**	**4**	**5**	**6**	**7**
SPI36	**1**	**1.0000**			0.5188		0.5536	
	2		**1.0000**		0.5717			
	3		0.5393	**0.9228**			0.5350	
	4	0.5167		0.6545	**0.9189**	0.6153		
	5		0.5526	0.6802	**0.7046**			
	6		0.6664	0.5466			**0.8571**	
	7	0.5543				**0.8636**	**1.0000**	0.5817
	8						**0.8532**	0.5575
	9						**0.8315**	
	10						0.5785	**0.9697**

The bold values show total interest values greater than 0.7.

Table 3.3 Statistics of attributes of cluster single of drought objects for December 1960.

CLUSTER OBJECT	**CENTROID DISTANCE**	**SPEI36**		**SPI36**	
		INT 50	**Area**	**INT 50**	**Area**
1	0.61	–1.32	505	–1.43	528
2	0.37	–1.13	6	–1.05	5
3	2.59	–1.05	30	–1.20	19
4	2.11	–1.12	26	–1.24	63
5	1.64	–1.59	13445	–1.58	11891
6	4.50	–1.09	12	–1.17	51
Sum		–7.30	14024	–7.67	12557
Mean		–1.22	2337.3	–1.28	2092.8
Median		**–1.13**	**28**	**–1.22**	**57**
Max		–1.05	13445	–1.05	11891
Min		–1.59	6	–1.58	5

Because there is a double match with SPEI36 object 4, SPI36 objects 4 and 5 are considered as a cluster. Similarly, there is a match between SPI36 object 7 and SPEI36 objects 5 and 6. The result of a double match with SPI36 object 7 yields a cluster of SPEI36 objects 5 and 6. Hence, the merging of objects within each field and the corresponding matching of simple

object pairs between the two fields result in a total of 6 matched (cluster single) objects between SPEI36 and SPI36 fields (Figs. 3.3c and 3.3d).

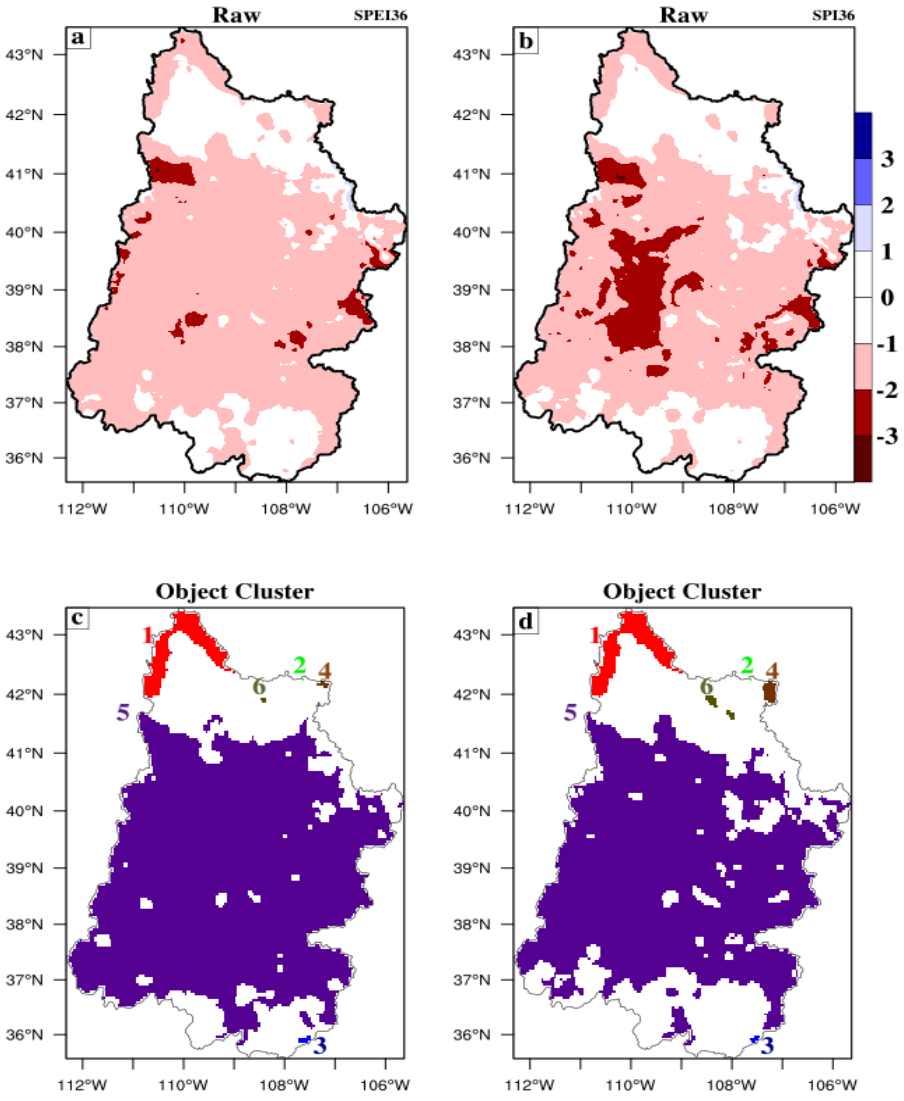

Figure 3.3 The spatial distributions of the values of (a) SPEI36, (b) SPI36, and clusters of drought objects identified for (c) SPEI36 and (d) SPI36 for 1960. The colored numbers in (c) and (d) indicate the objects that were matched between the two fields.

The total object area in SPEI36 is 14024 grid-points, while it is 12557 grid-points in SPI36 (Table 3.3). The difference in area between the matched object pairs is about 10%, or 1467 grid-points. Also, differences between the centroids distance are small, indicating that both drought indicators produce objects at about the same location. For instance, the centroid distance for cluster pairs object 2 is 0.37, while it is 4.5 for cluster pairs object 6 (Fig. 3.3). Consistent with the objects area and centroids, the median of drought intensity within the objects vary slightly from one object to another. The median of the 50th percentile intensity of drought objects ranges from –1.05 to –1.59 in SPEI36, while it ranges from –1.05 to –1.58 in SPI36.

Overall, the sample result presented here indicates that both SPEI36 and SPI36 produced drought objects over UCRB, although there is a slight difference in magnitude, location, and areal extent. The climatology of individual objects, in which this sample is a part, will be discussed in section 3.3, while the statistics of matched objects (cluster pairs) will be addressed in section 3.4.

3.3 Results of individual drought objects

3.3.1 Statistics of simple single drought objects

This section examines and compares the distributions of the median values of various object attributes (e.g., intensity {e.g., 10th, 50th and 90th percentiles}, centroid location {latitude and longitude}, and area) for all simple single drought objects from SPI36 and SPEI36.

Figure 4 shows the distributions of the median of the 10th, 50th, and 90th percentiles intensity attribute of SPI36 and SPEI36 drought objects, while the summary of the mean

values is shown in Table 3.4. Although the median of the percentile intensity attributes from SPI36 compared well with that from SPEI36, there are still slight differences. The SPI36 has

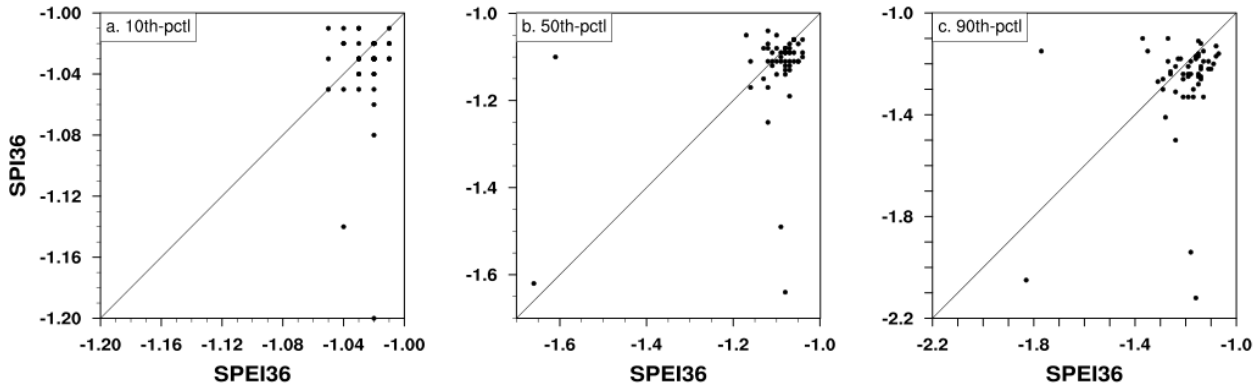

Figure 3.4 The median of the (a) 10th, (b) 50th, and (c) 90th percentile intensity attribute within the simple single drought objects for SPEI36 versus SPI36 for 1950–2012.

Table 3.4 Approximate mean values for drought objects attributes from the drought indices

Drought Index	Attributes of drought objects					
	Percentile Intensity			Centroid location		Log_{10} Area
	10th	50th	90th	Latitude (°N)	Longitude (°W)	
SPEI36	–1.040	–1.11	–1.21	38.9	108.9	1.28
SPI36	–1.038	–1.13	–1.27	38.9	108.9	1.32

drought intensities that are slightly higher than that of SPEI36. For the 10th percentile intensity attribute, the mean intensity for SPEI36 is approximately the same with that of SPI36 (Fig. 3.4a). The difference in mean intensity between the two indices, calculated using the Kolmogorov-Smirnov two-sample test statistics for non-normal data (Appendix 3A1) at the 5% level, is not statistically significant (p-value = 0.37). For the 50th percentile intensity attribute (Fig. 3.4b), the mean drought intensity in SPEI36 is slightly lower than that of

SPI36 (Table 3.4). Similarly, the difference in mean for the 50th percentile intensity attribute of the drought objects is not statistically significant (p-value = 0.08). Figure 3.4c shows the distribution of median of the 90th percentile intensity attributes for drought objects depicted by SPEI36 versus SPI36. The cluster around the diagonal line within –1.0 and –1.4 indicate a close match between the intensities produced by the two indicators. There are some cases during the period when SPI36 have considerably higher values than SPEI36, leading to a difference in drought severity (Table 3.4). The Kolmogorov-Smirnov test of significance for the difference between the two means indicates that the difference in mean of the 90th percentile intensity attribute of the drought objects from SPEI36 and SPI36 is not statistically significant at the 5% level as p-value equal 0.06.

Figure 3.5 shows the scatter plot of centroid locations (latitude and longitude) of drought object for SPEI36 versus SPI36, while the summary of the mean values is shown in Table 4. There is a linear relationship between the two drought indices as the latitude values are well clustered about the 1–to–1 diagonal line (Fig. 3.5a). For SPEI36, the median value of centroid latitude ranges from 36.0 to 42.5 °N, while for SPI36 it ranges from 36.4 to 41.9 °N. On average, the statistics of centroid latitude of drought objects show that the latitudes of drought objects retained by the two indicators are comparable, with approximately similar mean values (Table 3.4). Based on the Student's *t* test, there is no significant difference between their means (t = 0.09, p-value = 0.93). As in the centroid latitude, the median of centroid longitude of drought objects exhibit similar patterns for SPEI36 versus SPI36 (Fig. 3.5b). For SPEI36, the median of centroid longitude ranges from 106.5 to 110.8 °W, while for SPI36 it ranges from 106.5 to 111.8 °W. Although both indicators locate the drought object at about the same longitude, objects in SPI36 are displaced slightly further west than

in SPEI36. The test of significance for the difference of two means indicate non-significant difference between the means of the centroid longitude of drought objects from the two indices; t = –0.07, p-value = 0.94. In general, the statistics of centroid locations of drought objects in SPEI36 and SPI36 are similar. This indicates the similarity in the spatial patterns of drought from the two indicators.

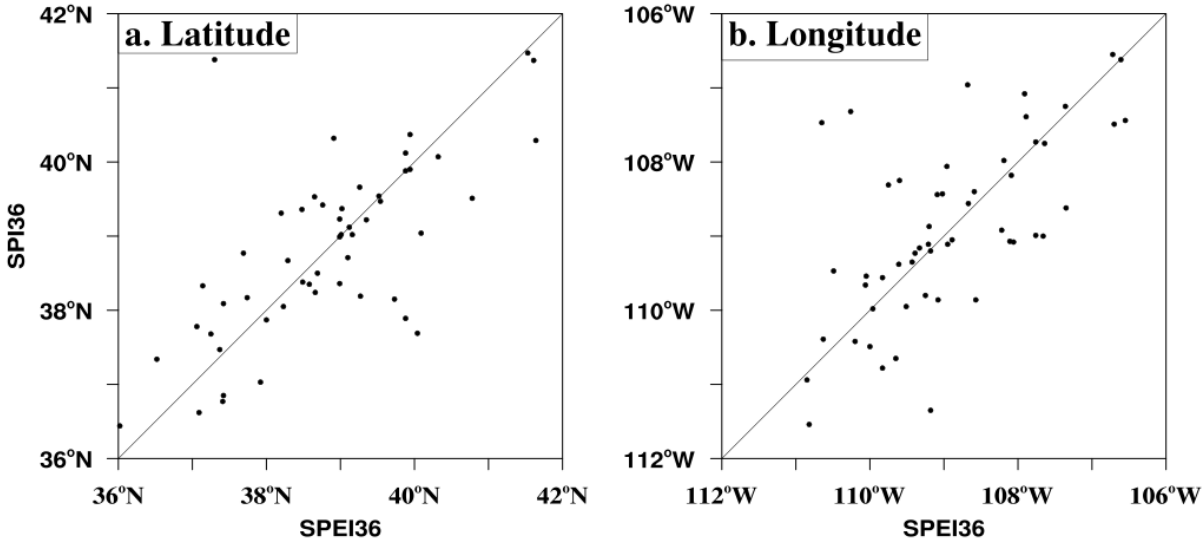

Figure 3.5 The median of centroid (a) latitude and (b) longitude within the simple single drought objects for SPEI36 and SPI36 for 1950–2012.

Figure 3.6 gives the scatter plot of the median and mean of area of drought objects. Given the fact that the area of drought objects vary in size and structure, the idea here is to examine the distributions of the median and mean values and then assess which of these statistics is suitable to represent the area attribute of drought objects. As with the size of drought area, the number of objects identified by the two indices can vary, leading to different median and

mean values among two fields. There are periods with such values in this study. For example, in 2007, SPEI36 identified 2 simple drought objects with areal extent given as {15, 1046}, leading to mean and median having the same value (530.5 grids), respectively. On the other hand, SPI36 has 4 simple drought objects. The areal extent in rank order gives {6, 14, 17, 461}, leading to mean value of 124.5 grids and median value of 15.5 grids. The scatter plots of the logarithm of the median of area of drought objects from the two indices show a cluster concentrated between 1.0 and 2.0 (Fig. 3.6a), however with some outliers showing when either of the two indices have considerably larger drought object areas than the other and also indicating the impact of the number of objects on the median statistic. In contrast, the distributions of the logarithm of the mean of area of drought objects (Fig. 3.6) show a fit well spread across the scale. In this case, the impact of object's number is not clearly obvious. These results suggest that users should apply the statistics that is appropriate to their need.

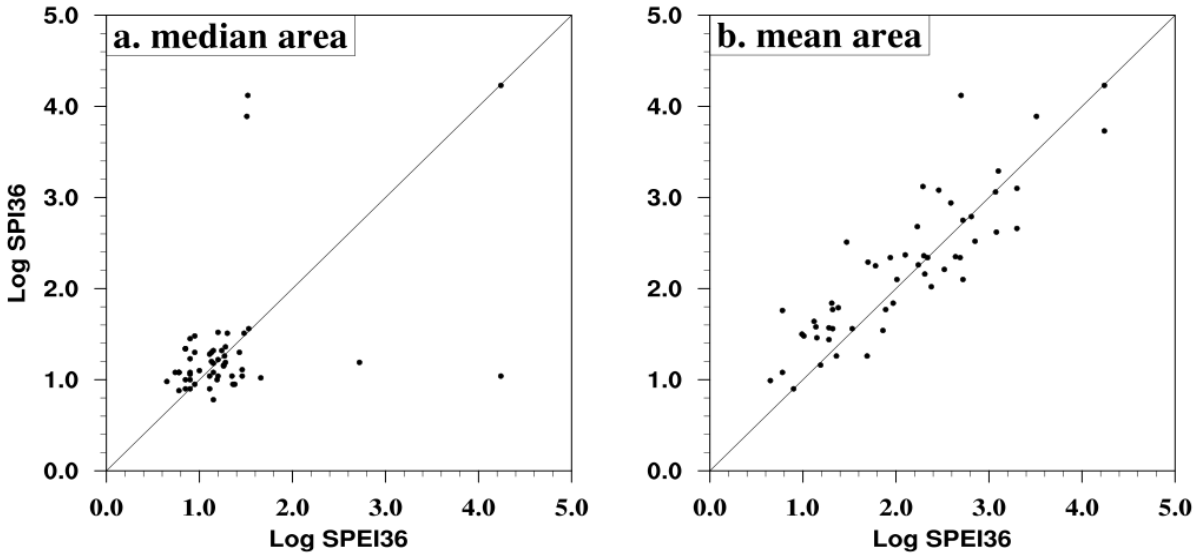

Figure 3.6 The median of area of simple single drought objects for SPEI36 and SPI36 for 1950–2012.

3.3.1.1 Composite statistics of simple single drought objects

This section summarizes the statistics of distributions discussed earlier, using concise box-whisker plots. The box-whisker plots offer a simple yet visually striking comparison of the drought attribute statistics. For the climatology of each of the object attributes in section 3.3.1, we extract a full range of statistics, such as the 5th percentile, first-quantile (25th), median, third-quantile (75th), 95th, and mean.

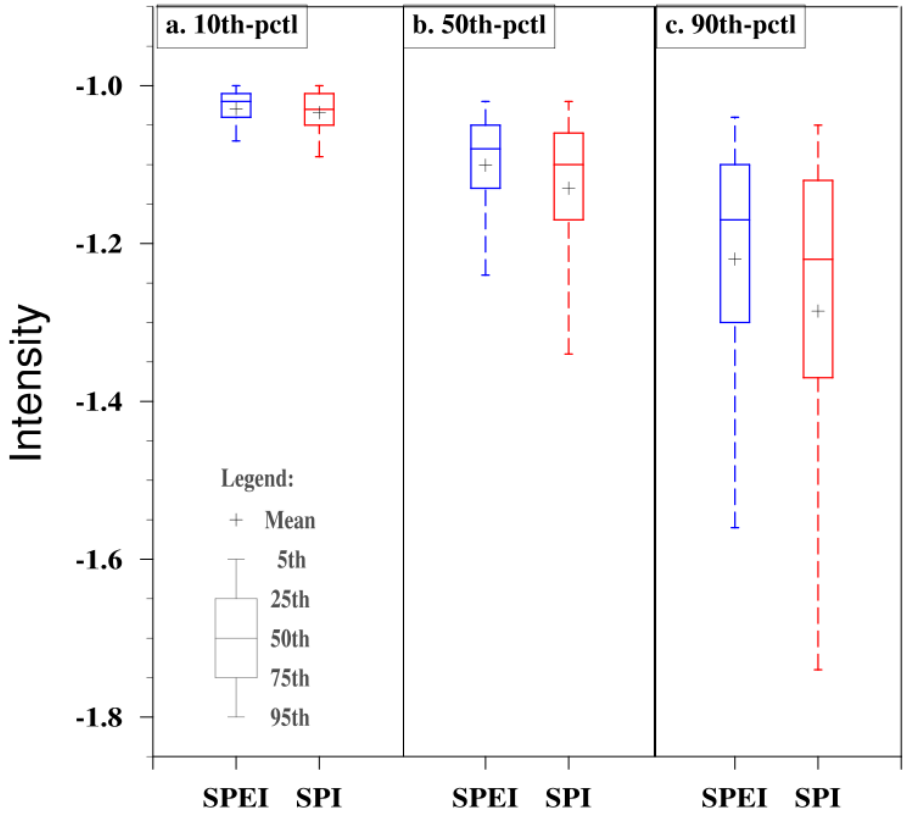

Figure 3.7 The statistics of (a) 10th, (b) 50th and (c) 90th percentile intensity attribute within drought objects for SPEI36 and SPI36 for 1950–2012.

Figure 3.7 shows the statistics of 10th, 50th, and 90th percentile intensity attributes of drought intensity within objects for SPEI36 and SPI36 for the period of 1950–2012. The

median of drought intensity for SPEI36 and SPI36 are slightly different from each other. Also, the spread in SPI36 is slightly wider than in SPEI36. Once more, this is likely the result of the number of drought objects identified (Fig. 3.2a). The median value of the 10th percentile intensity attribute is –1.02 and –1.03 for SPEI36 and SPI36, respectively. The 50th percentile intensity attribute shows that median value in SPEI36 is about 2% lower than that of SPI36. The median values are –1.08 and –1.10 for SPEI36 and SPI36, respectively. In contrast to the 10th and 50th percentile intensity attributes, the 90th percentile intensity attribute has large median difference. The median values for SPEI36 and SPI36 drought objects are –1.17 and –1.22, respectively. This indicates that SPI36 has severe drought intensities within the objects than SPEI36.

Figure 3.8 shows the distribution of statistics of the median of centroid location attribute for SPEI36 and SPI36. For the centroid latitude of drought objects, although the statistics are quite close, the distribution of the median statistics is slightly more spread out in SPI36 than in SPEI36 (Fig. 3.8a). However, Fig. 3.8b shows that centroid longitude of drought objects in SPI36 is located slightly west of the location in SPEI36, with the spread in location also greater than that of SPEI36.

Figure 3.9 shows the statistics of area attribute of drought objects from SPEI36 and SPI36. Consistent with the spread in the percentile intensity attribute, the spread in drought area is wider in SPI36 than in SPEI36 further showing that the area of some of the drought objects in SPI36 is larger than in SPEI36. Although the median value of the distributions is the same, there are differences in other statistics. For example, both indices skewed to the right, but the SPI36 has longer tail than SPEI. Similarly the temporal mean in SPI36 is higher than in SPEI36 (Table 3.4). Overall, there is consistency in the distributions of area,

percentile intensity, and number of drought objects during the drought conditions over UCRB.

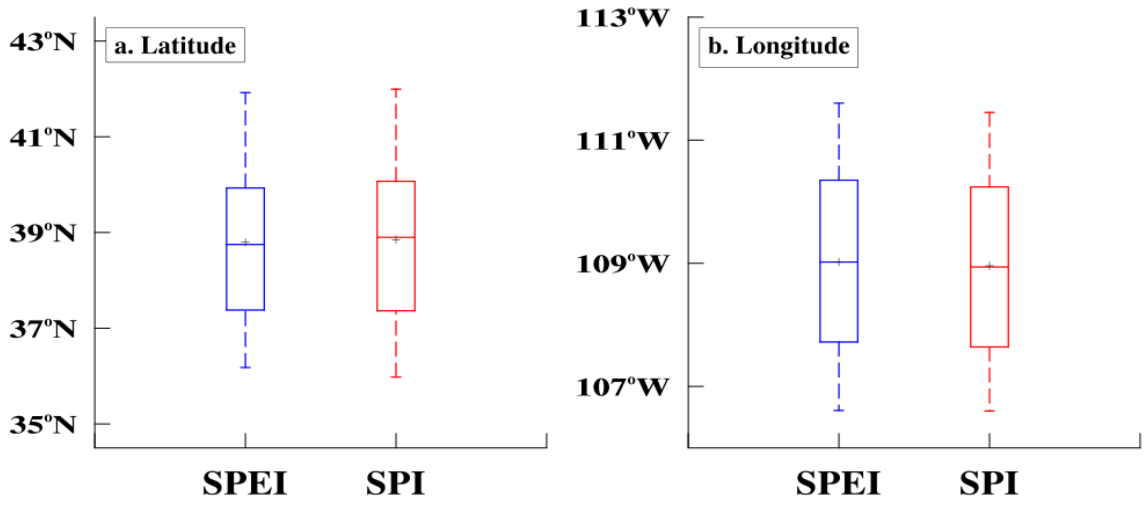

Figure 3.8 Boxplot comparing the statistics of centroid (a) latitude and (b) longitude of drought objects between SPEI36 and SPI36 for 1950–2012.

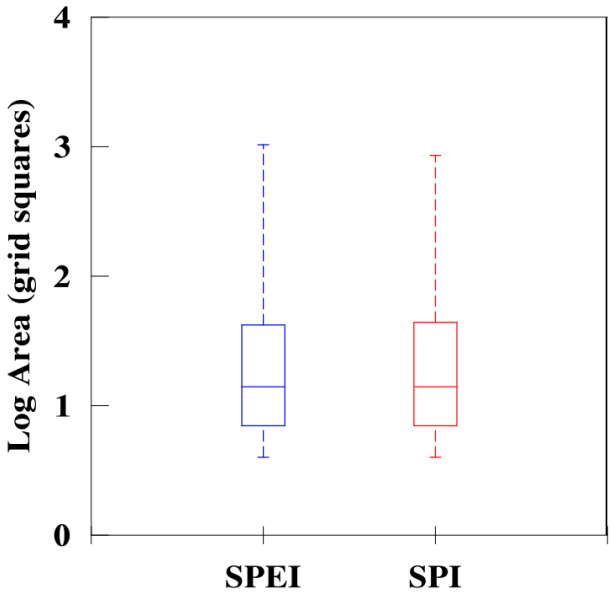

Figure 3.9 The statistics of area of drought objects for SPEI36 and SPI36 for 1950–2012.

3.3.2 Statistics of cluster single drought objects

Further, we analyze the relationship between SPEI36 and SPI36 for cluster single drought objects. As in the previous section, we present results only for intensity, centroids, and area attributes. As shown in Figure 3.10, there is a linear relationship between the two indices, although some scatter exists between the indices. For the 90% quantile attribute of drought intensity, SPEI36 show higher drought magnitude at about 67% of times, while SPI only has higher values at about 8% of time during the period when drought objects were identified. The difference in drought intensity identified by the two indices ranges from –0.58 to 0.17. A similar result is shown for the 10% and 50% quantiles, where SPEI36 exhibits higher drought intensity for the 10th percentile intensity attributes (43%) than in SPI36 (21%); while for the 50th percentile intensity attributes the SPEI36 value is higher at about 59% of times than in SPI36 (19%).

Figure 3.11 shows the relationship between the drought indicators for the centroid locations of the drought objects. A linear relationship exist between the SPEI and SPI centroid latitude (Fig. 3.11a), suggesting that both indices produce matched drought objects over UCRB at almost the same location. Similarly, we observe a nearly perfect relationship between SPEI and SPI for MODE centroid longitude (Fig. 3.11b). Figure 3.12 shows the median and mean of area of matched drought objects over UCRB. As in the case of simple single drought objects (Fig. 3.6), few outliers are observed in the median of area of cluster simple drought objects. In contrast to the median value, the mean of area of matched drought objects exhibit a close linear relationship between SPEI36 objects and SPI36 objects.

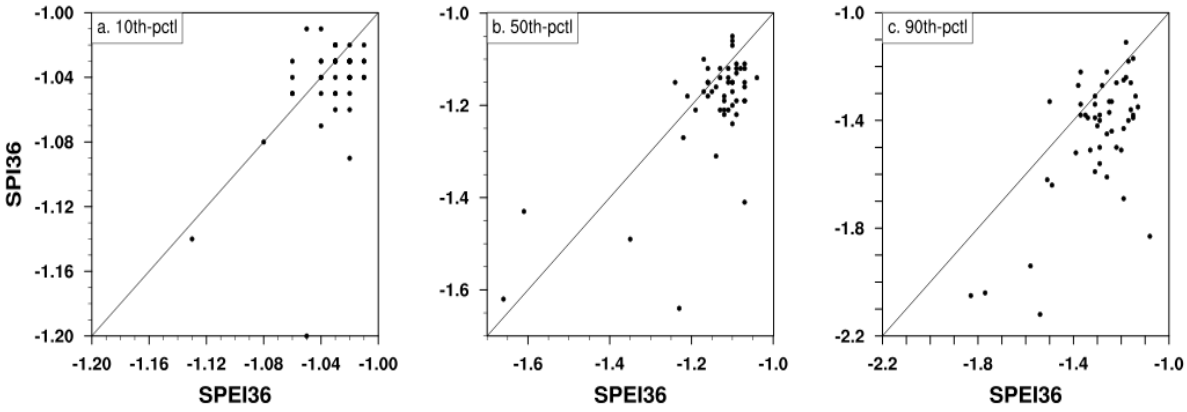

Figure 3.10 Relationship between SPEI36 and SPI36 median of the (a) 10th, (b) 50th, and (c) 90th percentile intensity attribute for cluster single drought objects.

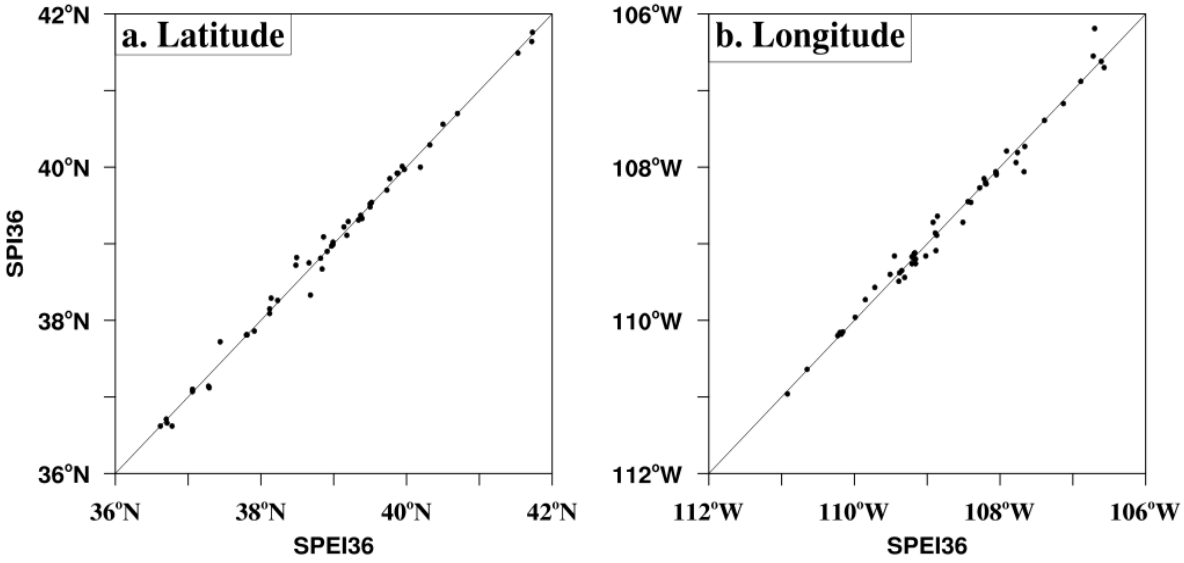

Figure 3.11 Relationship between SPEI36 and SPI36 median of centroid (a) latitude and (b) longitude attribute for cluster single drought objects.

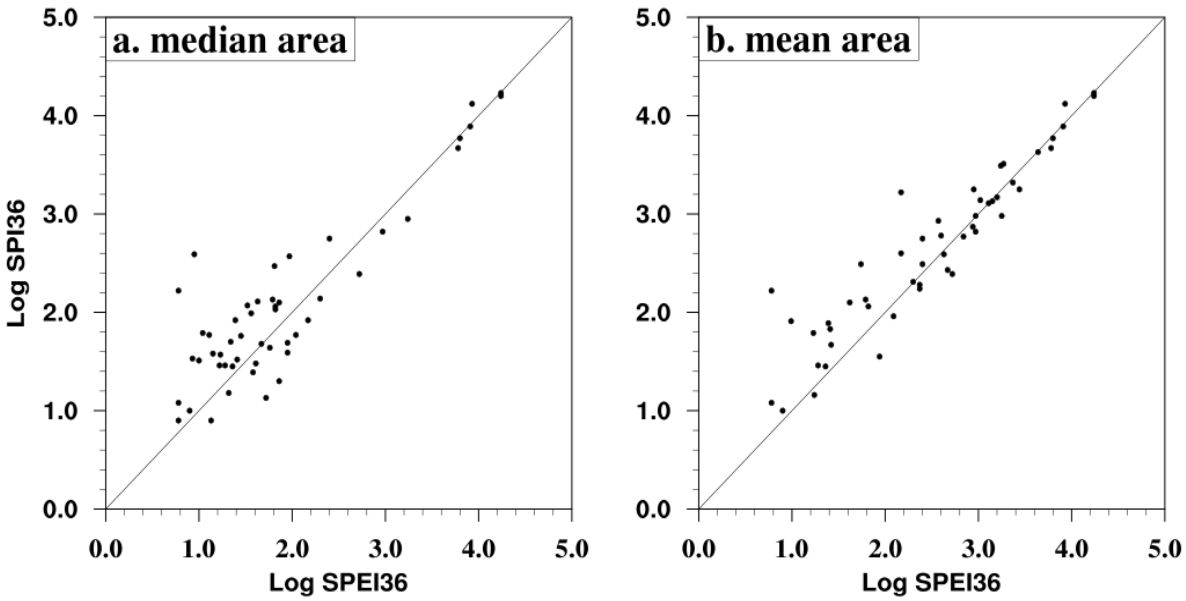

Figure 3.12 Relationship between SPEI36 and SPI36 (a) median and (b) mean of area of cluster single drought objects.

3.4 Results of matched drought objects

3.4.1 Statistics of cluster pair drought objects

Apart from the statistics of individual object attributes previously analyzed, MODE output files also provide information on the commonalities of drought objects from the two indices that can be explored. Among such information are the critical success index (CSI), the area and intensity biases. The object-based CSI is a measure of the frequency of matched objects. It is defined as the ratio of hits to the sum of hits, misses, and false alarms. In this study, an object is defined and counted as a miss when SPI-produced drought objects have no match in SPEI, while a false alarm is counted when SPEI objects have no match in the SPI.

This definition is analogous to that defined for forecast and observed systems (Davis et al. 2006a, 2006b).

Figure 3.13 shows the evolution of CSI over UCRB for the period 1950–2012. The gaps in the temporal pattern is a result of no drought objects during the period (Fig. 3.2a). The CSI is characterized by substantial interannual variability with higher values that indicate similarities between the spatial pattern of SPEI36 and SPI36 drought objects, supporting Fig. 12. Lower CSI values (< 1 standard deviation; 1σ = 0.28) occur at about 27% of times, again confirming a match between the drought objects identified by the two indices. Further to the CSI, biases in the drought object attributes are examined. The area bias for all matched cluster pairs of drought object normalized by the average of all matched SPI36 areas for a given year is given as;

$$B^t_{area} = \frac{\Sigma_i \left[A^t_{spei,i} - A^t_{spi,i}\right]}{\Sigma_i A^t_{spi}} \tag{3.1}$$

Analogously, the intensity bias is given as;

$$B^t_{intensity} = \frac{\Sigma_i \left[I^t_{spei,i} - I^t_{spi,i}\right]}{\Sigma_i I^t_{spi}} \tag{3.2}$$

where *B* refers to bias and the superscript *t* refers to the year when there is drought object.

Figure 3.14 shows the temporal evolution of area and percentile intensity biases for cluster pairs of drought objects. As shown in Fig. 3.14a, the area bias is very small confirming that both SPEI36 and SPI388 have roughly similar matched object sizes. With this, the area bias lies between ± 1σ at about 86% (43 of 50) of times. The area of drought objects identified by SPEI36 is wider than that of the SPI36 only 4 times (bias > 1σ), while the area of drought objects identified by SPI36 is wider than that of the SPEI36 only 3 times

(bias < 1σ). The bias in 10th and 90th percentile intensities within the cluster pairs of drought object areas is shown in Fig. 3.14b. The bias in 10th percentile intensity is small with values lying between ± 1σ at about 70% of the period. SPI36 has higher intensity values than SPEI36 at about 22% (11) of the period (bias < 1σ). Unlike the 10th percentile intensity, the negative bias in 90th percentile intensity of drought object is obvious. This shows that SPI36 has severe droughts than those identified by SPEI36 during the period of study. The earlier period of the study from 1950 to 1980 is characterized by strong negative bias, while the later period from 1981 to 2012 is dominated by periods with no drought and drought objects. This pattern is consistent with Figures 3d, 3e, and 5b of Abatan et al. (2017), although with differences in extreme magnitudes.

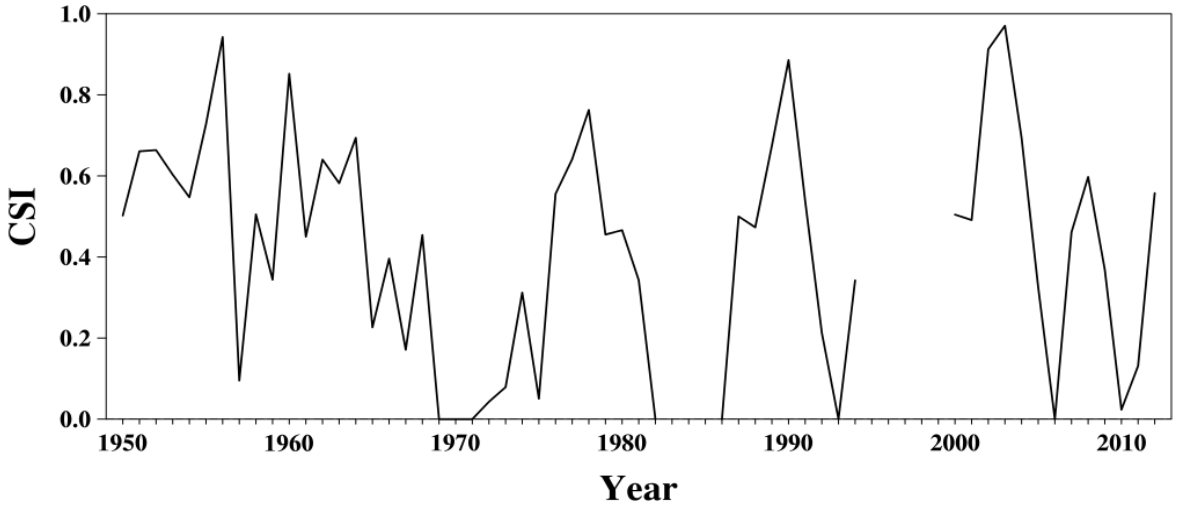

Figure 3.13 The CSI for matched drought object area. The horizontal dash-dash line is the standard deviation, σ.

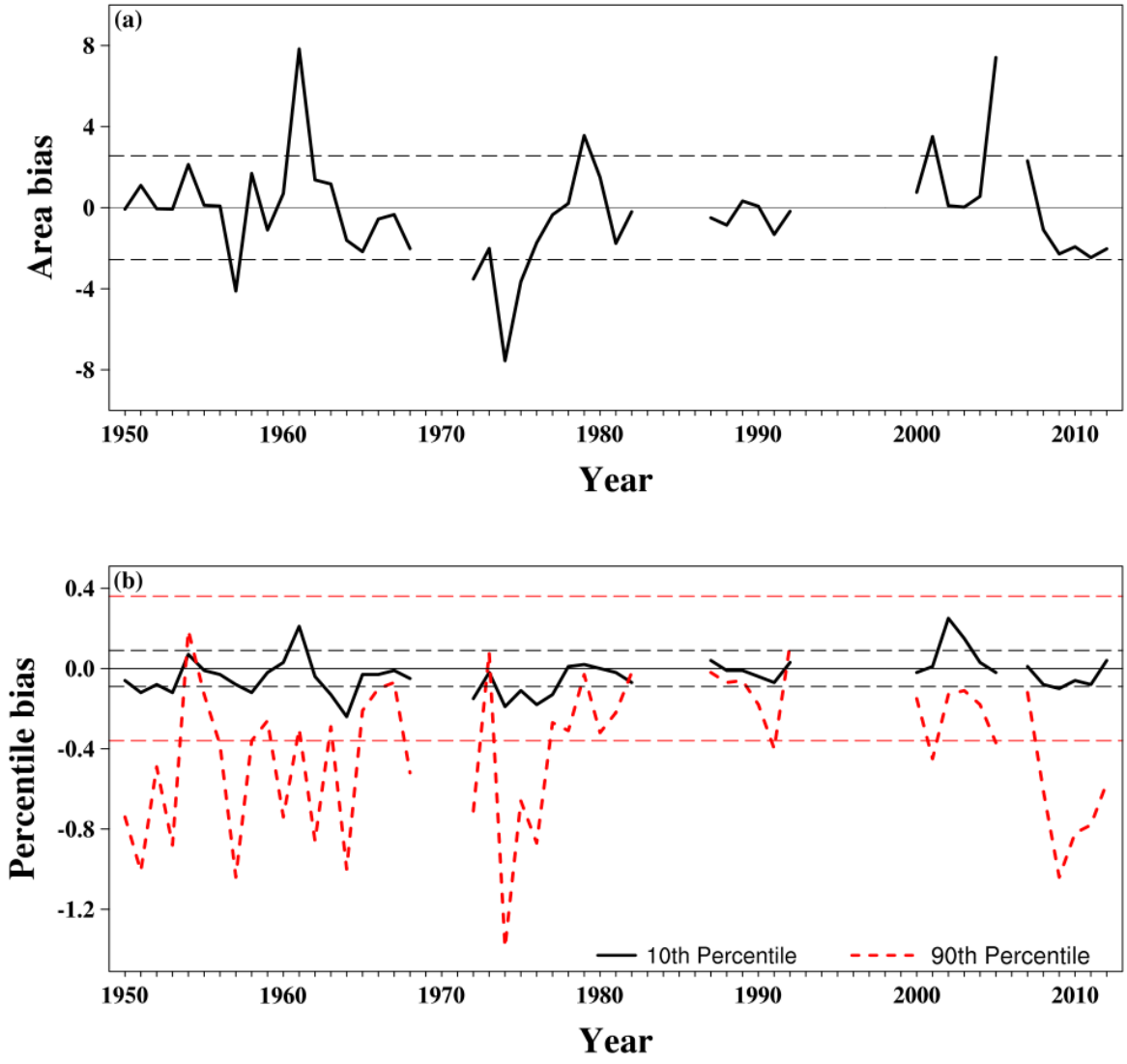

Figure 3.14 Bias in (a) area and (b) percentile intensity of matched cluster pairs of drought objects. The horizontal dash-dash line is the standard deviation, σ.

4. Conclusions

We use the MODE technique to examine and compare the statistics of attributes of drought objects from the SPEI and SPI at 36-month timescale UCRB. The two drought

indicators are calculated using the monthly climate variables from PRISM datasets from 1948 to 2012. MODE identifies several parameters of interest, but, in particular, we focus on object attributes such as centroid location, area and intensity percentiles. To the best of authors' knowledge, MODE has been widely used to obtain statistics of attributes of the objects of wet extremes at weather timescales, but it has not been used to examine drought characteristics. Because of this, we perform a sensitivity test to determine the best combination of parameter thresholds suitable for the number of objects identified and retained in the merging and matching process. We observe that a combination of convolution radius equal 0 (no smoothing) and an area threshold of 4 grid points is well suited for this study, contrary to a minimum of convolution radius of four grid lengths suggested by Davies et al. (2006a) for precipitation evaluation. This study provides an important first-hand information in using MODE to examine multi-year drought conditions over UCRB.

The median of the percentile intensity distribution of drought objects from SPI36 is similar to that from SPEI36, although slight differences exist. We find that SPI36 has severe drought intensities, however, the Kolmogorov-Smirnov test statistics for the difference of two means indicates that the difference in means is not statistically significant. Despite the differences in intensity, the climatology results show that both indices place the centroids (latitude and longitude) of the drought objects at about the same location.

The area of drought objects is characterized by substantial variability in size and number. From the analysis of the individual objects, we find that SPI36 has more and larger drought objects than does SPEI36. However, MODE clearly identifies the 2000s multi-year droughts over the study domain that peaked in 2002 in SPEI36, consistent with the previous study by

Abatan et al. (2017). This further highlights the importance of MODE utility in drought analyses.

In order to examine further the similarities/differences between the two drought indicators, we analyze the object-based CSI and area and intensity biases of the matched drought objects. The higher value of CSI during the period of study is suggestive of a close similarity between the area of matched drought objects identify by SPEI36 and SPI36. However, the negative bias in the 90th percentile intensity of drought objects further attests that some of the matched drought objects in SPI36 have more severe droughts that in SPEI36.

In conclusion, at the timescale considered in this study, SPI produces higher percentile intensity of drought objects, which is clearly obvious in the 90th percentile intensity of drought objects. Although both indices produced drought objects at about the same location over UCRB, the large difference between SPEI36 and SPI36 occurred in the area of drought objects during the recent period when UCRB experience drought conditions, which previous studies have linked to ongoing global warming. This indicated that drought indices that include the effects of temperature are increasingly important for drought evaluation and monitoring over UCRB.

Acknowledgements

We acknowledged the comments and contributions of the reviewers. This work is supported by the National Science Foundation through Earth System Modeling (EaSM) Grant AGS-1243030. We acknowledge high-performance computing support from Yellowstone

(ark:/85065/d7wd3xhc) provided by NCAR's Computational and Information System Laboratory. NCAR is supported by the National Science Foundation, and managed by the University Corporation for Atmospheric Research. We also thank the management of the Federal University of Technology, Akure, Nigeria for granting study leave to the first author. To God be all the glory.

Appendix: Comparison of SPEI using different PET methods

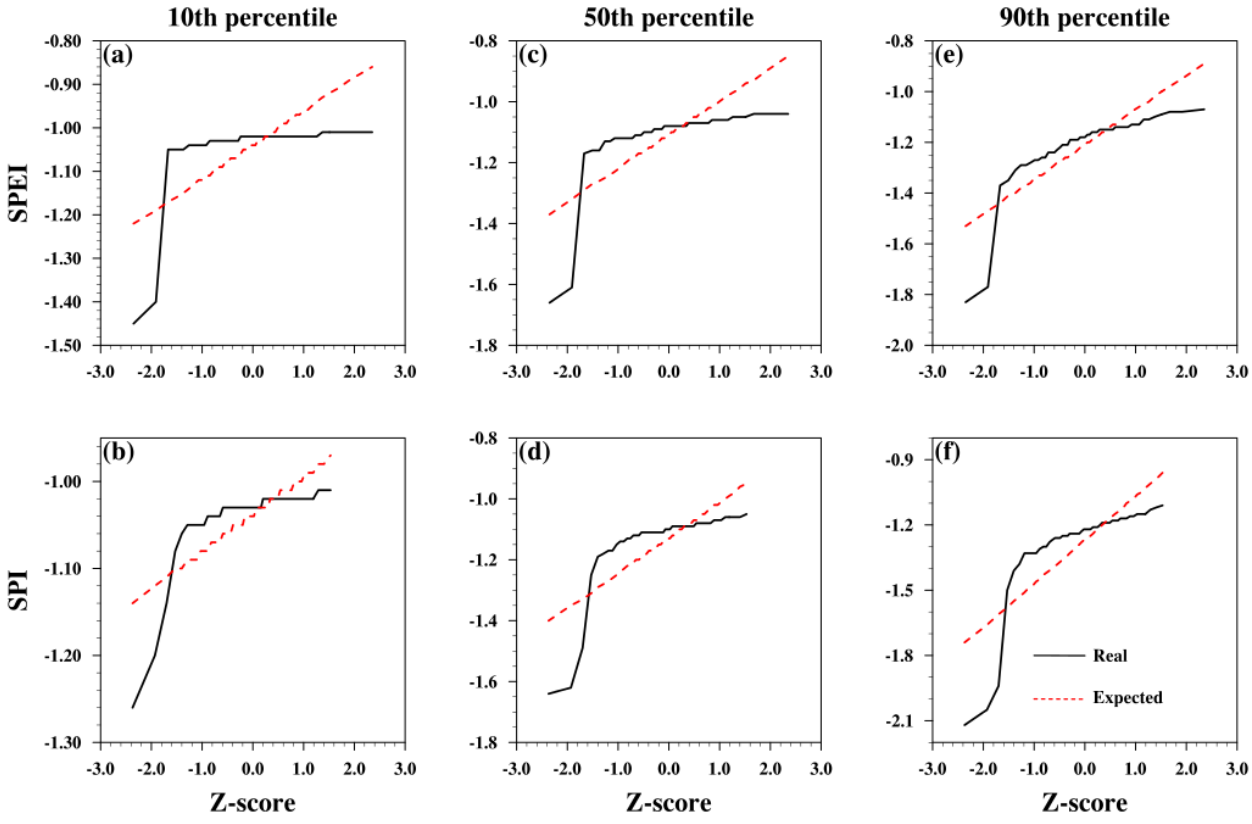

Figure 3.A1 Normality plot of (a, b) 10th, (c, d) 50th, and (e, f) 90th percentile intensity of drought objects from (top) SPEI36 and (below) SPI36.

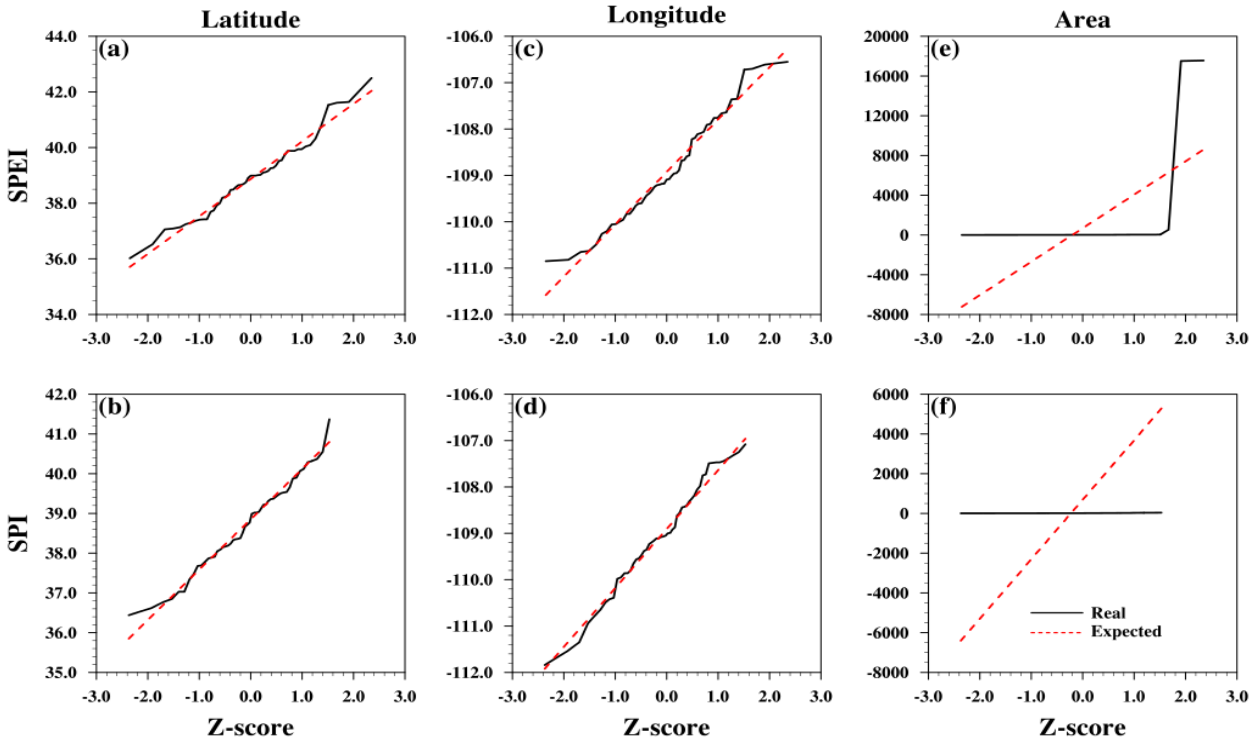

Figure 3.A2 Normality plot of (a, b) latitude, (c, d) longitude, and (e, f) area of drought objects from (top) SPEI36 and (below) SPI36.

References

Abatan AA, Gutowski WJ Jr., Ammann CM, Kaatz L, Brown BG, Buja L, Bullock R, Fowler T, Gilleland E, Gotway JH. 2017. Multi-year droughts and pluvials over Upper Colorado River basin and associated circulations. *J. Hydrometeor.*, **18,** 799–818, doi: 10.1175/JHM-D-16-0125.1.

Ahijevych D, Gilleland E, Brown BG, Ebert EE. 2009. Application of spatial verification methods to idealized and NWP-gridded precipitation forecasts. *Wea. Forecasting* **24:** 1485–1497.

American Meteorological Society. 1997. Meteorological drought—Policy statement. *Bull. Amer. Meteor. Soc*. **78:** 847–849.

Barry, R. G., 1992: Mountain weather and climate. Routledge, New York, 402 pp.

Beguería S, Vicente-Serrano SM. 2013. Calculation of the Standardised Precipitation-Evapotranspiration Index (SPEI). Available from: http://cran.r-project.org/web/packages /SPEI/SPEI.pdf [9 June 2015]

Beguería S, Vicente-Serrano SM, Fergus F, Latorre B. 2014. Standardized precipitation evapotranspiration index (SPEI) revisited: parameter fitting, evapotranspiration models, tools, datasets and drought monitoring. *Int. J. Climatol*. **34:** 3001–3023.

Brown BG, Gilleland E, Ebert E. 2011. Forecasts of spatial fields, Chapter 6, pp. 95–117, In: *Forecast Verification: A Practitioner's Guide in Atmospheric Science*, I. T. Jolliffe and D. B. Stephenson, Eds., John Wiley & Sons, Ltd, 274 pp.

Bullock RG, Brown BG, Fowler TL. 2016. *Method for Object-Based Diagnostic Evaluation*. NCAR Technical Note NCAR/TN-532+STR, 84 pp, doi:10.5065/D61V5CBS. Available from http://opensky.library.ucar.edu/search/?ky=technotes.

Burgman RJ, Jang Y. 2015. Simulated U.S. drought response to interannual and decadal Pacific SST variability. *J. Climate* **15:** 4688–4705.

Chen Y, Wang JZ. 2002. A region-based fuzzy feature matching approach to content-based image retrieval. *IEEE Pattern Anal. Mach. Intell*. **24:** 1252–1267.

Chen T, van der Werf GR, de Jeu RAM, Wang G, Dolman AJ. 2013. A global analysis of the impact of drought on net primary productivity. *Hydrol. Earth Syst. Sci*. **17:** 3885–3894.

Christensen NS, Lettenmaier DP. 2007. A multimodel ensemble approach to assessment of climate change impacts on the hydrology and water resources of the Colorado River Basin. *Hydrol. and Earth System Sci.* **11:** 1417–1435.

Christensen NS, Woods AW, Voisin N, Lettenmaier DP, Palmer RN. 2004. The effects of climate change on the hydrology and water resources of the Colorado River Basin. *Climatic Change* **62:** 337–363.

Cook BI, Seager R, Smerdon JE. 2014a. The worst North American drought year of the last millennium: 1934. *Geophys. Res. Lett*. **41:** 7298–7305, doi: 10.1002/2014GL061661.

Cook BI, Smerdon JE, Seager R, Coats S. 2014b. Global warming and 21st century drying. *Clim. Dyn.* **43:** no. 9-10, 2607–2627, doi: 10.1007/s00382-014-2075-y.

Cook BI, Ault TR, Smerdon JE. 2015. Unprecedented 21st century drought risk in the American Southwest and central Plains. *Science Advance* **1:** 1–7.

Daly C, Halbleib M, Smith JI, Gibson WP, Doggett MK, Taylor GH, Curtis J, Pasteris PP. 2008. Physiographically-sensitive mapping of temperature and precipitation across the conterminous United States. *Int. J. Climatol*. **1:** 2031–2064.

Daly C, Neilson RP, Phillips DL. 1994. A statistical–topographic model for mapping climatological precipitation over mountainous terrain. *J. Appl. Meteor.* **33:** 140–158.

Davis C, Brown B, Bullock R. 2006a. Object-based verification of precipitation forecasts. Part I: Methods and application to mesoscale rain areas. *Mon. Wea. Rev*. **134:** 1772–1784.

Davis C, Brown B, Bullock R. 2006b: Object-based verification of precipitation forecasts. Part II: Application to convective rain systems. *Mon. Wea. Rev*. **134:** 1785–1795.

Davis CA, Brown BG, Bullock R, Halley-Gotway J. 2009. The Method for Object-based Diagnostic Evaluation (MODE) applied to numerical forecasts from the 2005 NSSL/SPC Spring Program. *Wea. Forecasting* **24:** 1252–1267.

Dracup JA, Lee KS, Paulson EG. 1980. On the statistical characteristics of drought events. *Water Resources Research* **16:** 289–296.

Ebert EE, Gallus WA. 2009. Toward better understanding of the Contiguous Rain Area (CRA) method. *Weather and Forecasting* **24:** 1401–1415.

Ebert EE, McBride JL. 2000. Verification of precipitation in weather systems: Determination of systematic errors. *J. Hydrol.* **239:** 179–202.

Fowler TL, Bullock R. 2010. Examination of Spatial Wind Features Associated with Ramping Events using MODE. First Conference on Weather, Climate, and the New Energy Economy. American Meteorological Society, Atlanta, January 16–20, 2010.

Gallus WA Jr. 2010. Application of Object-based verification techniques to ensemble precipitation forecasts. *Wea. Forecasting* **25:** 144–158.

Gilleland E, Ahijevych D, Brown BG, Casati B, Ebert EE. 2009. Intercomparison of spatial verification methods. *Wea. Forecasting* **24:** 1416 – 1430.

Guttman NB. 1998. Comparing the Palmer drought index and the standardized precipitation index. *J. Amer. Water Resources Assoc.* **34:** 113–121.

Hargreaves GL, Samani ZA. 1985. Reference crop evapotranspiration from temperature. *Appl. Eng. Agric.* **1:** 96–99.

Hayes MJ, Svoboda MD, Wilhite DA, Vanyarkho OV. 1999. Monitoring the 1996 drought using the Standardized Precipitation Index. *Bull. Amer. Meteor. Soc.* **80:** 429 – 438.

Jarrett RD. 1990. Paleohydrologic techniques used to define the spatial occurrence of floods. *Geomorphology* **3:** 181–195.

Johnson A, Wang X. 2012. Verification and calibration of neighborhood and object-based probabilistic precipitation forecasts from a multimodel convection-allowing ensemble. *Mon. Wea. Rev*. **140:** 3054–3077.

Kalnay E, and Coauthors. 1996. The NCEP/NCAR 40-Year Reanalysis Project. *Bull. Amer. Meteor. Soc*. **77:** 437–471.

Lloyd-Hudges B. 2014. The impracticality of a universal drought definition. *Theor. Appl. Climatol*. **117:** 607–611.

Lloyd-Hughes B, Saunders MA. 2002. A drought climatology for Europe. *Int. J. Climatol*. **22:** 1571–1592.

Matthai HF. 1969. Floods of 1965 in the United States: Floods of June 1965 in South Platte River basin, Colorado. U.S. Government printing office, Washington, D.C. 20402. Geological survey water-supply paper 1850-B. pp62.

Mittermaier MP, R Bullock. 2013. Using MODE to explore the spatial and temporal characteristics of cloud cover forecasts from high-resolution NWP models. *Meteor. Applications* **20:** 187–196.

McCabe GJ, Palecki MA Betancourt JL. 2004. Pacific and Atlantic Ocean influences on multidecadal drought frequency in the United States. *Proceedings of the National Academy of Sciences* **101:** 4136–4141.

McKee TB, Doesken NJ, Kleist NJ. 1993. The relationship of drought frequency and duration to time scales. Preprints, *Eighth Conf. on Applied Climatology*, Anaheim, CA, American Meteorological Society 179–184.

Meehl GA, Zwiers F, Evans J, Knutson T, Mearns L, Whetton P. 2000. Trends in extreme weather and climate events: Issues related to modeling extremes in projections of future climate change*. *Bull. Amer. Meteor. Soc*. **81(3):** 427–436.

R Development Core Team. 2012. R: A language and environment for statistical computing. R Foundation for Statistical Computing, Vienna, Austria. ISBN 3-900051-07-0. Available from: http://www.R-project.org.

Seager R, Kushnir Y, Ting M, Cane M, Naik N, Miller J. 2008. Would advance knowledge of 1930s SSTs have allowed prediction of the Dust Bowl drought? *J. Climate* **21:** 3261–3281.

Schubert SD, and Coauthors. 2009. A U.S. CLIVAR project to assess and compare the responses of global climate models to drought-related SST forcing patterns: Overview and results. *J. Climate* **22:** 5251–5272.

Trenberth KE, Jones PD, Ambenje P, Bojariu R, Easterling D, Klein Tank A, Parker D, Rahimzadeh F, Renwick JA, Rusticucci M, Soden B, Zhai P. 2007. Observations: Surface and Atmospheric Climate Change. In *Climate Change 2007: The Physical Science Basis*. Contribution of Working Group I to the Fourth Assessment Report of the Intergovernmental Panel on Climate Change, Solomon S, Qin D, Manning M, Chen Z, Marquis M, Averyt KB, Tignor M. Miller HL (eds). Cambridge University Press: Cambridge, UK and New York, NY.

Yu M, Li Q, Hayes M.J, Svoboda MD, Heim RR. 2014. Are droughts becoming more frequent or severe in China based on the standardized precipitation evapotranspiration index: 1951–2010? *Int. J. Climatol*. **34:** 545–558.

Vicente-Serrano SM, Beguería S, López-Moreno JI. 2010. A multiscalar drought index sensitive to global warming: The Standardized Precipitation Evapotranspiration Index. *J. Climate* **23:** 1696–1718.

Wernli H, Paulat M, Hagen M, Frei C. 2008. SAL—A novel quality measure for the verification of quantitative precipitation forecasts. *Mon. Wea. Rev*. **136:** 4470–4487.

WMO. 2006. Drought monitoring and early warning: Concepts, progress and future challenges. WMO.

Yager RR, Ovchinnikov S, Tong RM, Hguyen HT. 1987. Fuzzy sets and applications, Selected Papers by L. A. Zadeh. John Wiley and Sons.

CHAPTER 4. USING MODE TO EVALUATE THE CAPABILITY OF CESM IN SIMULATING MEGA-HYDROLOGICAL DROUGHT OVER THE UPPER COLORADO RIVER BASIN

A paper to be submitted to

The Journal of Hydrometeorology

Abayomi A. Abatan[6,1,*], William J. Gutowski, Jr.[1], Caspar M. Ammann[2], Laurna Kaatz[3], Barbara G. Brown[2], Lawrence Buja[2], Randy Bullock[2], Tressa Fowler[2], Eric Gilleland[2] and John Halley Gotway[2]

[1]Department of Geological and Atmospheric Sciences, Iowa State University, Ames, Iowa USA
[2]Research Applications Laboratory, National Center for Atmospheric Research, Boulder, Colorado USA
[3]Denver Water, Denver, Colorado USA
[*]Department of Meteorology and Climate Science, Federal University of Technology, Akure, Nigeria

Abstract

The southwest US, including the upper Colorado River basin (UCRB), has witnessed multi-year drought events with significant impacts on human and ecosystems. Understanding the day-to-day operation of water resource management in this region in the face of the current climate requires knowledge of extreme events from modeling outputs. However, there is need to evaluate the performance of the models before any actionable decision can be derived

[6]Corresponding author address: Abayomi A. Abatan, 3134 Agronomy Hall, Department of Geological and Atmospheric Sciences, Iowa State University, Ames, Iowa 50011 USA.

E-mail address: abatanaa@iastate.edu yomiabatan69@gmail.com

from their outcomes. The Method for Object-based Diagnostic Evaluation (MODE) is one of the tools currently being used to evaluate climate models. This study uses MODE to diagnose the ability of 34 Community Earth System Model Large Ensemble (CESM-LE) members to reproduce drought objects' attributes including intensity percentiles, area, and centroid locations. The drought objects are based on the standardized precipitation evapotranspiration index at 36-month timescale over UCRB. The results of the study show that CESM-LE performs reasonably well over UCRB, although uncertainties due to the model internal variability exist among the ensemble members. MODE indicates that CESM-LE members give higher intensity percentile of drought objects with smaller drought object area relative to observed drought objects. Although the simulated centroid location of drought objects have wider spread than observation-based objects, MODE shows that the location of the ensemble mean is fairly close to the observed centroid locations. The results provide insight to the usefulness of MODE and CESM-LE as tools for climate study over the UCRB.

Keywords: MODE; SPEI; Drought objects; CESM Large Ensemble; Denver Water

1. Introduction

Extremes in precipitation and temperature variability often result in droughts or floods. Drought is a temporary multiscalar natural hazard characterized by increased temperature and precipitation deficit over an extended period of time (Bryant, 2005; Wilhite and Buchanan, 2005; Vicente-Serrano et al. 2010a; Wilhite, 2000; Dai 2011; Sheffield et al. 2012; Abatan et al. 2017). This extreme of the climate system can have large environmental,

societal and economic consequences. For example, 2012 moderate to severe drought-related agricultural loss over 64% of the contiguous U.S. was worth tens of billions of U.S. dollars (Burgman and Jang, 2015). Drought can impair water resource management and planning, thus dangerously decrease crop yields and cattle inventories. Droughts deplete the strength of streamflow and pose a great challenge to many river basins, including the upper Colorado River basin (UCRB) which supplies water to the Denver metropolitan area. In addition, this extreme climate event can deplete soil moisture and groundwater reservoirs, which can lead to water shortages both for human consumption and agricultural purposes. For instance, the 2000 – 2010 drought in southwest U.S. resulted in Colorado River water shortfalls. This had important potential implications for the region's supplies and prices of agricultural commodities such as fruits, tree nuts, and corn. Also, the impact of droughts on the reservoirs can undermine the generation of hydropower and cripple financial economic sectors including resort centers, tourism, and hotel management, thus reducing the gross domestic per-capita income of a nation.

The current warming of the earth's surface has potential to increase the frequency and severity of drought, because studies have shown that drought severity increases with temperature (Dai, 2011; Vicente-Serrano et al. 2010b), with even more devastating impacts on millions of people in the world. For instance, the century-long observed trends in precipitation, temperature, and sea-level pressure, supported by climate model results, strongly suggest that anthropogenic forcing has increased the probability of severe and persistent droughts in Syria (Kelley et al. 2015). This event led to massive migration of rural farmers to urban locations, with increased stress on already limited natural resources resulting in social conflict. In the central United States, GCM simulations in the context of

global warming suggested a marked increase in the frequency and duration of extreme droughts (Gregory et al. 1997; Woodhouse and Overpeck, 1998). The Intergovernmental Panel on Climate Change (IPCC) Fourth Assessment Report (Meehl et al. 2007) and Fifth Assessment Report (IPCC, 2013) projected a continuous increase in global mean surface air temperature over the twenty-first century, when models simulate the Representative Concentration Pathway GHG forcing scenario RCP8.5, a high-level GHG concentration forcing scenario. The projected climate change can cause some regions including southwest U.S. to experience even more serious drought conditions in the near future.

The impact of drought can be very costly; as a result, several studies have been carried out to monitor, understand and characterize this climatic extreme. Given the complex nature of drought coupled with different drought types (e.g., agricultural, hydrological, and meteorological), researchers have employed several drought identification tools including the standardized precipitation index (SPI) and the standardized precipitation evapotranspiration index (SPEI) to characterized this phenomenon. Of these indicators, the SPEI developed by Vicente-Serrano et al. (2010a, 2010b) has been chosen for this study. We choose SPEI because it is a multiscalar index that incorporates potential evapotranspiration in its algorithm using Hargreaves' method (Hg; Hargreaves and Samani, 1985), thus allowing an evaluation of a complete climatic water balance. These attributes make SPEI an essential tool for monitoring drought and for evaluating the future impact of global warming on droughts (Ujeneza and Abiodun, 2015). Several studies have examined drought using the SPEI. For example, Diasso and Abiodun (2017) examine the spatial structure of drought over West Africa using the SPEI calculated from CORDEX regional climate models simulation outputs. Ujeneza and Abiodun (2015) use SPEI to evaluate the performance of suites of global

climate models in simulating the spatial and temporal patterns of drought regimes over Southern Africa. Abatan et al. (2017) use the index to characterize observed hydrological drought over the UCRB. These studies showed that SPEI is a useful tool to characterize drought in a warmer climate.

Nowadays, drought studies are undertaken using model simulation. This is because many regions lack suitable historical observational datasets to describe the spatial extent of historic droughts. The Community Earth System Model, version 1, with the Community Atmosphere Model, version 5 (CESM1-CAM5; Hurrell et al. 2013) from the CESM Large Ensemble (CESM-LE) project has been developed for studying the influence of internal climate variability and climate change on climatic variables. The CESM1-CAM5 is one of the contributors to the Coupled Model Intercomparison Project Phase 5 (CMIP5). Although climate models such as CESM1-CAM5 are important tools for climate studies, their usefulness depends on how the statistics of present-day climate and climate variability are simulated (Phillips et al. 2014). In particular, the confidence in the accuracy of simulations of future scenarios hinges on how well the models are able to simulate the present-day mean climate. Thus, the ability of CESM1-CAM5 ensemble simulations (hereafter CESM-LE) to reproduce the basic features of atmospheric variables has been examined in some studies (e.g., Kay et al. 2015; Hagos et al. 2016; Scherrer et al. 2016). However, detailed drought analysis using CESM-LE is still lacking.

In order to establish our confidence in future projection from a model, such a model must first be able to reproduce the basic features of the present climate including internal variability and dynamics. Commonly used methods often do not provide adequate information about the capability of a climate model for users' needs. The inherent limitations

associated with commonly used approaches have led to developing the spatial verification tool *Method for Object-Based Diagnostic Evaluation* (MODE; Davis et al. 2006a, 2006b). MODE was developed for verification of forecast systems and observation sources. Several studies have used MODE for rainfall fields (e.g., Davis et al. 2006a, 2006b; Ahijevych et al. 2009; Davis et al. 2009; Gallus, 2010). Recently, Mittermaier and Bullock (2013) used MODE and the more recently developed time-domain version of MODE to explore the spatial and temporal characteristics of total cloud cover over the United Kingdom. Abatan et al (2017) examined and compared the statistics of attributes of observed drought objects produced by SPEI and SPI at 36-month timescale over the UCRB using MODE. MODE has emerged as an efficient tool to compare objects between two fields.

The aim of this study is to use MODE to evaluate the skill of CESM-LE in simulating the statistics of drought object attributes. In particular, we apply MODE to examine the spatial structure of multi-year droughts objects produced by SPEI at 36-month timescale over the UCRB, the region that supplies water for Denver Water. The analysis in this study is rooted on object attributes such as centroid of distribution, area, and intensity percentiles.

2. Data and methods

This study uses gridded monthly precipitation and temperatures (mean, Ta; minimum, TN; and maximum, TX) outputs from 35 CESM-LE members (Kay et al. 2015). All CESM-LE members use the same model, CESM1-CAM5, and they are driven by anthropogenic greenhouse gases, aerosols, and natural external radiative forcing. The model consists of coupled atmosphere, sea ice, land use, and ocean components. Ensemble member 1 was

integrated from 1850 to 2100, while ensemble members 2 to 35 were all started on 1 January 1920 using slightly different initial conditions. Details of the CESM-LE experimental design and coupled simulations that have been done with CESM1-CAM5 appear in Kay et al. (2015) and in a special collection of the *Journal of Climate*[7]. Additional information can also be found at the CESM homepage[8,9]. Although the historical simulations are available from 1920–2005 on a 1.25° longitude × 0.935° latitude grid resolution, this study analyses the outputs from 34-member ensemble simulations for the period 1950–2005.

For the model validation, we use observed monthly temperatures and precipitation datasets for the same period as the model for consistency. The observed datasets are from Climatic Research Unit of the University of East Anglia (CRU, TS3.21; Harris et al. 2014) and the Precipitation-Elevation Regression on Independent Slopes Model (PRISM; Daly et al. 1994, 2008). These datasets are land-only and defined at a different spatial resolution and time scale While CRU datasets are available at a spatial resolution of 0.5° longitude × 0.5° latitude for the period 1901–present, the PRISM datasets are available on a 4 km × 4 km grid from 1895–present. However, for consistency and ease of comparison, we regrid all observations to the CESM-LE model grid using the conservative interpolation method in the National Center for Atmospheric Research (NCAR) Command Language (NCL[10]) library.

MODE is a user-friendly object-based spatial verification tool developed to identify and determine how features of interest in a forecast and observed fields are merged and/or matched. Object identification is performed by a fuzzy logic engine. The object's

[7] http://journals.ametsoc.org/page/CCSM4/CESM1
[8] https://www2.cesm.ucar.edu/models/experiments/LENS
[9] http://www.cesm.ucar.edu/experiments/cesm1.1/LE/
[10] https://www.ncl.ucar.edu/

identification and subsequent merging and matching process involve raw data convolution and thresholding. The first major operation in MODE, the convolution process, is simply data smoothing using a specified convolution radius. Next, the thresholding process is applied. Here, the smoothed field is extracted by seeking field values exceeding a user-specified threshold. This step produces a masked field, that is, a binary matrix of ones and zeroes. Finally, the raw data is restored to the locations of the ones in the matrix, while the raw data occupying the locations of the zeroes are discarded. This process yields a contiguous field of objects of interest from which various objects attributes including centroid location, shape {orientation angle and aspect ratio}, intensity, and area can be calculated and eventually used to perform object merging and matching processes within and between the two fields. Further details on MODE appear in studies including Davis et al. (2006a, 2006b), Ahijevych et al. 2009, Davies et al. (2009), Gallus Jr., (2010), Johnson and Wang (2012), and Abatan et al. (2017).

As in Abatan et al. (2017), we run MODE for this study using a convolution radius of zero and an area threshold of four data grid point to identify drought objects from the SPEI at 36-month timescales. The output files from the run contain the attributes' information for individual drought objects (simple single and merged-cluster single) and matched drought objects (simple pairs and cluster pairs). In this study, only the data for simple single drought objects are analyzed. An example of drought objects presented by MODE from observations and one of the CESM-LE ensemble members (029) appears in Fig. 4.1. The top panel in this figure is the raw data, while the middle and bottom panels are the objects identified by MODE. The banded colored numbers identify objects that are matched between the two fields. Various statistics of the individual and matched drought objects appear in the table

below the panels. For the analysis presented in section 3b, we separately extract all observed and simulated data for the attributes of interest (intensity, area, and centroids location), during the period of study. Then, we compute and compare various statistical measures.

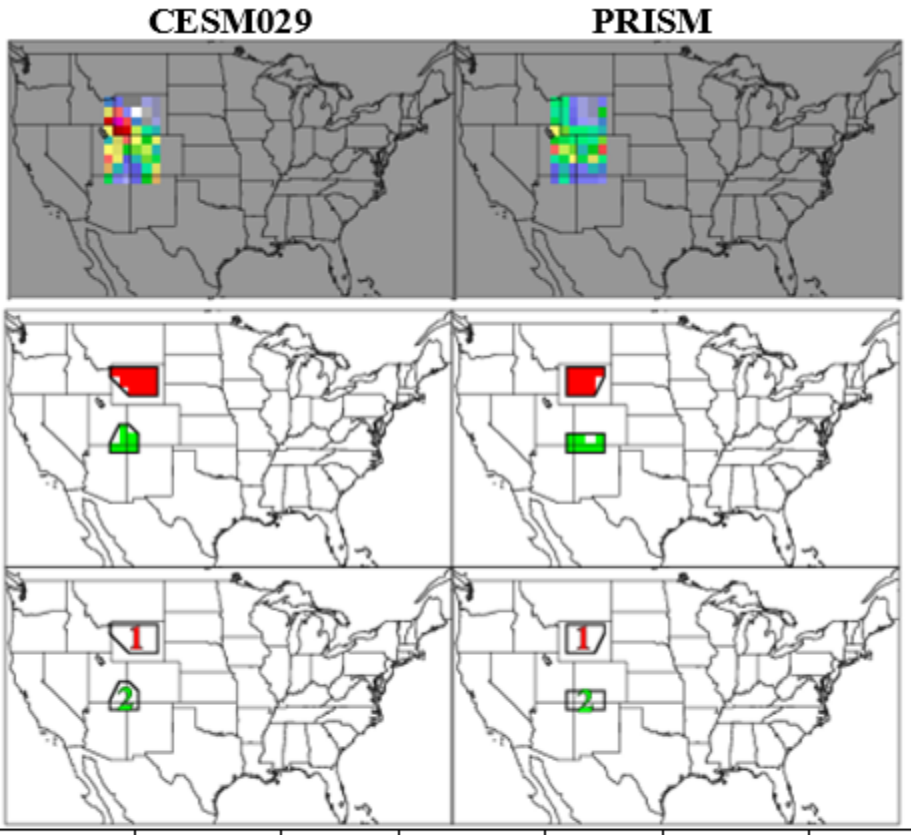

CLUSTER PAIR	CESM029 AREA	PRISM AREA	CESM029 INT 50	PRISM INT 50	CESM029 INT 50	PRISM INT 50
1	12	10	-1.41	-1.30	-1.16	-1.14
2	6	7	-1.13	-1.17	-1.05	-1.07

Figure 4.1 The 2001 spatial distributions of model (CESM 029) and observed (PRISM) SPEI36 (top rows) and clusters of drought objects identified (middle rows). The colored numbers in the bottom panels indicate the objects that were matched between the two fields. The table below the panels shows various statistics calculated for the matched drought objects.

We present results of some of our analysis using box and whisker plots. In this study, the horizontal line in the middle of the box represents the median, the top and bottom of the box are the 25th and 75th percentiles, and the whisker endpoints are the 5th and 95th percentiles values of the fields in question. In addition, we also use the Taylor diagram (Taylor, 2001) to compare the statistics of climatological fields of temperature and precipitation between the CESM-LE and observations. The observations are the reference fields for the Taylor diagrams presented here.

3. Results and discussion

a. Model evaluation

The ability of the CESM-LE in reproducing several aspects of near-surface climate variables has been evaluated by earlier studies highlighted in section 1. However, those studies performed the evaluations on a global scale. Such evaluations offered limited information on how well the model ensemble members reproduce basic features of the variables of interest for climate users interested in a specific region, as in the case here. We begin the analysis in this study with the evaluation of the mean annual cycle of the CESM-LE precipitation and mean, maximum, and minimum temperatures over UCRB. We focus only on temperatures (mean, minimum, and maximum) and precipitation because they are key variables in drought analysis in this study.

Figure 4.2 shows the mean annual cycle of precipitation and temperatures as represented by the CESM-LE and the observations. Several similarities and differences among the ensemble members and observations appear. The temporal patterns of observed

precipitations are similar with less spread during May to October (Fig. 4.2a). The mean annual cycle exhibits double peaks in precipitation. The CRU has its primary peak in August (39.6 mm month^{-1}) and a secondary peak in May (34.7 mm month^{-1}). Similarly, the two peaks in PRISM dataset occur in May (39.8 mm month^{-1}) and August (38.8 mm month^{-1}). A dip in precipitation over the region occurs in June. The amplitude of the annual cycle is higher in the simulations than in the observations, showing a wet bias of seasonal precipitation over the UCRB. The spread among the ensemble members is wider than that of the observations, with the widest spread in May and December. Although the CESM-LE ensemble reproduces the temporal pattern of the mean annual cycle of precipitation, they miss the peak: all the ensemble members show the primary peak in precipitation in May (median = 75.0 mm month^{-1}) and the secondary peak in July (median = 71.7 mm month^{-1}).

The mean annual cycles of observed and simulated temperatures (Ta, TX, and TN) over UCRB during the period of study appear in Figures 4.2b – 4.2d. Although differences can be identified, the similarities in amplitude and phase of the annual cycle of temperatures indicate that the CESM-LE reproduces well the distributions of temperatures over UCRB. On a monthly basis, the spread in simulated temperatures is slightly wider than that of the observations. The annual-cycle pattern of observed and simulated temperature is parabolic in nature with maximum values in July and August. While the CESM-LE ensemble members reproduce fairly well the mean Ta (Fig. 4.2b), they slightly underestimate the mean TX (Fig. 4.2c) and overestimate the mean TN (Fig. 4.2d). As in Fig. 4.2, Fig. 4.3 shows that the ensemble members overestimate both precipitation (Fig. 4.3a) and mean TN (Fig. 4.3d) and underestimate mean TX (Fig. 4.3c), while the temporal evolution of observed mean Ta is within the spread of the simulated mean Ta (Fig. 4.3b).

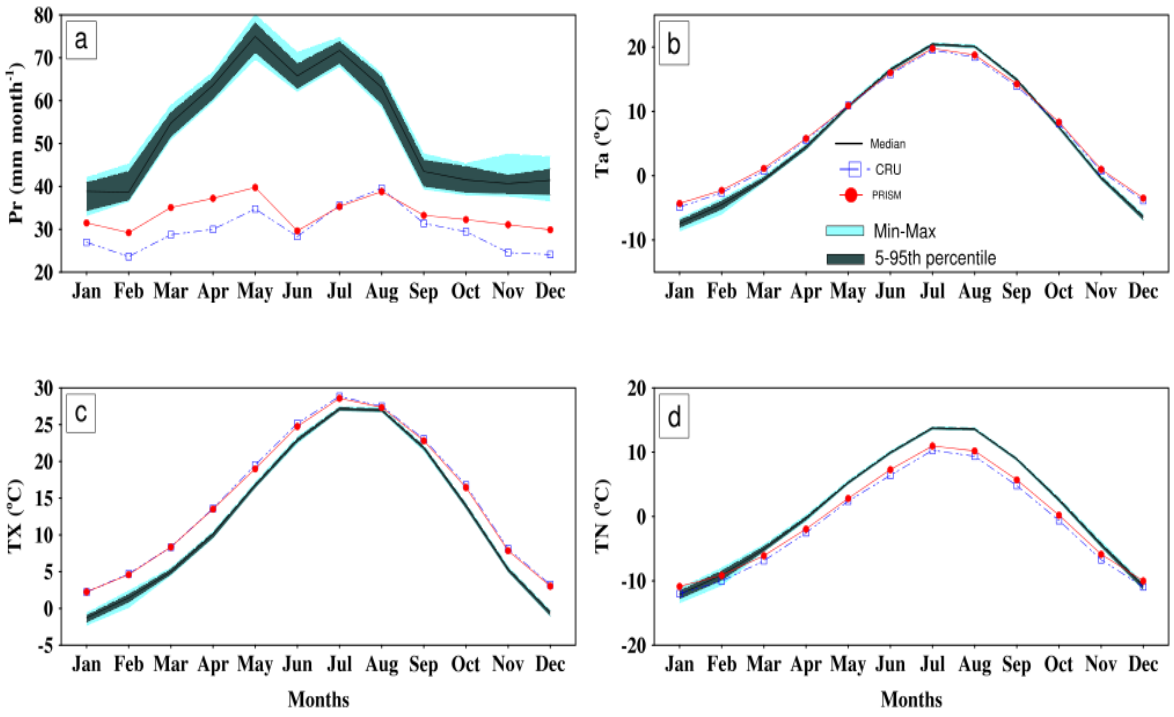

Figure 4.2 Annual cycle of observed and simulated (a) precipitation, (b) mean temperature; Ta, (c) maximum temperature; TX, and (d) minimum temperature; TN over UCRB for the period 1950–2012. The measure of spreads among the 34 ensemble members of the CESM-LE is shown by the minimum–maximum range and the 5–95th percentile range. Also shown in the figures are the ensemble median (thin black line), CRU (blue square), and PRISM (red dot).

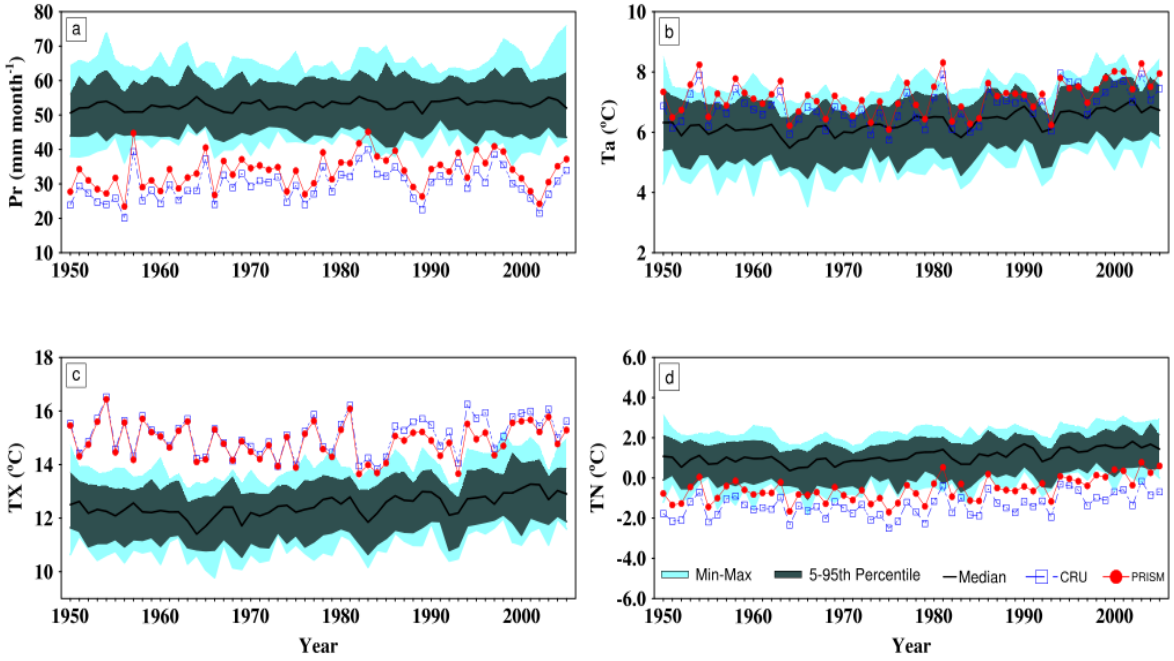

Figure 4.3 Interannual variability of observed and simulated (a) precipitation, (b) mean temperature; Ta, (c) maximum temperature; TX, and (d) minimum temperature; TN over UCRB for the period 1950–2012. The measure of spreads among the 34 ensemble members of the CESM-LE is shown by the minimum–maximum range and the 5–95th percentile range. Also shown in the figures are the ensemble median (thin black line), CRU (blue square), and PRISM (red dot).

The Taylor diagram provides a simple way of showing the skill with which multi-model ensembles simulate the spatial patterns of variables in terms of correlation coefficient, normalized standard deviation, and the root-mean-square difference from a reference field. Figure 4.4 shows a Taylor diagram of the spatial climatology of precipitation and temperatures from CESM-LE in comparison with observations. The Taylor diagram shows

that the CESM-LE perform fairly well in simulating the climate variables. The correlations between simulated climate variables and observations generally lie between 0.6 and 1.0. Among the temperatures, the mean TN shows the lowest correlations between observations and the CESM-LE ensemble members, with a mean value of about 0.65 for CESM-LE versus CRU (Figs. 4.4b) and 0.8 for CESM-LE versus PRISM (Figs. 4.4d). The normalized standard deviations of the simulated TN lie between 1.0 and 1.5, which indicates that each ensemble member has a higher spatial variability of mean TN than observed. The correlation coefficients between the observed and the simulated mean Ta are very strong with a mean value of about 0.97 (Figs. 4.4b and 4.4d). Also, there is a strong relationship between observed and simulated mean TX as indicated by the high correlation value of about 0.99. There appears to be a similarity in spatial patterns between observed and simulated mean Ta, as well as between observed and simulated mean TX climatology. This is supported by the normalized standard deviations values closer to 1.0, which suggests less spatial variability. For precipitation, the correlations between the CESM-LE ensemble members and CRU cluster between 0.95 and 0.97 (Fig. 4.4a), while the correlations between the ensemble members and PRISM cluster between 0.90 and 0.96 (Fig. 4.4c), with a mean value of about 0.95. Although the correlations are high, the normalized standard deviations of simulated precipitation climatology are greater than 1 indicating that each of the ensemble members has more spatial variability than observations. The statistics suggest that the model did not capture well the observed spatial variability in TN, as indicated by the cluster of the ensemble members that is farther off from the unity line. The normalized standard deviations of simulated precipitation ranges from 2.0 to 2.3 for CESM-LE versus CRU (Figs. 4.4a), while it ranges between 1.0 and 1.4 for CESM-LE versus PRISM (Figs. 4.4c). This further

confirms the wet biases shown in Figs. 4.2 and 4.3. The consistency between multimember ensemble statistics of the simulated variables suggests there is a good agreement between the CESM-LE ensemble members.

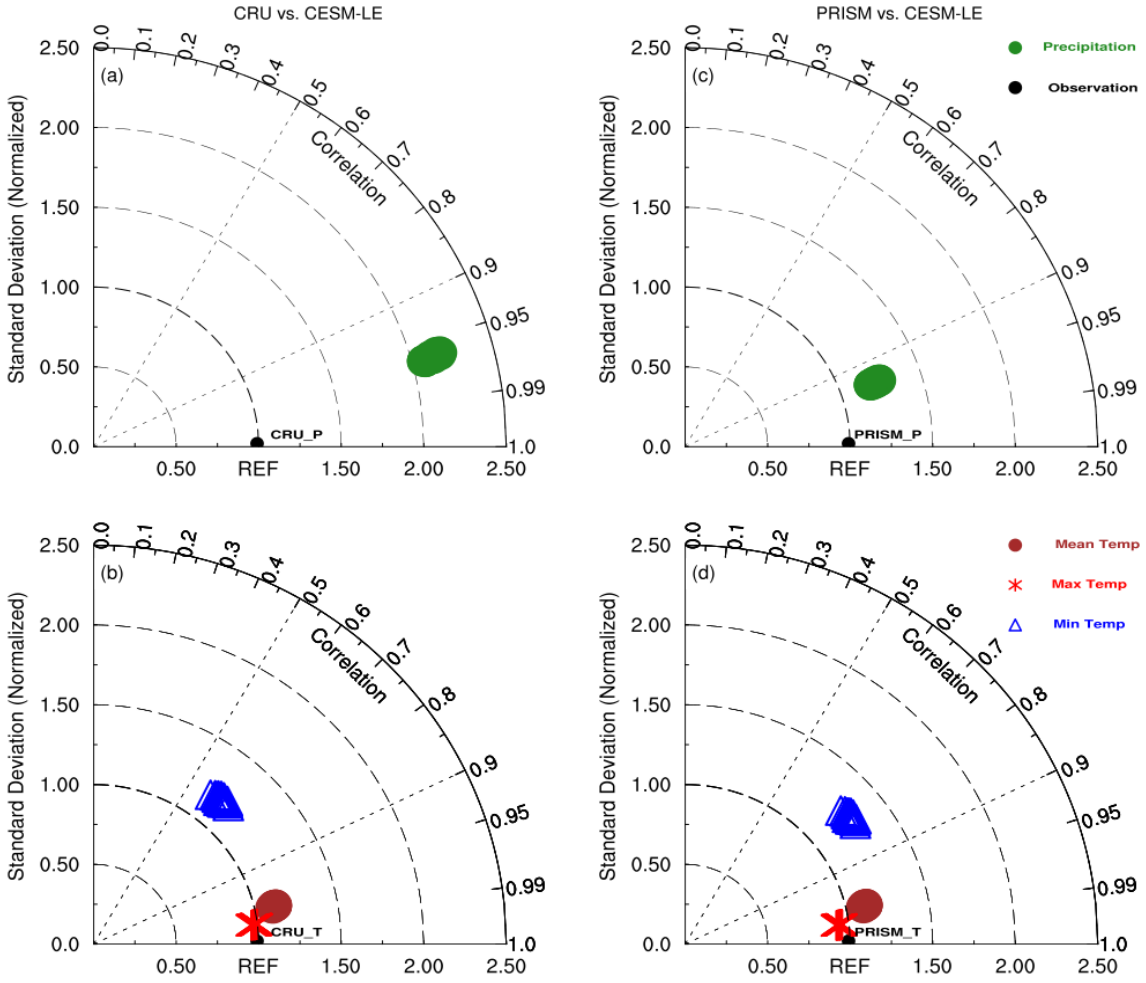

Figure 4.4 Taylor diagram of spatial correlation between CESM-LE ensemble members and observations (CRU; left, and PRISM; right) for (a and c) precipitation and (b and d) temperatures (mean; brown, maximum; red, and minimum; blue) climatology over UCRB for the period 1950–2012. The observations provide the reference datasets.

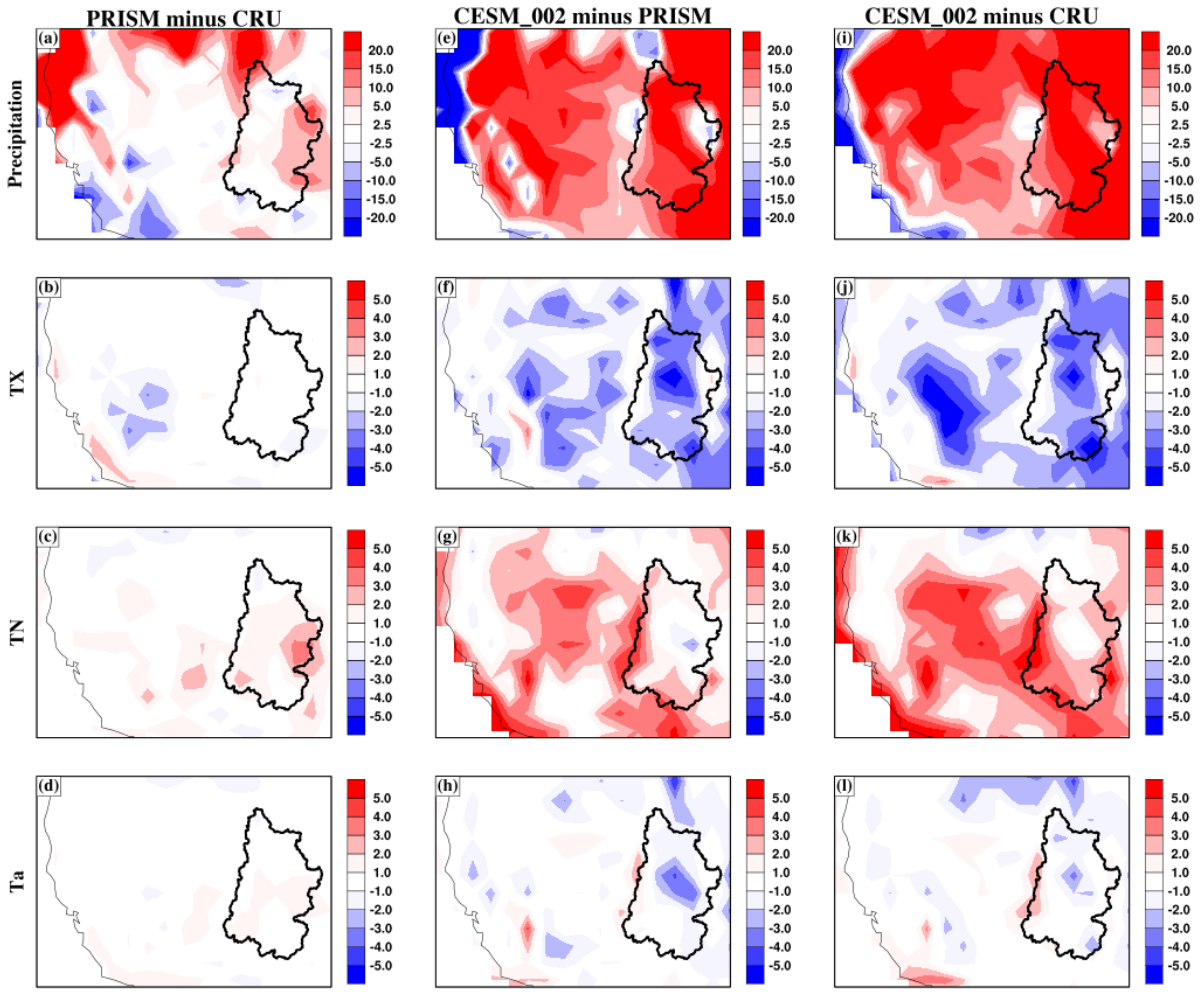

Figure 4.5 Bias in CRU in reference to PRISM, and biases in CESM002 simulations in reference to PRISM and CRU: precipitation (1st row), maximum temperature (TX; 2nd row), minimum temperature (TN; 3rd row), and mean temperature (Ta; 4th row). Precipitation has a unit of mm month^{-1} and temperature has a unit of °C.

Figure 4.5 shows the spatial patterns of the differences between simulation (for CESM 002) and observed climate variables. For clarity, the CRU bias in reference to PRISM is in

column 1 and CESM bias in reference to PRISM (CRU) is in column 2 (column 3). The difference between observed precipitation (Fig. 4.5a) generally ranges from –20 to 20 mm month^{-1}, with PRISM precipitation slightly higher than CRU precipitation over the eastern sector of the UCRB, Oregon, northern California, and the extreme northern half of the western sector of U.S. For most parts, there is similarity between the two observed datasets. Figures 4.5e and 4.5i for CESM 002 minus PRISM and CESM 002 minus CRU generally indicate that the model overestimates the observed precipitation. As a result, a wet bias in excess of 5 – 20 mm month^{-1} widely spread over the region is observed.

For TX (Fig. 4.5b), there seems to be little or no difference between the two observations over the UCRB. However, the model underestimates the observed TX over the region. Pockets of lower TX that ranges from –1.0 to –5.0 ℃ are shown in Figures 4.5f and 4.5j. In contrast to TX, there is a slight difference between observed and simulated TN over the UCRB and other parts of the western U.S. (Fig. 4.5c). The CRU TN appears to be colder than the PRISM TN with a difference of at least 1 ℃. We find that the nighttime temperature (TN) in the model is considerably higher than observed (Figs. 4.5g and 4.5k). The magnitude of the warm bias is higher and more widespread in CRU than in PRISM. Figures 4.5h and 4.5l indicate that the model capture the spatial pattern of mean Ta over the region, although with a slight mixture of warm and cold biases. The difference between observed Ta is relatively weak (Fig. 4.5d); less than 2 ℃. A similar result is noted for other CESM ensemble members (not shown), although with slight differences.

b. Evaluation of CESM-LE drought simulation performance

1) INTERANNUAL VARIABILITY OF SINGLE DROUGHT OBJECT ATTRIBUTES

The interannual variability of percentile intensity attributes of drought objects appears in Fig. 4.6. In this figure, the shaded area represents the spread among the 34 ensemble members of the CESM-LE, while the thick black line indicates the median values. The spread is measured by the distance between the maximum and minimum drought intensity values. The percentile intensity for the observations is depicted by the solid blue line (CRU) and the thin red dash-dash line (PRISM). We note that it is not logical to compare the model and observations on a yearly basis because the time series of unforced, internal variability may differ between the model and observations. However, we can glean some useful information from the climatology. In general, there is a good agreement between the observational datasets, but differences exist in some years. For example, MODE did not identify drought objects in CRU in 1953, 1963, 1968, 1977-78, and 1981 when PRISM produce drought objects. Also, there are no drought objects in PRISM in 1958 and 1996 in contrast to CRU. These results show that uncertainty exists among the observation-based datasets.

The temporal evolution of the median of drought intensity for the ensemble members and the observations shows increasing trends in the percentile intensity attribute, indicating that some of the ensemble members capture the variability in drought intensity attribute. The magnitude of trends in the median of drought intensity for the ensemble members is roughly half of the magnitudes in PRISM. For the 10th percentile intensity attribute (Fig. 4.6a), the trend values are 0.038, 0.046, and 0.071 per decade for CESM-LE, CRU, and PRISM respectively. The Welch two-sided *t* test statistics for the difference of two means indicate that there is no statistically significant difference between the mean of CESM-LE drought intensity and either of the two observations. We further assess the statistical significant using

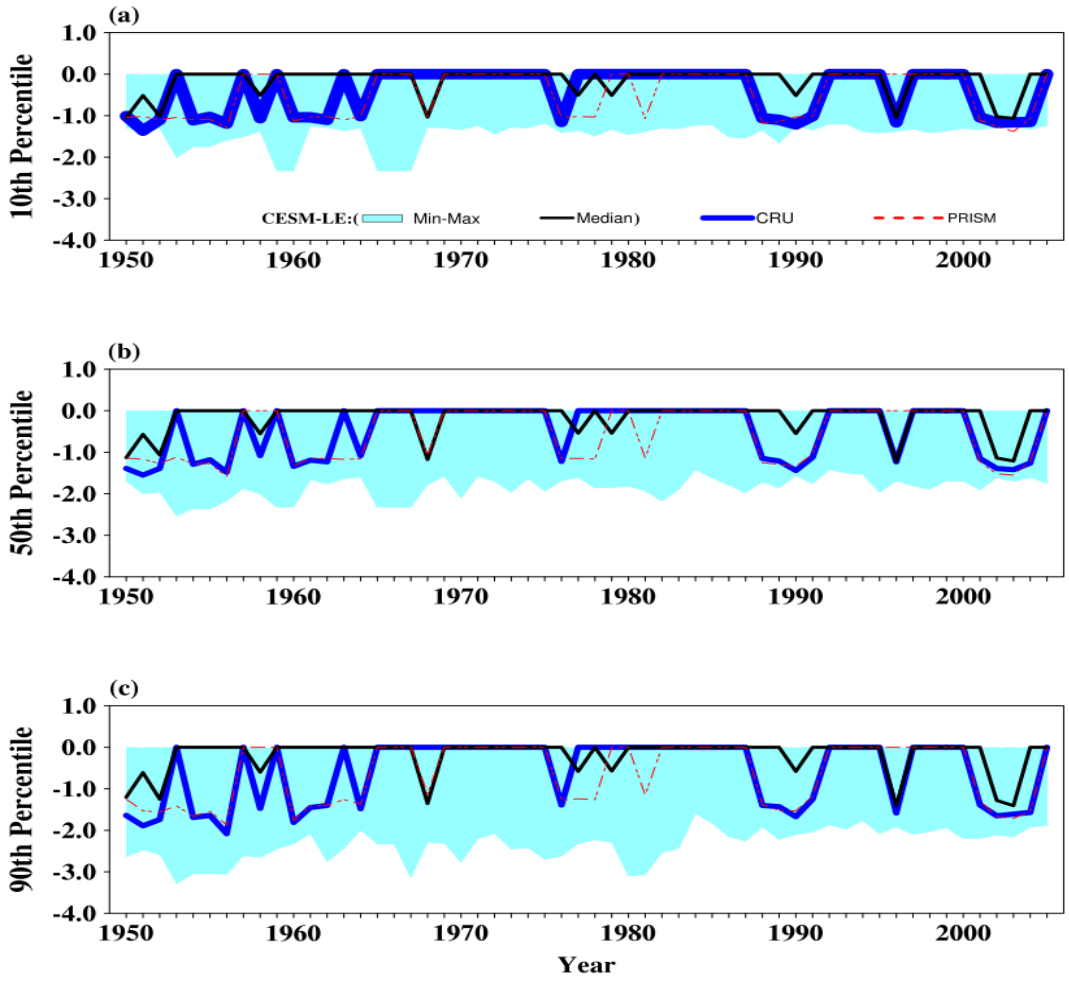

Figure 4.6 Interannual variability of (a) 10th, (b) 50th, and (c) 90th percentile intensity attribute of MODE drought objects. The cyan shade represents the minimum-maximum range and the thick black line is the median of drought intensity for the CESM-LE ensemble members. The solid blue (CRU) and dash-dash red (PRISM) lines indicate observed intensities, respectively.

Fisher's least significant different test, and obtain the same result. For the 50th percentile intensity attribute (Fig. 4.6b), the slope of best-fit lines are 0.047, 0.062, and 0.081 per decade, while for the 90th percentile intensity attribute (Fig. 4.6c) the slopes are 0.063,

0.092, and 0.11 per decade for CESM-LE, CRU, and PRISM, respectively. Consistent with the 10th percentile intensity attribute, there are no statistically significant differences between the mean of CESM-LE drought intensity and the two observations for both the 50th and 90th percentile intensity attributes of drought objects.

Figure 4.7 shows the temporal variability of area attribute of MODE drought objects during the period of study over UCRB. Consistent with Fig. 4.6, Fig. 4.7 shows that some of the ensemble members have smaller drought objects as indicated by the median value. During the period when there is no observed drought, some of the ensemble members simulate large drought objects area. This shows the presence of spread among the ensemble members, with some of the ensemble members exhibiting outlier behavior in their climate variables.

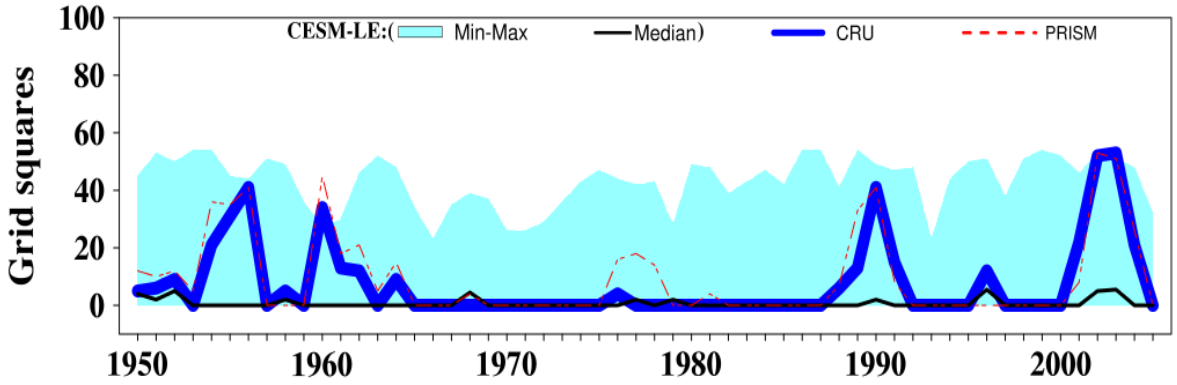

Figure 4.7 Interannual variability of area attribute of MODE drought objects. The cyan shade represents the minimum-maximum range and the thick black line is the median of drought intensity for the CESM-LE ensemble members. The solid blue (CRU) and dash-dash red (PRISM) lines indicate observed intensities, respectively.

2) STATISTICS OF SINGLE DROUGHT OBJECT ATTRIBUTES

Considering data for all the identified drought objects during the period of study for each CESM ensemble members and observations, we obtain a data series for each ensemble members and observations separately by taking the average of all the data. Then, we calculate various statistics of the data. Figures 4.8 – 4.11 show the statistics of MODE drought object attributes (percentile intensity, area, and centroid locations) for the ensemble members and observations (CRU and PRISM). We use the box-and-whisker plots to present the statistics of the percentile intensity and area attributes, while that of the location attribute is shown on the UCRB map.

Figure 4.8 shows the box-and-whisker plots of the 50th percentile intensity of observed and simulated MODE drought objects. As shown in Fig. 4.8a, there is a considerable spread in the statistics of the 50th percentile intensity of drought among the CESM-LE ensemble members. The median value of this attribute ranges from –1.22 to –1.45, with ensemble member 17 and 29 (CESM 017 and CESM 029) with the lowest magnitude and ensemble member 12 (CESM 012) with the highest magnitude. Only 11 (32%) of the ensemble members have median values within the spread of the observed median. The simulated inter-quartile range (IQR) is wide. This statistic varies between –0.15 and –0.36, with a median value of –0.25 and a standard deviation (StDev) of 0.06. The observed IQR are –0.14 and –0.23 for PRISM and CRU, with a mean of –0.19 and a StDev of 0.07, respectively. About 59% of the ensemble members have IQR values closer to –0.19 ± 0.07 of observed IQR, indicating that CESM ensemble members fairly reproduce the observed IQR. Similarly, there exists a large spread in the range (max – min) of the 50th percentile intensity of drought among the CESM-LE ensemble members. This value varies from –0.36 to –1.38, with a

median of –0.80 and a StDev of 0.27. Again, for some of the ensemble members this value is considerably higher than observed range, indicating the possibility of outliers. Considering the CESM ensemble mean (Fig. 4.8b), we find that the observed mean values are lower than the least of the simulated mean (values outside of the lower tail of the distribution), confirming that the CESM ensemble members overestimates the observed 50th percentile intensity of drought.

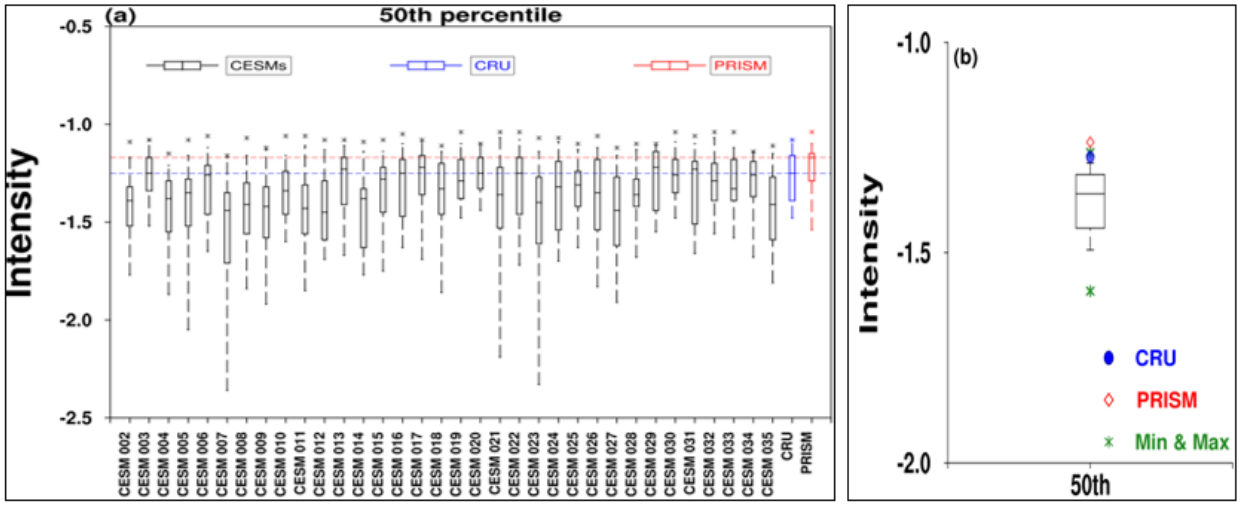

Figure 4.8 Boxplots of (a) 50th percentile intensity attribute of MODE drought objects for CESM-LE ensemble members and observation, and (b) the ensemble mean of CESM-LE ensemble members. The whiskers indicate 5th and 95th – percentiles, respectivly. The asterisks indicate the minimum and maximum drought intensities.

Consistent with the 50th percentile intensity attribute of drought objects, the simulated median of the 90th percentile intensity of MODE drought objects shows considerable

variability, with values that range from –1.47 to –1.80 (Fig. 4.9a). The mean and StDev of this statistic are –1.62 and 0.10, respectively. The observed median of the 90th percentile intensity of drought objects are –1.58 and –1.40 for CRU and PRISM, respectively. About

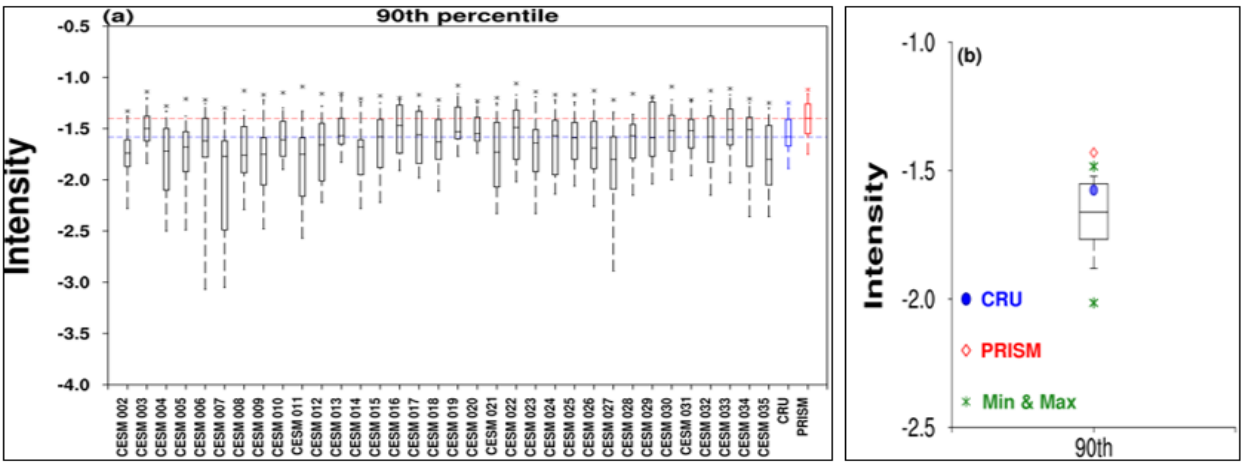

Figure 4.9 Boxplots of (a) 90th percentile intensity attribute of MODE drought objects for CESM-LE ensemble members and observation, and (b) the ensemble mean of CESM-LE ensemble members. The whiskers indicate 5th and 95th – percentiles, respectivly. The asterisks indicate the minimum and maximum drought intensities.

62% (21) of the CESM ensemble members have their median values near or within the spread of the observed median. In general, the simulated IQR ranges from –0.23 to –0.87, with some ensemble members found with higher values (e.g., CESM 007 {–0.87}, CESM 021 {–0.62}, and CESM 004 {–0.61}). The observed IQR is –0.25 for CRU and –0.29 for PRISM. In fact, these values are within the spread of the simulated IQR. Also, Fig. 9a indicates that about 41% of simulated IQR are closer to –0.29 ± 0.05 of observed IQR. This

shows that there is a good agreement among some of the model ensemble members in simulating the upper 10% of the drought intensity. Taking the statistics of the mean of the 90th percentile intensity of drought objects from each ensemble members, Fig. 4.9b further confirms that CESM-LE overestimate the drought intensity over UCRB as the median value of the simulated means is considerably higher than both the observed mean drought intensities.

For further understanding of the ability of CESM-LE to simulate drought objects, we assess the performance of CESM-LE ensemble members to simulate the area of drought objects over UCRB. Figure 4.10 shows the box-and-whisker plots of observed and simulated area of drought objects. As shown in Fig. 4.10a, the median value of observed area is 14 and 15.5 for CRU and PRISM, respectively. The slight difference in values further confirms the presence of uncertainty in observational datasets. Figure 4.10a also shows that the median values of simulated area of objects are very different from each other. We find 20 of the ensemble members with median values below the observed median values, while 4 have median values above the observed median values. However, among those 20 ensemble members, there are 10 of them with median values closer or within 14.75 ± 1.06 of observed median. The observed IQR is also slightly different, 22.3 grid squares (CRU) and 26.9 grid squares (PRISM). The spread of the simulated IQR is considerably wide. This statistic ranges from 7.5 to 30.0 grid squares, indicating that some CESM ensemble members (4) have higher IQR than observations. Figure 4.10b shows that CESM-LE ensemble members simulated smaller area of drought objects as the observed means lie outside the IQR box of the ensemble mean, supporting the results in Fig. 4.10a. This is further confirm by the leftward skewness of the median value, where we find that the upper tail (95th percentile) of the

whiskers is considerable shorter than the lower tail (5th percentile) and the maximum area is well extended beyond the 95th percentile value, confirming the existence of outliers in drought area among the ensemble members.

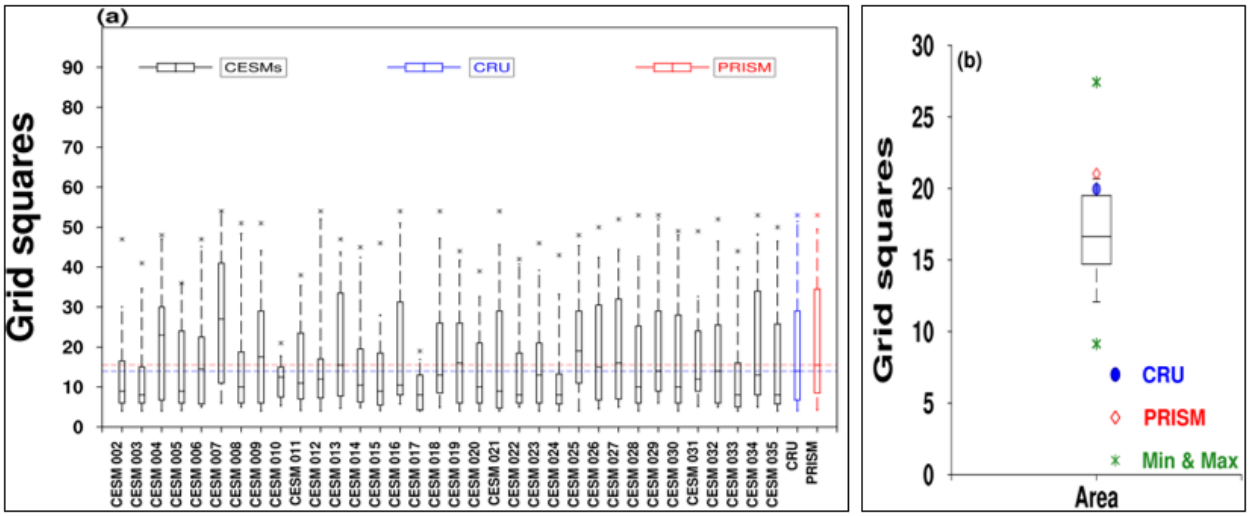

Figure 4.10 Boxplots of (a) area of MODE drought objects for CESM-LE ensemble members and observation, and (b) the ensemble mean of CESM-LE ensemble members. The whiskers indicate 5th and 95th – percentiles, respectivly. The asterisks indicate the minimum and maximum drought areas.

Figure 4.11 displays the spatial distribution of the mean of observed and simulated centroid location attribute of MODE drought objects during the period of study.

Consistent with previous observed attributes, the observed centroid location also exhibits slight differences in their mean values. The observations are spatially separated by about 0.2° latitude and 0.5° longitude. In general, the CESM-LE ensemble members are characterized by wider latitudinal spread. The spread in simulated centroid latitude of drought objects

ranges from 39.2 – 42.1 °N (median at 40.8 °N), while the spread in simulated centroid longitude of drought objects ranges from 107.7 – 109.9 °W (median at 108.2 °W). This leads to the ensemble mean located at 40.5 °N, 108.3 °W. In general, the CESM-LE ensemble mean shows drought object centroid location that is slightly closer to centroid location of observed drought objects.

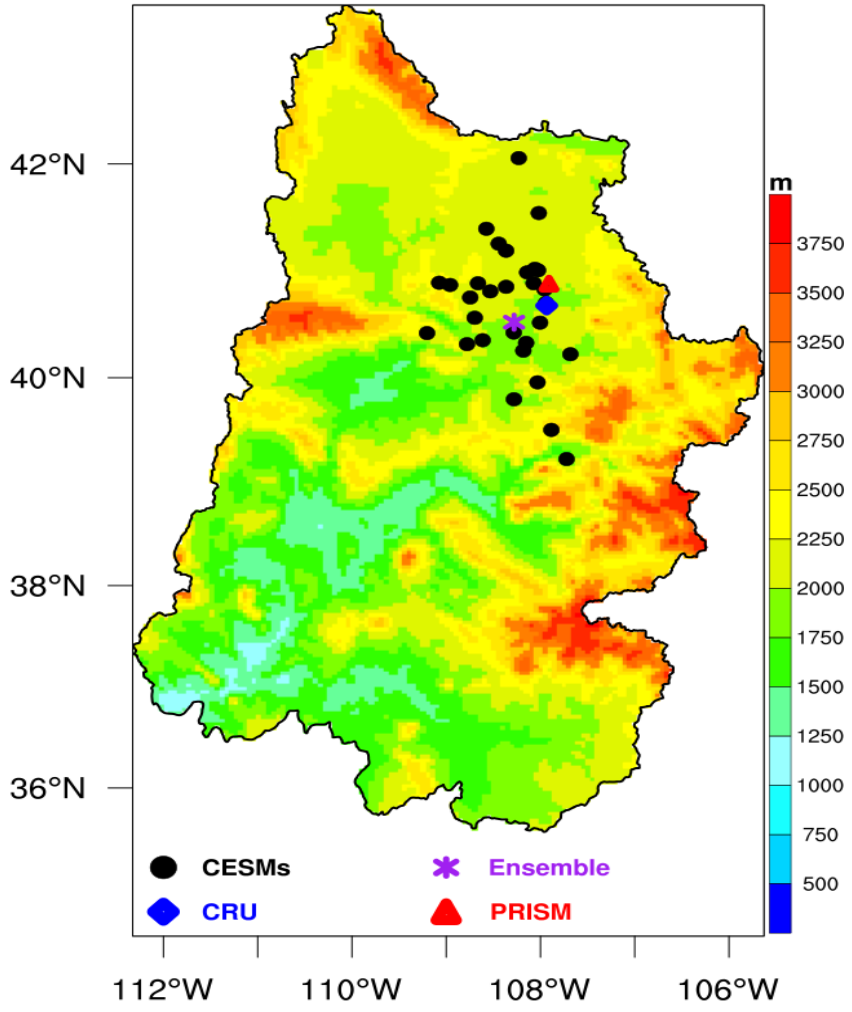

Figure 4.11 Spatial distribution of mean of centroid location attribute of MODE drought objects for CESM-LE ensemble members and observations.

4. Conclusions

This study uses the MODE analysis tool developed by Davies et al. (2009) to evaluate the performance of the CESM-LE in reproducing the statistics of drought object attributes including centroid location, area, and intensity percentile over the UCRB. MODE has been applied in several studies to evaluate precipitation forecasts (e.g., Gallus Jr., 2010). However, this study provides an initial application of MODE to evaluate the performance of the CESM-LE to reproduce the climatological statistics of drought object attributes. We characterize drought using the SPEI at the 36-month time scale. This drought index is calculated individually for two observed datasets (CRU and PRISM) and for 34 members of the CESM Large Ensemble. In this analysis, we use the monthly means of precipitation and daily maximum and minimum temperature for the period 1948–2005.

The performance of the CESM-LE in simulating the climate variables (TX, TN, Ta, and Pr) over UCRB is examined. The analyses show that the ensemble members have a mixed performance in simulating the climate over the region. For Pr, the ensemble members are characterized by a wet bias. At both the seasonal and annual timescale, the CESM-LE capture the temporal patterns fairly well, but misses the peak of the amplitude. Similarly, we find a large disparity between observed and simulated Pr during the warm season. The simulated TX exhibits a cold bias, while simulated TN shows a warm bias. However, simulated Ta appears to be a balance between TX and TN; thus this climatic variable is simulated fairly well. The assessment of the spatial variability of the climatic variables using Taylor diagrams indicates that the observed spatial distributions of both the Pr and TN are not well reproduced by the ensemble members. The uncertainties among the ensembles

members in these important drought variables indicate that miss values will show up in the simulated attributes of drought objects.

The MODE depiction of the CESM-LE drought object attributes shows consistency among the model ensemble members in simulating higher percentile intensity attribute of drought object, although outliers occur. The CESM-LE shows wider spread in the statistics of this attribute. We find that there is agreement among the CESM-LE ensemble members in simulating smaller drought area than observed. Twenty of the CESM ensemble members have median value of area below the observed median values, while 4 of the CESM ensemble members have higher median values than the observed median values. For the centroid location attribute of drought objects, there is a considerable spread in the simulated locations of MODE drought objects, with the ensemble centroid locations closer to observed locations of drought objects.

This study presents a preliminary result of the application of MODE to evaluate simulated simple drought objects over the UCRB. The analyses are based on three object attributes for only the simple single objects, therefore there is opportunity for further work. However, the results from this three attributes show that MODE can offer an effective evaluation opportunity for model developers and water resources managers in their daily operations for onward societal application. In addition, the outcomes of this study show the usefulness of MODE to monitor and characterize extreme climatic events including droughts.

A motivation for this study is to analyze the utility of the CESM-LE to project changes in the UCRB hydrology that could be used by Denver Water in its long-term planning. The results show that the CESM-LE can produce medium and strong droughts with about the same frequency as observed, but with some biases that must be kept in mind when looking at

projected changes. For example, the CESM-LE tends to produce smaller regions of drought, but with more intense drought in those region. The CESM-LE also tends to locate drought regions farther west from the continental divide than do the observations, apparently because its topography at approximately 1˚ grid spacing is smoother than observed topographic features that influence the location of precipitation in the UCRB.

Acknowledgements

We appreciate the contributions of the Denver Water management in this study. This work provides tool, metric, and information to serve the needs of Denver Water resource management to identify actionable climatic resources that influence day-to-day decision-making. The high-performance computing support from Yellowstone (ark:/85065/d7wd3xhc) provided by the National Center for Atmospheric Research (NCAR) is greatly appreciated. We perform the computations and analyses using the NCAR Command Language (Version 6.3.0). This work is supported by the National Science Foundation through Earth System Modeling (EaSM) Grant number AGS-1243106. Also, we thank the anonymous reviewers for their comments.

References

Abatan, A. A., W. J. Gutowski Jr., C. M. Ammann, L. Kaatz, B. G. Brown, L. Buja, R. Bullock, T. Fowler, E. Gilleland, J. Halley Gotway, 2017. Multi-year droughts and pluvials over the upper Colorado River basin and associated circulations. *J. Hydrometeorol.,* **18,** 799–818, doi: 10.1175/JHM-D-16-0125.1.

Abatan, A. A., W. J. Gutowski Jr., C. M. Ammann, L. Kaatz, B. G. Brown, L. Buja, R. Bullock, T. Fowler, E. Gilleland, J. Halley Gotway, 2017. Statistics of multi-year droughts from the Method for Object-based Diagnostic Evaluation (MODE). *Int. J. Climatol.,* (Submitted).

Ahijevych D, Gilleland E, Brown B. G., Ebert E. E. 2009. Application of spatial verification methods to idealized and NWP-gridded precipitation forecasts. *Weather and Forecasting*, **24,** 1485 – 1497.

Bryant, E., 2005: Natural Hazards. Cambridge University Press, Second Edition, 312 pp.

Burgman, R. J. and Y. Jang, 2015: Simulated U.S. drought response to interannual and decadal Pacific SST variability. *J. Climate*, **15,** 4688–4705.

Dai A. 2011. Drought under global warming: a review. *Wiley Interdiscip Rev Clim Change*, **2**(1), 45–65, doi:10.1002/wcc.81.

Daly, C., M. Halbleib, J. I. Smith, W. P. Gibson, M. K. Doggett, G. H. Taylor, J. Curtis, and P. P. Pasteris, 2008: Physiographically-sensitive mapping of temperature and precipitation across the conterminous United States. *Int. J. Climatol*., **1,** 2031–2064.

Daly, C., R. P. Neilson, and D. L. Phillips, 1994: A statistical–topographic model for mapping climatological precipitation over mountainous terrain. *J. Appl. Meteor.,* **33,** 140–158.

Davis, C., B. Brown, R. Bullock, 2006a: Object-based verification of precipitation forecasts. Part I: Methods and application to mesoscale rain areas. *Mon. Wea. Rev*., **134,** 1772–1784.

Davis, C., B. Brown, R. Bullock, 2006b: Object-based verification of precipitation forecasts. Part II: Application to convective rain systems. *Mon. Wea. Rev*., **134,** 1785–1795.

Davis, C. A., B. G. Brown, R. Bullock, Halley-Gotway J. 2009. The Method for Object-based Diagnostic Evaluation (MODE) applied to numerical forecasts from the 2005 NSSL/SPC spring program. *Weather and Forecasting*, **24,** 1252–1267.

Diasso, U. and and B. J. Abiodun. 2017: Drought modes in West Africa and how well CORDEX RCMs simulate them. *Theor. Appl. Climatol.*, **128,** 223–240, doi:10.1007/s00704-015-1705-6.

Gallus, Jr. W. A. 2010. Application of Object-based verification techniques to ensemble precipitation forecasts. *Weather and Forecasting*, **25,** 144–158.

Gregory, J. M., J. F. B. Mitchell, and A. J. Brady, 1997: Summer drought in northern midlatitudes in a time-dependent CO2 climate experiment. *J. Climate,* **10,** 662–686.

Hagos, S. M., L. R. Leung, J.-H. Yoon, J. Lu, and Y. Gao, 2016: A projection of changes in landfalling atmospheric river frequency and extreme precipitation over western North America from the Large Ensemble CESM simulations. *Geophys. Res. Lett.*, **43,** 1–7, doi:10.1002/2015GL067392.

Hargreaves, G. L., and Z. A. Samani, 1985: Reference crop evapotranspiration from temperature. *Appl. Eng. Agric.* **1**: 96–99.

Harris, I., P. Jones, T. Osborn, and D. Lister, 2014: Updated high resolution grids of monthly climatic observations—The CRU TS3.10 dataset. *Int. J. Climatol*., **34,** 623–642.

Hurrell, J. W., M. M. Holland, P. R. Gent, S. Ghan, J. E. Kay, P. J. Kushner, J.-F. Lamarque, W. G. Large, D. Lawrence, K. Lindsay, W. H. Lipscomb, M. C. Long, N. Mahowald, D. R. Marsh, R. B. Neale, P. Rasch, S. Vavrus, M. Vertenstein, D. Bader, W. D. Collins, J. J. Hack, J. Kiehl, and S. Marshall, 2013: The community earth system model: A framework for collaborative research. *Bull. Amer. Meteorol. Soc*., 1339–1360, doi:10.1175/BAMS-D-12-00121.1.

IPCC, 2013: Summary for Policymakers. In: Climate Change 2013: The Physical Science Basis. Contribution of Working Group I to the Fifth Assessment Report of the Intergovernmental Panel on Climate Change [Stocker, T.F., D. Qin, G.-K. Plattner, M. Tignor, S. K. Allen, J. Boschung, A. Nauels, Y. Xia, V. Bex and P.M. Midgley (eds.)]. Cambridge University Press, Cambridge, United Kingdom and New York, NY, USA.

Johnson A, Wang X. 2012. Verification and calibration of neighborhood and object-based probabilistic precipitation forecasts from a multimodel convection-allowing ensemble. *Mon. Wea. Rev*. **140:** 3054–3077.

Kay, J. E., C. Deser, A. Phillips, A. Mai, C. Hannay, G. Strand, J. M. Arblaster, S. C. Bates, G. Danabasoglu, J. Edwards, M. Holland, P. Kushner, J.-F. Lamarque, D. Lawrence, K. Lindsay, A. Middleton, E. Munoz, R. Neale, K. Oleson, L. Polvani, and M. Vertenstein, 2015: The community earth system model (CESM) large ensemble project: A community resource for study climate change in the presence on internal climate variability. *Bull. Amer. Meteorol. Soc*., 1333–1349, doi:10.1175/BAMS-D-13-00255.1.

Kelly CP, Mohtadi S, Cane MA, Seager R, Kushnir Y. 2015. Climate change in the Fertile Crescent and implications of the recent Syrian drought. *PNAS*, **112,** 3241–3246.

Meehl GA, Stocker TF, Collins WD, Friedlingstein P, Gaye AT, Gregory JM, Kitoh A, Knutti R, Murphy JM, Noda A, Raper SCB, Watterson IG, Weaver AJ, Zhao Z.-C. 2007. Global Climate Projections. In: *Climate Change 2007: The Physical Science Basis.* Contribution of Working Group I to the Fourth Assessment Report of the Intergovernmental Panel on Climate Change [Solomon, S., D. Qin, M. Manning, Z. Chen, M. Marquis, K.B. Averyt, M. Tignor and H.L. Miller (eds.)]. Cambridge University Press, Cambridge, United Kingdom and New York, NY, USA.

Mittermaier M. P., R. Bullock, 2013: Using MODE to explore the spatial and temporal characteristics of cloud cover forecasts from high-resolution NWP models. *Meteorological Applications*, **20,** 187–196.

Phillips, A. S., C. Deser and J. Fasullo 2014: Evaluating modes of variability in climate models, *Eos Trans. AGU, **95(***49), 453, 455, 2014EO490002.

Scherrer, S. C., E. M. Fischer, R. Posselt, M. A. Liniger, M. Croci-Maspoli, and R. Knutti, 2016: Emerging trends in heavy precipitation and hot temperature extremes in Switzerland. *J. Geophys. Res. Atmos*., **121,** 1–12, doi:10.1002/2015JD024634.

Sheffield, J., E. F. Wood, and M. Roderick, 2012: Little change in global drought over the past 60 years. *Nature*, **491**, 435–438.

Taylor, K. E. 2001: Summarizing multiple aspects of model performance in a single diagram. *J. Geophys. Res*., **106,** 7183–7192.

Ujeneza, E. L. and B. J. Abiodun. 2015: Drought regimes in Southern Africa and how well GCMs simulate them. *Climate Dynamics*, **44,** 1595–1609.

Vicente-Serrano SM, Beguería S, López-Moreno JI, 2010a: A multiscalar drought index sensitive to Global Warming: the Standardized precipitation evapotranspiration index. *J Climate,* **23,** 1696–1718, doi:10.1175/2009JCLI2909.1.

Vicente-Serrano, S. M., S. Beguería, J. I. López-Moreno, m. Angulo, and A. EL Kenawy, 2010b: A new global 0.5º gridded dataset (1901–2006) of a multiscalar drought index: Comparison with current drought index datasets based on the Palmer Drought Severity Index. *Amer. Meteor. Soc.,* **11,** 1033–1043.

Wilhite, D. A., 2000: Drought as a natural hazard: Concepts and definitions. In: *Drought: A Global Assessment*, Vol. 1, Wilhite, D.A. (ed.). Routledge, New York, pp. 1–18.

Wilhite, D.A. and Buchanan, M. (2005). Drought as hazard: Understanding the natural and social context. In: *Drought and Water Crisis: Science, Technology, and Management Issues*, Wilhite, D.A. (ed.). CRC Press (Taylor and Francis), New York, pp. 3–29.

Woodhouse, C. A., and J. T. Overpeck. 1998: 2000 years of drought variability in the central United States. *Bull. Amer. Meteorol. Soc*., **79,** 2693–2714.

CHAPTER 5. GENERAL CONCLUSIONS

Water is essential to life. However, the quality and quantity of this natural resource are depleting at a faster rate as a result of climate variability and change. In recent times, a large percentage of the world has experienced an unprecedented drought episodes resulting from warming and reduction in precipitation. The future of human on earth requires detail understanding of the characteristics of extremes of climate, such as drought, that promotes the variability in the intensity, frequency, and duration of precipitation leading to reduction in streamflow in many regions of the world including the UCRB in Denver, US. Although we cannot put an end to drought occurrence, but we can mitigate the impact on human and natural ecosystems through informed planning and decision making. The water resource managers have a great role to play in this mitigation process for a better future on earth. As such, the Denver Water management has increased their interest in climate science to foster their daily activity and water management planning. This study was carried out in conjunction with Denver Water, a major water utility in the western US. Denver Water is particularly vulnerable to multi-year droughts, which can have severe consequences on water resources management, and for maintaining both supply and operating revenue. The focus of this study is to use a water applications perspective to:

- Understand the characteristics of past droughts and, for contrast, pluvials and how they might change in the future, through the analysis of the two most widely used drought indicators; SPI and SPEI, over UCRB.

- Adapt tool successfully applied to numerical weather prediction evaluation, MODE, to examine and compare the statistics of attributes of drought objects from the SPEI and SPI over UCRB.
- Use MODE to evaluate the ability of CESM-LE to provide credible insight into the statistics of attributes of drought objects from the SPEI over UCRB so that their output can be used for planning.
- Identify biases to improve models and develop usable information that can guide water managers.

Our analyses focus on the 36-month SPI (SPI36) and SPEI (SPEI36), and we adapt MODE tool to explore the probabilistic nature of climate-simulation evaluation, focusing on UCRB, the region that supplies Denver Water. The analyses yield drought and pluvial characteristics in observations and climate simulations and the atmospheric large-scale features associated with the initiation and maintenance of multi-year droughts and pluvials. We diagnose the processes that sustain droughts and pluvials revealed by the SPEI and SPI indices. We also find that the droughts and pluvials are not simply the opposite phases of each other. These analyses reveal the capabilities and limitations of climate simulations produced by the NCAR CESM Large Ensemble.

MODE lend itself has an important technique to evaluate climate models. MODE allows us to quantify model-observation differences in intensity, shape, and location of events. We demonstrate opportunities and challenges that emerge when adapting weather forecast verification tools to climate problems in the water sector.

In summary, CESM-LE is a reasonable climate model to study several aspects of droughts over UCRB, although there is still room for improvements of the basic climate

variables, in particular precipitation. The study conclude that the application of SPEI as an alternate to SPI to study the characteristics of extreme climate events including droughts at longer timescale over the study domain is viable.

Future research

This study has in particular, shown some basic characteristics of past observed and simulated droughts using relevant drought indices and evaluation tool. We believe that knowledge of climate systems from past occurrences will promote our understanding of how the system might change in future, thus enable us to mitigate the impacts. For future research, it is important to do further analysis on:

- Dynamical comparison between 21st-century and earlier drought
- Comparison of 21st-century droughts with 20st-century droughts
- Changes in drought characteristics
- The physical mechanism related to 21st-century drought, and possibly compare with 20th-century